BEHAVIOR OF REINFORCED CONCRETE INFILLED FRAMES UNDER DYNAMIC LOADING: PART 2

by

NESTOR ROBERTO RUBIANO-BENAVIDES

Ingeniero Civil, Magister en Ingenieria Civil

THESIS

Presented to the Faculty of the Graduate School of

The University of Texas at Austin

in Partial Fulfillment

of the Requirements

for the Degree of

MASTER OF SCIENCE IN ENGINEERING

THE UNIVERSITY OF TEXAS AT AUSTIN

August 1995

BEHAVIOR OF REINFORCED CONCRETE INFILLED FRAMES

UNDER DYNAMIC LOADING: PART 2

.

APPROVED BY

SUPERVISING COMMITTEE:

_____

Richard E. Klingner

_____

Jose M. Roesset

To my son, Nestor Raul

ACKNOWLEDGMENTS

The research described in this thesis was conducted at the Phil M. Ferguson Structural Engineering Laboratory of the University of Texas at Austin by Mr. Tarek R. Bashandy and the author, under the supervision of Dr. Richard E. Klingner. Funding and technical information was provided by the U. S. Army Construction Engineering Laboratory (USACERL), under the direction of Steven Sweeney. Partial financial support was also provided to the author by the "Fundación para el Futuro de Colombia, COLFUTURO."

The author is greatly indebted to Dr. Richard E. Klingner for his continuous and invaluable guidance and support as teacher, supervisor, and friend. No part of this thesis would have been possible without his assistance. Likewise, the author wishes to express his gratitude to Dr. Jose M. Roesset for his comments and suggestions. Assistance from the staff of Ferguson Lab is gratefully acknowledged as well, particularly that from Cindy McCright, who helped formatting this thesis.

Finally, completion of this thesis was possible only because of the understanding and love given to the author by his wife, Janet.

Nestor Roberto Rubiano-Benavides

June 12, 1995

ABSTRACT

BEHAVIOR OF REINFORCED CONCRETE INFILLED FRAMES UNDER DYNAMIC LOADING: PART 2

by

Nestor Roberto Rubiano-Benavides, M.S.E.
The University of Texas at Austin, 1995
SUPERVISOR: Richard E. Klingner

A recent survey of U. S. Army buildings showed that a considerable percentage of them can be classified as reinforced concrete frames with infill masonry walls. In order to evaluate the strength and seismic behavior of such structures, the U. S. Army Construction Engineering Laboratory (USACERL) carried out an experimental program on several half-scale infilled frame specimens subjected to dynamic loading. Using a shaking table, both in-plane and out-of-plane simulated earthquake motions were applied to virgin, previously damaged, and repaired specimens. The experimental data obtained from this test series were then analyzed at the University of Texas at Austin. The objective of this work was to develop reliable analysis tools to predict the real strength and the dynamic response of infilled frames. Evaluation of in-plane and out-of-plane behavior of the infilled frames was performed using their load-displacement response. Maximum base shears, deflections, and internal strains were measured and assessed. Using various mathematical idealizations, the dynamic response of the specimens was predicted analytically. Finally, simplified analytical idealizations were developed to predict the strength and stiffness of infilled frames, and several design procedures were reviewed.

TABLE OF CONTENTS

Page

LIST OF FIGURES

Page

LIST OF TABLES

Page

CHAPTER 1

INTRODUCTION

1.1. General

A recent inventory of essential and high-risk buildings used by the U.S. Army showed that nearly 40% of them were classified as reinforced concrete frames with infill shear walls (Al-Chaar et al, 1994). Generally, those buildings were designed and constructed following different specifications and construction practices, and the infill panels were not usually intended to be part of the structural system. Therefore, the real capacity of these structures and their ability to withstand moderate and large earthquakes must be evaluated. Evaluation of the buildings' seismic resistance requires accurate models for predicting the behavior of infilled frames subjected to in-plane and out-of-plane loads. The in-plane strength and stiffness of the infills is likely to dominate the overall seismic response of the building, while their out-of-plane strength will determine whether or not individual panels will collapse under strong lateral motions.

Extensive experimental and analytical research on analysis, design, and behavior of concrete infilled frames has been conducted worldwide during the last three decades. Based on the results of such investigations, a number of design approaches have been developed and used. However, most of the experimental evidence has been obtained from static and pseudo-dynamic tests, and thus, the dynamic nature of the seismic response of these structures has not been completely assessed. Therefore, to fully understand the response of concrete infilled frames under seismic loads, and to develop rational methods for analysis and design that consider the dynamic response of these frames, more experimental work using dynamic loading is required.

Because of this need, the U.S. Army Construction Engineering Research Laboratories (USACERL) initiated in 1992 a comprehensive multi-year research program to develop methods for assessing the seismic vulnerability of existing infilled-frame structures. From early 1992 through May 1993, USACERL carried out a series of shaking-table tests on half-scale models of infilled reinforced concrete frames. The original objective of those tests was to aid in the development of engineering models for estimating the load-deflection behavior of the infilled frames under earthquake ground motions, considering elastic and inelastic response, in-plane and out-of-plane response, and the effects of damage due to in-plane excitation on the out-of-plane strength.

Moreover, some of the tests were intended to assess the effectiveness of rehabilitation methods for infills with low out-of-plane strength.

A large amount of data was gathered during that test program, including accelerations, displacements, and internal deformations of the specimens. As part of the research study reported here, such data were thoroughly interpreted and analyzed using state-of-the-art analytical models as well as simplified engineering design models.

In this thesis, a detailed description of the test specimens and setup is first presented. Then, experimental results obtained from the series of tests are reviewed and interpreted. Several analytical models used to predict the response of infills are presented, and the specimens' behavior is compared with those analytical predictions. Then, simplified engineering models are developed and applied to predict the in-plane and out-of-plane strength and stiffness of the infilled frames.. Finally, conclusions on the overall dynamic behavior of the frames is presented and recommendations for implementation of simplified mathematical models is made.

Next section presents the main objectives of the research program conducted for this thesis and the scope of the study. The final section of this chapter reviews previous analytical and experimental research on the in-plane and out-of-plane design and behavior of infilled frames.

1.2. Objectives and Scope

The main objective of this thesis is to present in detail the experimental results obtained by the USACERL during the test series, verify their consistency, and interpret them to evaluate the dynamic characteristics and response of the specimens. Additionally, several analytical idealizations are used to predict the experimental results and simplified engineering models for use in analysis and design are reviewed. No additional experimental work was performed at The University of Texas at Austin.

The specific objectives of this thesis are:

a) Describe the test program, the characteristics of the specimens, and the test setup and procedure
b) Present in detail the results of the shaking-table tests conducted at USACERL

c) Discuss the internal consistency of the results
d) Synthesize and evaluate the observed responses
e) Compare the experimental response with analytical predictions
f) Review simplified engineering models for estimating the earthquake response of the infilled frames

1.3. Overview of Previous Research

Research on masonry infilled frames started in the 1950's, even before studies on reinforced concrete shear walls (Kwan and Xia, 1995). Both in-plane and out-of-plane loading have been investigated thereafter, and even today, ongoing research is continuing worldwide. This section, based mainly on a literature survey made by Angel et al. (1994), briefly reviews the most significant previous experimental and analytical research for in-plane and out-of-plane behavior of infilled frames. Other research program reviews are given by Thomas and Klingner (1990) and Beavers, Bennett and Flanagan (1992).

1.3.1. Tests with In-Plane Loading

The most extensive experimental work has been performed on one-story, one-bay specimens, although a limited number of investigations have included multi-story structures (up to 7 stories) and three-bay frames. Parameters that have been studied are frame material (steel and concrete), infill material (clay brick, hollow clay tile, and concrete block), the type of failure mechanism (infill diagonal cracking, infill crushing, column shear, and column hinge), scale effects (1/8- to full-scale), infill confinement from adjacent panels, and relative frame/infill strength and stiffness (Angel et al., 1994).

Results show that for strong and stiff frames with weak infills, system behavior is dominated by the frame; the panel cracks and deforms while adapting to the frame deflection. On the other hand, behavior of weak frames infilled with strong panels is controlled by the infill, which cracks in an X-crack pattern and may produce a brittle failure or induce shear failure in columns. Regarding lateral deflections, systems with low frame-to-infill strength ratio showed drifts of 0.5% at cracking and 1.0% at peak load. For systems with high frame-to-infill strength ratios, drifts up to 1.5% for cracking and as large as 3% for peak load were measured.

1.3.2. Analytical Studies for In-Plane Loading

The shear beam model is probably the simplest approach that has been used to estimate the stiffness of infilled frames, by combining the shearing and flexural deflections under a unit lateral load. However, stiffness at cracking of the infill is generally overestimated (Thomas and Klingner, 1990).

Another idealization that has been used extensively is to replace the infills by equivalent diagonal compression struts to form a braced frame that can be analyzed statically (Holmes, 1961, 1963; Stafford Smith, 1962, 1966, 1967a, 1967b, 1969; Stafford Smith and Riddington, 1978; Saneinejad and Hobbs, 1995). Several methods have been proposed to estimate the dimensions of the struts, and therefore their strength and stiffness. In general, strut characteristics have been related to the frame and infill material properties, the thickness and aspect ratio of the panel, and the frame/infill stiffness ratio.

A similar, but more sophisticated idealization uses multiple struts (diagonal and vertical) to model the infill panels (Thiruvengadam, 1985). Using this approach, frame -infill interaction and interface separation can be accounted for. Moreover, infill openings can be modeled by appropriately selecting the location of the struts. Finally, this idealization has been found to perform well under both static and dynamic loading (Thiruvengadam, 1985).

More elaborate idealizations, using the finite element method, have been also used extensively. Initially, only linear elastic masonry behavior was considered, and no frame/infill interaction was modeled. Then, some studies included the frame-infill interface separation and the loss of friction along the remaining contact length (Riddington and Stafford Smith, 1977). Recently, brick-size finite elements connected by mortar linking elements have been introduced (Page, 1978). Finally, material nonlinearity has been used for inelastic analyses considering cracking, tension stiffening, and compression softening of the masonry.

Predictions of in-plane stiffness and strength of infilled frames using both simple (diagonal struts) and complex (nonlinear finite element analysis) idealizations are presented in Chapters 6 and 7. Comparisons between such predictions are discussed and recommendations on their application are made.

1.3.3. Tests with Out-Of-Plane Loading

In this case the main parameters that have been studied are frame material (steel and concrete), infill material (clay brick, hollow clay tile, and concrete block), frame stiffness (flexible and rigid), frame-infill connection (free, simple support, and fixed), scale effects (1/2- to full-scale), and repair methods. Most of the limited experimental work has been performed on one-story, one-bay specimens, with a single-wythe masonry infill. A great variety of test setups have been used: detonation of high explosives; tunnel air blasts; static concentrated loads (simulating dynamic inertial loads) applied by hydraulic actuators; and uniform load of the lateral surface of the infill using air bags (Dawe and Seah, 1990; Angel et al., 1994).

Results of tests have shown that out-of-plane strength depends mainly on the compressive strength of masonry (rather than on its tensile capacity), and also on the in-plane stiffness of the confining frame. Furthermore, two non-dimensional parameters, representing the geometry of the infill, have been found useful in describing the out-of-plane behavior of the system: the aspect ratio of the frame (length/height, l/h); and the slenderness ratio of the panel (height/thickness, h/t). The range for l/h has been from 1.0 to 3.0, while ranges for h/t have been from 8 to 31 for concrete masonry and from 8 to 24 for clay masonry. For h/t ratios over 30, the effect of arching action has been found to be small (Angel et al., 1994).

Several repair and restrengthening techniques have been investigated in many countries. Such rehabilitation methods include: pressure injection of cement grout in infill cracks, attachment of diagonal steel tie-bars, and addition of a reinforced concrete surface topping connected to the infill by steel anchors.

1.3.4. Analytical Studies for Out-Of-Plane Loading

Initial approaches used to estimate out-of-plane strength were based on elastic plate solutions assuming isotropic and homogeneous materials and uniform loading pressures. Failure is assumed to occur when the masonry tensile strength is reached, and therefore any capacity of the cracked wall is neglected. Moreover, stiffness is generally overestimated using this idealization.

Theories that include the additional out-of-plane strength of the panel due to the effect of arching action were developed as early as in the 1950's (McDowell et al., 1956). Many of these approaches were based on one-way action and a completely rigid confining frame. Then, more involved theories have developed to include the effect of the frame stiffness, frame-infill interface gaps, and infill shrinkage (Anderson, 1984). More recent developments have considered two-way

action using wall segments defined by, and rotating about, yield (cracking) lines. Also, compressive crushing of the masonry, instead of its tensile resistance, has been considered to limit the infill strength. Finally, support rotation and deflection to model frame flexibility have been introduced (Dawe and Seah, 1990) as well as existing cracks due to previous in-plane loading (Angel et al., 1994).

In summary, currently available analytical models vary from simplified expressions based mainly on the *h/t* (height to thickness) ratio, to sophisticated computer programs based on the yield line approach. However, very few of these idealizations consider previous damage of the infill (due, for example, to prior in-plane loading).

CHAPTER 2

DESCRIPTION OF EXPERIMENTAL PROGRAM

2.1. General Background

During 1992 and 1993, the USACERL performed a series of earthquake-simulated dynamic tests on small-scale reinforced concrete frames infilled with masonry panels. The main investigators of this project were Ghassan Al-Chaar and Steven Sweeney. One set of test specimens, referred to from now on as “weak frames,” was intended to represent buildings designed by the 1956 ACI Code and old construction practices. A second set of specimens, referred to as "strong frames," was designed by the 1989 ACI Code, and was intended to represent modern building construction. In this section, the test program, specimens, test setup and testing procedure are reviewed.

2.2. Experimental Program

The experimental program consisted of a series of dynamic tests with increasing ground motions applied to 8 “Models.” Each Model consisted of a reinforced concrete frame (strong or weak, bare or infilled, and tested in- or out-of-plane) supported by a foundation beam which was attached to the shake table. An overall view of a typical infilled frame specimen is shown in Figure 2.1. For each type of frame, the sequence described below was followed.

First, a bare frame specimen consisting of two parallel frames was tested in-plane. Gradually increasing levels of ground motion were applied parallel to the frames. Their dynamic properties were measured and a certain level of damage was produced in the specimens. The frames were then infilled with masonry, and gradually increasing levels of ground motion were again applied. The specimens’ dynamic properties were again measured, and the maximum ground motion was gradually increased until the infills cracked. Finally, one infilled frame of the specimen was rotated 90 degrees and subjected to out-of-plane ground motions until severe cracking occurred.. No specimen was tested in-plane after out-of-plane excitations had been applied; therefore, the effects of out-of-plane excitation on in-plane response cannot be assessed. In all cases, random vibrations were applied to the specimens to measure their fundamental frequency of vibration, from which its stiffness can be readily estimated. The overall experimental program is summarized in Table 2.1.

For the strong-frame specimen, the infill was repaired after the out-of-plane excitation and subsequently retested to evaluate the effectiveness of the repair method. The weak-frame specimen was not repaired. Finally, a strong infilled frame, to which no previous in-plane excitation had been applied, was tested out-of-plane until severe damage was apparent, to estimate the effect of in-plane ground motions on out-of-plane response.

Table 2.1 Overall Experimental Program Table

	In-Plane Seismic Tests		**Out-of-Plane Seismic Tests**	
Frame Type	**Bare Frame**	**Infilled**	**Unrepaired**	**Repaired**
Strong Frame	Model #1	Model #2	Model #3 Model #5 (Virgin)	Model #4
Weak Frame	Model #6	Model #7	Model #8	Not tested

2.3. Description of Specimens and Test Setup

The specimens were half-scale models of bare and infilled reinforced concrete frames. Each specimen consisted of two parallel one-story, one-bay frames, connected at their top levels by a stiff concrete slab. The slab was attached to the top beams by transverse steel rods. The frame columns were founded on massive beams that were rigidly connected to the shaking-table floor. Figures 2.2 and 2.3 show the layout and dimensions of the frames. For the strong frame the beams were 5 in. × 6 in. and the columns were 6 in. × 6 in. For the weak frame the beams were 4 in. × 6 in. and the columns were 5 in. × 5 in. Infills, with a height-to-thickness ratio of 18, were made of half-scale clay brick laid with a Type N mortar. The measured masonry prism compressive strength was 5000 psi (35 MPa).

Detailing of both longitudinal and transverse reinforcement is also shown in Figures 2.2 and 2.3 for the strong and weak frames respectively. Ratios of longitudinal reinforcement used for the strong frame were 1.2% for the beams (top and bottom) and 2.4% for the columns. For the weak-frame beams, the reinforcement ratios were 1.6% for the top steel and 1.0% for the bottom steel, while for the columns the ratio was 1.8%. Identical transverse reinforcement, in the form of closed stirrups, was provided in beams and columns of both weak and strong frames. However, while for the weak frames spacing was maintained constant at approximately the effective depth of the members, for the strong frames the spacing was reduced to one-fourth the

effective depth of the member near and at the beam-column joints, and to one-half elsewhere (Al-Chaar et al., 1994).

Post-tensioning cables were threaded through each column to increase their axial load, and therefore simulate the effects of the vertical gravity loads generated by overlying stories of a multi-story building. In addition, masses of 8.0 kips (36 kN) and 6.0 kips (27 kN) were added to the slab of the strong- and weak-frame specimens respectively. These masses were intended to simulate the lateral inertial forces generated in the full-scale prototype under base excitation.

Ground accelerations were input to the specimens using the USACERL Biaxial Shock Testing Machine (BSTM). The foundation beams of the specimens were rigidly attached to the shaking table to avoid sliding of the frames. At very small time increments, accelerations and displacements were recorded at various locations and reinforcing-bar strains were measured at critical zones of columns and beams.

2.4. Testing Procedure

The first series of tests, performed on strong-frame specimens, comprised Models #1 through #5. The bare-frame specimen (Model #1) was subjected to a series of in-plane ground motions until cracks appeared in the structural elements. Varying levels of axial prestress were applied to the columns of this specimen during the tests. Infills were then added to the frame, and the specimen was re-named Model #2. A new series of gradually increasing in-plane ground motions was applied to this model until the infills cracked. One infilled frame of this specimen was then rotated 90 degrees and its tip was fixed with cables to the shaking-table floor.

This specimen, named Model #3, was subjected to a series of out-of-plane ground motions until severe cracking occurred in the infills. After this, the masonry infill was repaired on both sides by 1/4-inch x 1/4-inch x 23-gage steel wire mesh, covered by a 1/4-inch (6-mm) ferrocement coating designed for high compressive strength and high workability. The steel mesh was not anchored to the infill nor the frame; all bond between the infill and the coating was achieved at the coating-infill interface itself.

This repaired specimen was named Model #4; it was subjected to a new series of increasing out-of-plane ground motions until severe damage occurred. Tables 2.2 through 2.5 describe the sequence of seismic tests for these models, including the span, the maximum base acceleration (A_{max}), the axial prestress in the columns (P_t) and remarks made by the

experimenters. Additionally, a number of random vibration tests were performed on the specimens, as the series of seismic tests was conducted, in order to estimate their dynamic properties.

Table 2.2 Seismic Tests for Model #1

Test #	DATE	SPAN (%)	A_{max} (g)	P_t (kips)	Remarks
1	3/3/92	10.0	—	0.0	Time scale = 1.4142. BAD TEST
2	3/3/92	25.0	0.192	0.0	
3	3/3/92	55.0	0.378	0.0	
4	3/3/92	—	0.379	0.0	
5	3/3/92	55.0	0.372	6.0	
6	3/3/92	55.0	0.375	9.0	Cracks
7	3/3/92	55.0	0.371	12.0	
8	3/3/92	8.0	0.311	12.0	Filtered. f_c = 2 Hz
9	3/3/92	20.0	0.838	12.0	Filtered
10	3/3/92	30.0	1.204	12.0	Filtered
11	3/3/92	40.0	0.984	12.0	Filtered
12	3/3/92	55.0	0.394	12.0	Unfiltered
13	3/4/92	55.0	0.384	9.0	Unfiltered
14	3/4/92	55.0	0.380	6.0	Unfiltered
15	3/4/92	55.0	0.386	3.0	Unfiltered

Table 2.3 Seismic Tests for Model #2

Test #	DATE	SPAN (%)	A_{max} (g)	P_t (kips)	Remarks
16	6/8/92	10.0	0.389	0.0	Filtered
17	6/8/92	30.0	1.198	0.0	
18	6/8/92	60.0	3.317	0.0	D9 data bad for this and previous tests.
19	6/8/92	90.0	5.933	0.0	

The second series of tests was performed on a “virgin” infilled frame, referred to as Model #5. Gradually increasing levels of out-of-plane shaking were applied until severe damage to the panel was apparent. No previous in-plane ground motions had been applied to this specimen. Table 2.6 describes the sequence of seismic tests for Model #5. A random vibration test was performed, before conducting the seismic-test series, to measure the dynamic properties of this model.

Table 2.4 Seismic Tests for Model #3

Test #	DATE	SPAN (%)	A_{max} (g)	P_t (kips)	Remarks
20	7/9/92	10.0	0.304	0.0	Filtered
21	7/9/92	30.0	0.906	0.0	Recording problems.
22	7/10/92	60.0	1.834	0.0	Filtered.
23	7/10/92	90.0	2.786	0.0	
24	7/10/92	10.0	0.334	0.0	Filtered (new) fc = 4 Hz.
25	7/10/92	30.0	1.098	0.0	

Table 2.5 Seismic Tests for Model #4

Test #	DATE	SPAN (%)	A_{max} (g)	P_t (kips)	Remarks
26	1/7/93	30.0	1.194	0.0	
27	1/7/93	60.0	3.142	0.0	
28	1/7/93	90.0	8.418	0.0	
29	1/7/93	10.0	0.927	0.0	
30	1/7/93	30.0	3.738	0.0	A15 = 3.80g
31	1/7/93	60.0	8.597	0.0	
32	1/8/93	60.0	—	0.0	ABORTED
33	1/8/93	45.0	2.747	0.0	A15 max = -10.72g

Table 2.6 Seismic Tests for Model #5

Test #	DATE	SPAN (%)	A_{max} (g)	P_t (kips)	Remarks
34	2/18/93	30.0	0.579	0.0	
35	2/18/93	60.0	1.558	0.0	A16 peak = -3.40g
36	2/18/93	90.0	3.472	0.0	Filtered. Change input. Accels. saturated
37	2/18/93	10.0	0.460	0.0	
38	2/18/93	45.0	3.907	0.0	
39	2/18/93	60.0	4.124	0.0	
40	2/18/93	75.0	4.884	0.0	

A third series of tests, performed on weak-frame specimens, consisted of Models #6 through #8, and followed a sequence similar to that of the first series of tests. Model #6 was a

bare-frame specimen, tested in-plane. Fairly constant axial prestress was applied to the columns during all seismic tests of this Model.

It was then infilled with masonry, and re-named Model #7. This Model was tested in-plane until its infills cracked; one of its panels (Model #8) was rotated and excited out-of-plane. However, Model #8 was not repaired after the out-of-plane excitation. Tables 2.7 through 2.9 describe the sequence of the seismic tests for these models. For each one of these models, two random vibration tests were performed to measure their dynamic properties, before and after conducting the seismic-tests series.

Table 2.7 Seismic Tests for Model #6

Test #	**DATE**	**SPAN (%)**	**A_{max} (g)**	**P_t (kips)**	**Remarks**
41	4/30/93	10.0	0.082	8.0	Filtered.
42	4/30/93	20.0	0.139	8.0	
43	4/30/93	30.0	0.203	8.0	
44	4/30/93	50.0	0.316	8.0	
45	4/30/93	70.0	0.443	8.0	
46	4/30/93	30.0	1.119	8.0	Switch to 2 Hz filtered El Centro
47	4/30/93	40.0	1.563	8.0	

Table 2.8 Seismic Tests for Model #7

Test #	**DATE**	**SPAN (%)**	**A_{max} (g)**	**P_t (kips)**	**Remarks**
48	5/18/93	20.0	0.785	0.0	
49	5/18/93	40.0	1.609	0.0	
50	5/18/93	60.0	3.044	0.0	
51	5/18/93	75.0	6.384	0.0	
52	5/18/93	85.0	7.254	0.0	Severe damage, especially in East infill.

All seismic tests were performed by subjecting each specimen to a series of earthquake records scaled from the North-South component of the El Centro 1940 ground motion. In some cases, high-pass filters with cut-off frequencies ranging from 2.0 to 4.0 Hz were used to remove the low-frequency components of the shaking-table input, permitting the application of higher

maximum shaking-table accelerations without exceeding the table's velocity or displacement limits.

Table 2.9 Seismic Tests for Model #8

Test #	DATE	SPAN (%)	A_{peak} (g)	P_t (kips)	Remarks
53	5/20/93	50.0	2.235	0.0	There was a problem with A9
54	5/20/93	75.0	7.021	0.0	
55	5/20/93	90.0	6.624	0.0	
56	5/20/93	20.0	1.917	0.0	
57	5/20/93	50.0	7.150	0.0	Retensioned the four bracing cables
58	5/20/93	70.0	7.985	0.0	

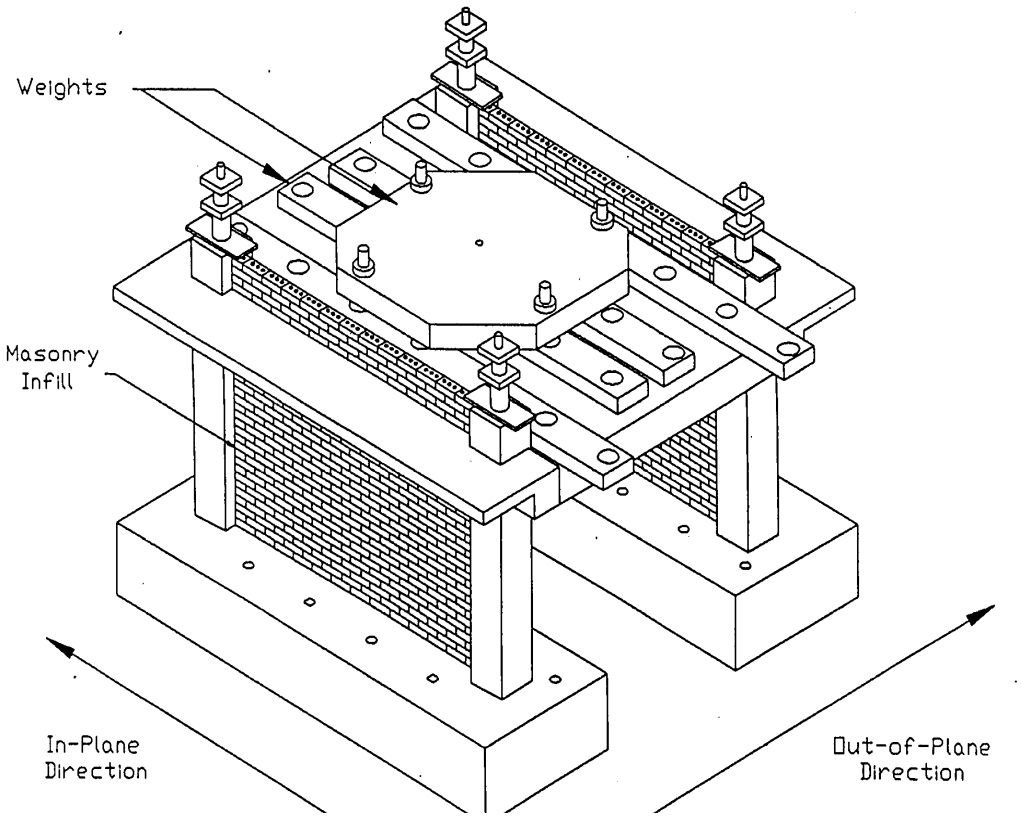

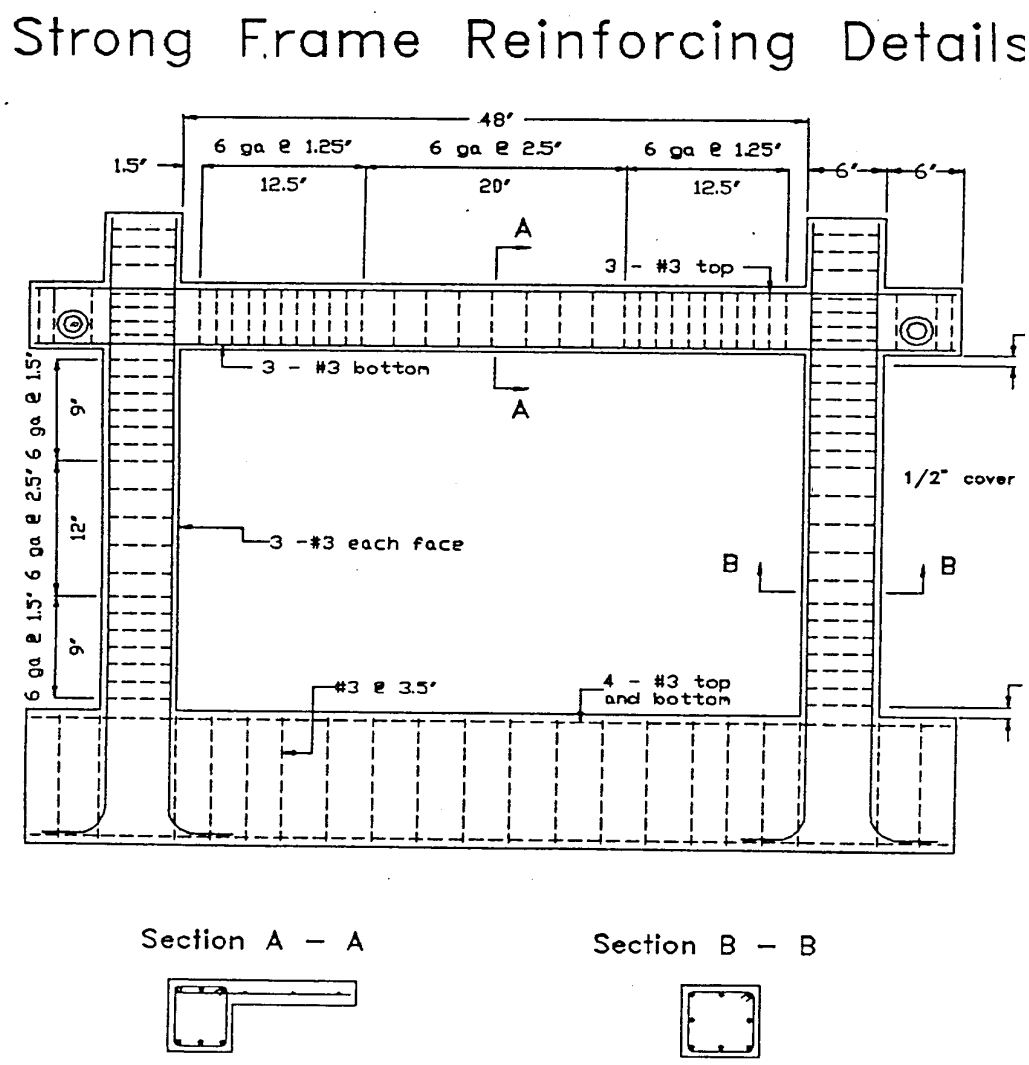

Figure 2.2 *Geometry and Reinforcement of the Strong Frame*

Weak Frame Reinforcing

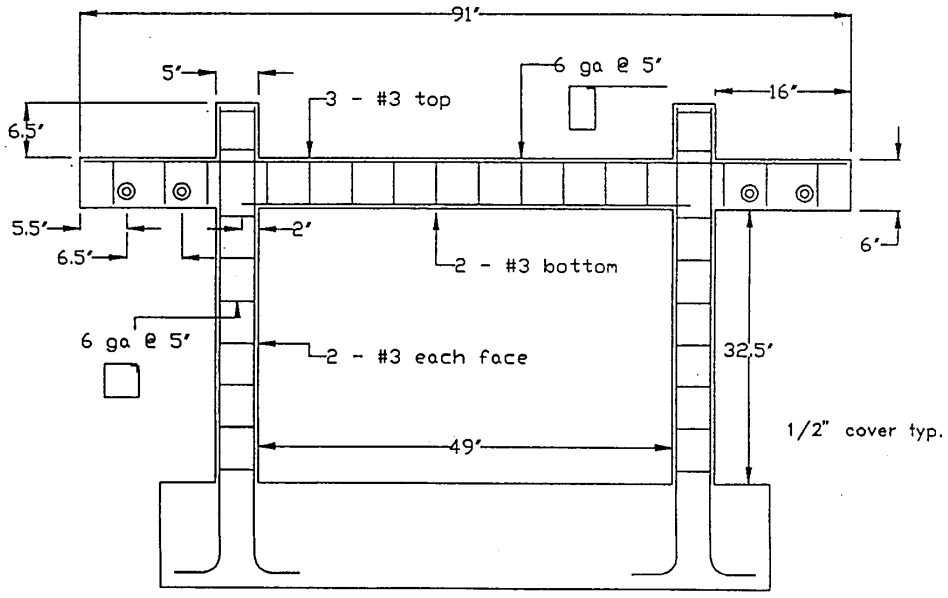

CHAPTER 3

OVERALL EXPERIMENTAL RESULTS

3.1. General Description of Experimental Results

A total of fifty-eight seismic tests were performed on 8 specimens (or "Models") following the experimental program summarized in Table 2.1 and described in detail in Section 2.4. For each model, increasing levels of ground acceleration were applied. Additionally, twenty-two random vibration tests were conducted on the specimens to determine their dynamic properties as the seismic-test series progressed. Since all test specimens were fully instrumented, accelerations, displacements and strains were recorded at multiple locations of the beams, columns, joints, and infills. All recorded displacements were absolute (that is, measured with respect to a fixed datum on the laboratory floor).

The load-displacement response for all fifty-eight seismic tests has been reported by Bashandy Rubiano, and Klingner (1995). Here, the load-displacement response of only those tests believed to represent the dynamic behavior of the specimens is presented and discussed in detail. Elastic response spectra for all seismic tests were also plotted by Bashandy, et al.(1995). Results from the most significant random tests are presented in Appendix B and discussed in this chapter. Local member response is described in Chapter 4, while a summary of all the experimental findings and their implications is provided in Chapter 5.

3.2. Data Reduction Process

All experimental data recorded during the tests were processed and converted to engineering units by the USACERL research staff. As a result, computer-readable files were produced containing the time history of absolute displacements and accelerations at several places on the specimens. A portion of one of these data files is shown in Figure A.1 of Appendix A.

Each specimen had a unique instrumentation configuration for acceleration and displacement measurement. Thus, separate computer programs, one for each specimen, were developed to generate displacement and acceleration time history graphs, as well as load-displacement diagrams at selected locations. The listing of one of those programs is shown in Appendix A. The base shear or inertial force acting on a specimen was computed as the response acceleration at the top of the frame times the effective mass of the structure. Displacements relative

to the base of the specimens were obtained by subtracting the shaking table's displacement from the absolute displacement at the desired location.

The following sections describe in detail the arrangement of the recording instruments for each specimen. Then, the characteristics of the load-displacement response during each seismic test are presented for every specimen. Finally, the results of the random vibration tests are summarized and discussed.

3.3. Synopsis of Overall Experimental Results

3.3.1. Synopsis of Overall Experimental Results for Model #1

Using this strong bare frame, 15 in-plane seismic tests were conducted. Accelerations were recorded at the following locations:

- BSTM floor (Gage A1);
- East base beam (Gage A2);
- Mid-height of the east columns (Gages A3 and A4);
- Center of the east top beam (Gage A5);
- Center of the north face of the slab (Gage A6);
- Top of the steel mass (Gage A7);

Displacements were recorded at the following locations:

- East base beam (Gage L1);
- Mid-height of the northeast column (Gage L2);
- East top beam (Gage L3);
- Center of the north face of the slab (Gage L4);

Load-displacement diagrams, plotted at the center of the north side of the slab and at the east top beam, are evaluated below for each seismic test:

- *Seismic Tests #1 and #2*: These first two seismic tests were stopped in their early stages, and no response information was available.

- *Seismic Tests #3 through #8:* Values of tip displacements and base shear are very small; all tests have very distorted load-displacement patterns. These tests were intended only to produce some damage to the specimen under very low levels of base shear.

- *Seismic Test #9*: The peak ground acceleration for this test was 0.84g. This test has relatively regular load-displacement diagrams, with higher values of both base shear and tip displacement than in the previous tests. Load-displacement diagrams for Test #9 are shown in Figures 3.1 and 3.2. A peak base shear of about 13 kips (58 kN) was reached and a maximum lateral displacement of about 0.09 inches (2.3 mm), corresponding to a 0.3% drift, was measured. An average secant stiffness (for all loops) of 150 kips/inch (26 kN/mm) was measured. From the two load-displacement diagrams, it is apparent that the frame did not yield. Finally, comparison of these two figures shows that the specimen's recorded response was reasonably consistent at the two different locations.

- *Seismic Test #10*: The peak ground acceleration for this test was 1.20g. This test has a regular load-displacement diagram, with higher values of both base shear and tip displacement than in the previous tests. Figures 3.3 and 3.4 show the load-displacement response at two locations on the specimen. A maximum base shear of 19 kips (85 kN) was reached, and a maximum displacement of about 0.17 inches (4.3 mm) corresponding to a drift over 0.5%. Both diagrams have an average secant stiffness of about 140 kips/inch (25 kN/mm). As before, no yielding of the frame is apparent, and both figures show consistent force-displacement behavior measured at different locations on the specimen.

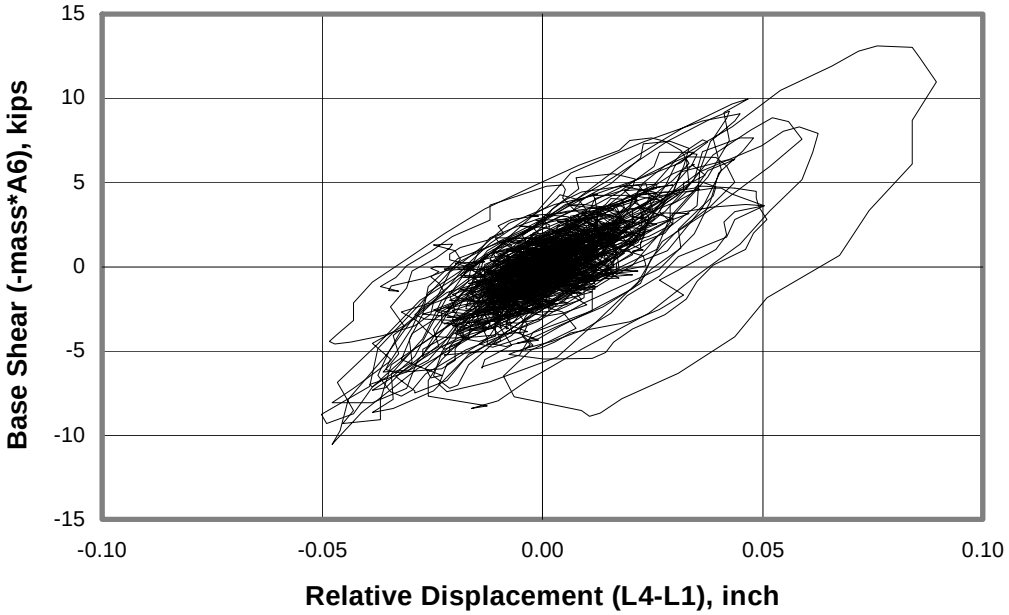

Figure 3.1 *Load-Displacement Response at Center of North Side of Slab, Model #1, Seismic Test #9*

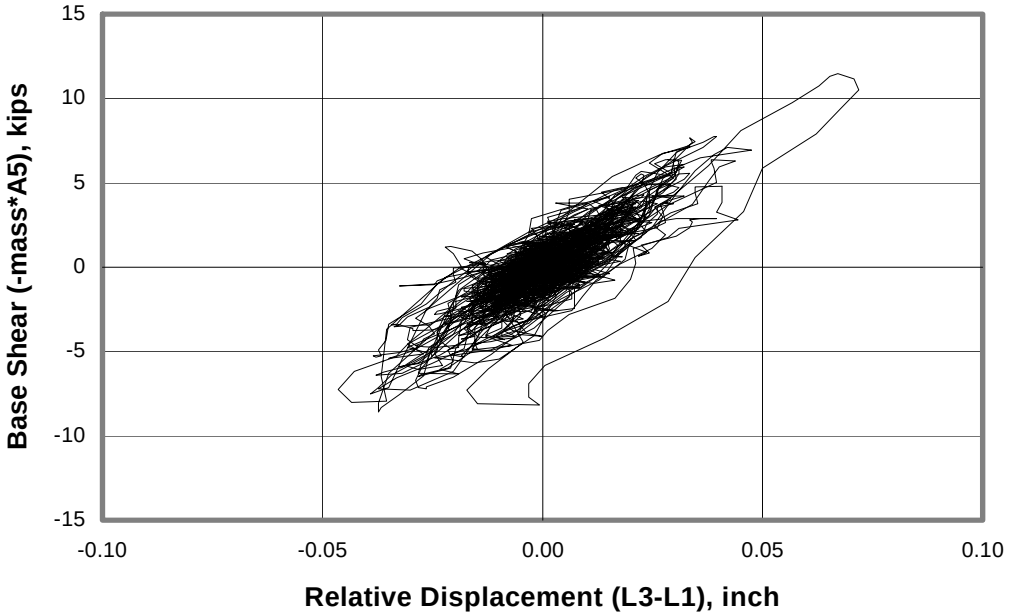

Figure 3.2 *Load-Displacement Response at Center of Top East Beam, Model #1, Seismic Test #9*

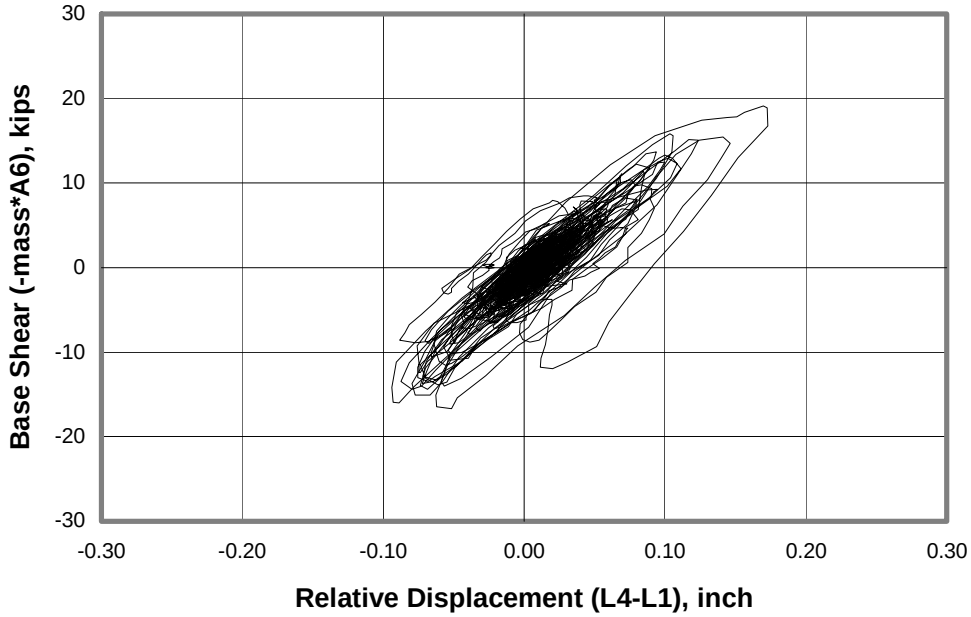

Figure 3.3 *Load-Displacement Response at Center of North Side of Slab, Model #1, Seismic Test #10*

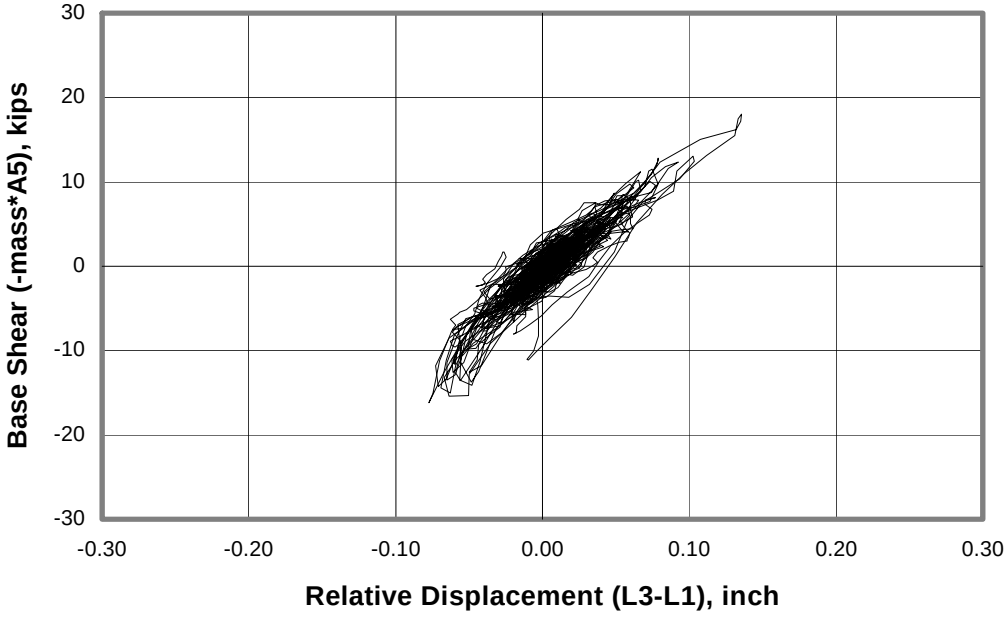

Figure 3.4 *Load-Displacement Response at Center of Top East Beam, Model #1, Seismic Test #10*

- *Seismic Test #11*: The peak ground acceleration for this test was 0.98g. Figures 3.5 and 3.6 show the load-displacement response for this test. Both of these diagrams show an approximate backbone stiffness of 120 kips/inch (21 kN/mm), a maximum load of 20 kips (89 kN) (which seems to be the yielding load of the frame), and a maximum displacement of about 0.3 inches (7.6 mm) which corresponds to a drift of 0.9%. The load-displacement diagram at the center of the north side of the slab, shown in Figure 3.5, suggests that some yielding of the frame occurred. This behavior, however, is not as obvious in Figure 3.6. The consistency of the displacements and accelerations, measured at different locations on the specimen, is relatively apparent in from these diagrams.

- *Seismic Tests #12 through #15:* Load-displacement diagrams show an irregular pattern. Values of base shear and tip displacement are inconsistent with those of the previous three tests: the tip displacements have similar values, but the base shear values are much lower.

A total of ten random tests was performed on this model. Figure B.1 of Appendix B shows the results of three of such tests.

Random Test #3 was conducted in between Seismic Tests #4 and #5. The measured fundamental frequency is about 12 Hz from which a stiffness of nearly 150 kips/inch (26 kN/mm) has been estimated. This stiffness can be regarded as the initial (uncracked) stiffness since previously conducted Seismic Tests #2 to #4 introduced very low levels of base shear to this model.

Random Test #6 was performed in between Seismic Tests #10 and #11, and the measured fundamental frequency in this case is about 11 Hz. This frequency implies a stiffness of about 120 kips/inch (21 kN/mm) which can be regarded as the cracked stiffness of the specimen since the applied base shear levels during Seismic Tests #9 and #10 were rather high.

Finally, Random Test #8, conducted after Seismic Test #13, shows a fundamental frequency of about 9 Hz, implying a stiffness of 80 kips/inch (14 kN/mm). This is the final stiffness of the strong bare frame, since the seismic tests performed after this random test had very low base shear levels.

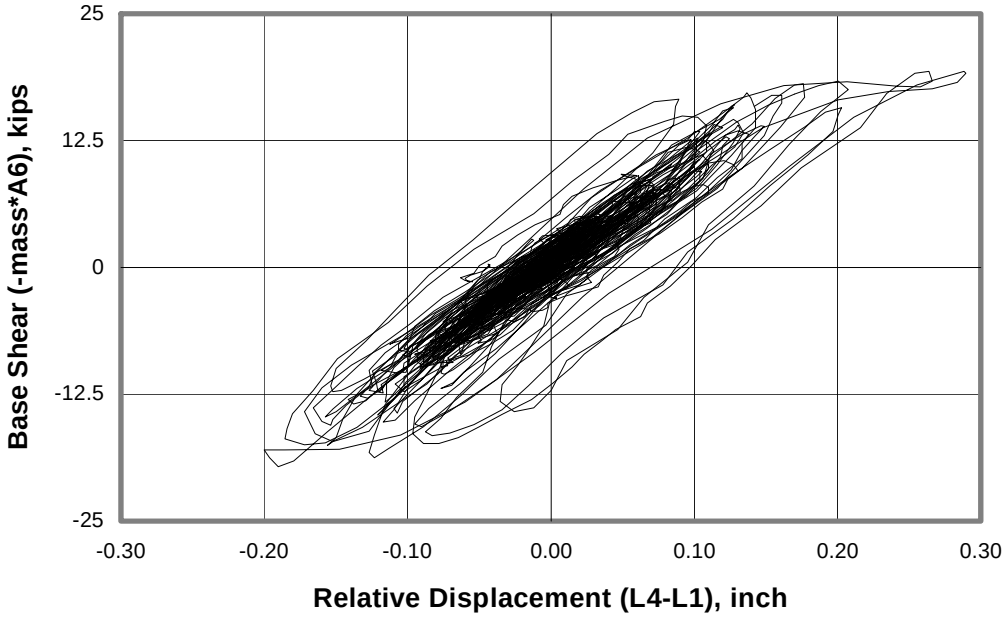

Figure 3.5 *Load-Displacement Response Center of North Side of Slab, Model #1, Seismic Test #11*

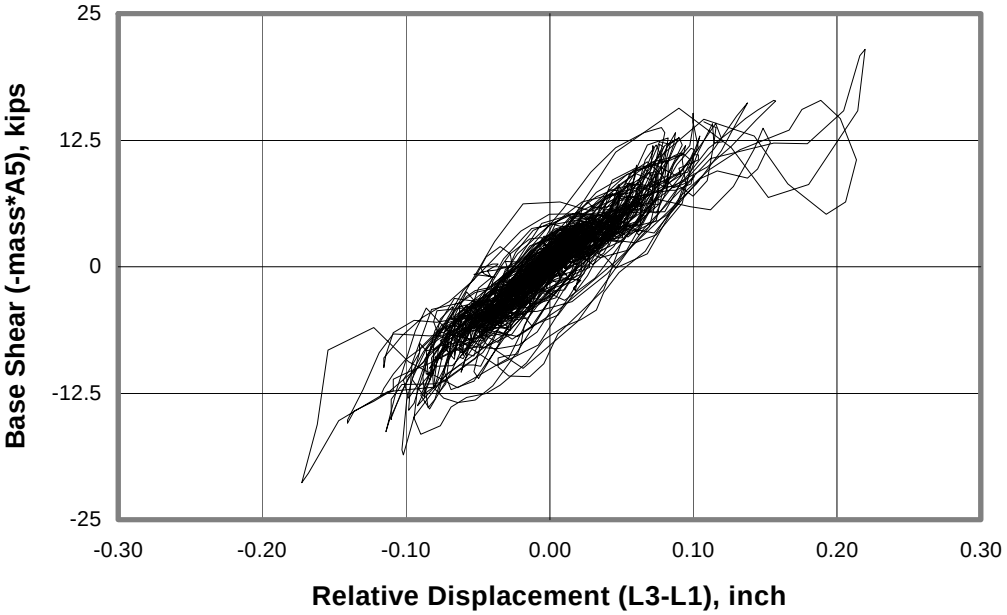

Figure 3.6 *Load-Displacement Response at Center of Top East Beam, Model #1, Seismic Test #11*

3.3.2. Synopsis of Overall Experimental Results for Model #2

This specimen was constructed by infilling the strong bare frames of Model #1. Four in-plane seismic tests were conducted. Accelerations were recorded at the following locations:

- BSTM floor (Gage A1);
- East base beam (Gage A2);
- Mid-height of the east columns (Gages A3 and A4);
- Center of the east top beam (Gage A5);
- Center of the north face of the slab (Gage A6);
- Top of the steel mass (Gage A7);
- Center of the east infill (Gage A8).

Displacements were recorded at the following locations:

- East base beam (Gage L1);
- Mid-height of the northeast column (Gage L2);
- East top beam (Gage L3);
- Center of the north face of the slab (Gage L4).

Load-displacement diagrams, plotted at the center of the north side of the slab and at the east top beam, are evaluated below for each seismic test:

- *Seismic Tests #16 and #17:* Load-displacement diagrams plotted based on gages at the center of the slab are completely different from those plotted using gages located at the east top beam. This could be due to severe cracking of one panel only, causing significant torsional response of the frame. However, this does not seem to be a reasonable explanation, because large cracks are not expected during these initial tests, when the base shear is so low (4 to 12 kips, or 18 to 53 kN). In later tests, for the same model, diagrams plotted using records at both locations looked relatively similar to

each other. In both tests, the backbone stiffness is less than 10% that for the bare frame.

- *Seismic Test #18:* The peak ground acceleration for this test was 3.32g. Values of tip displacements for both diagrams are very high (0.2 inches or 5 mm), corresponding to a drift of 0.6%, and are accompanied by low values of base shear. The load level reached 40 kips (89 kN), while higher than for the bare frame, is less than that reached by the weak infilled frame (Model #7, discussed in Section 3.3.7). Based on the load-displacement diagrams, an average backbone stiffness varying from 100 kips/inch to 250 kips/inch (17.5 kN/mm to 43.8 kN/mm) was measured.

- *Seismic Test #19:* The peak ground acceleration for this test was 5.93g. For this test, load-displacement diagrams at the center of the slab differ from those for the east top beam. Values of tip displacements are also very high (over 0.7 inches, or 18 mm), corresponding to a drift of 2.2%, accompanied again by low values for base shear (about 60 kips or 267 kN). Based on the load-displacement diagrams, an average backbone stiffness varying from 50 kips/inch to 120 kips/inch (8.8 kN/mm to 21.0 kN/mm) was measured.

Random Tests #11 and #12 were conducted on this specimen immediately before and after the seismic tests series, respectively. Their results are shown in Figure E.2 of Appendix B. The initial fundamental frequency, obtained from the results of Random Tests #11, is about 24 Hz, from which the initial stiffness is estimated as 590 kips/inch (103 kN/mm). The final fundamental frequency, obtained from Random Test #12, is about 11 Hz. Thus, the final stiffness is estimated as 120 kips/inch (21 kN/mm).

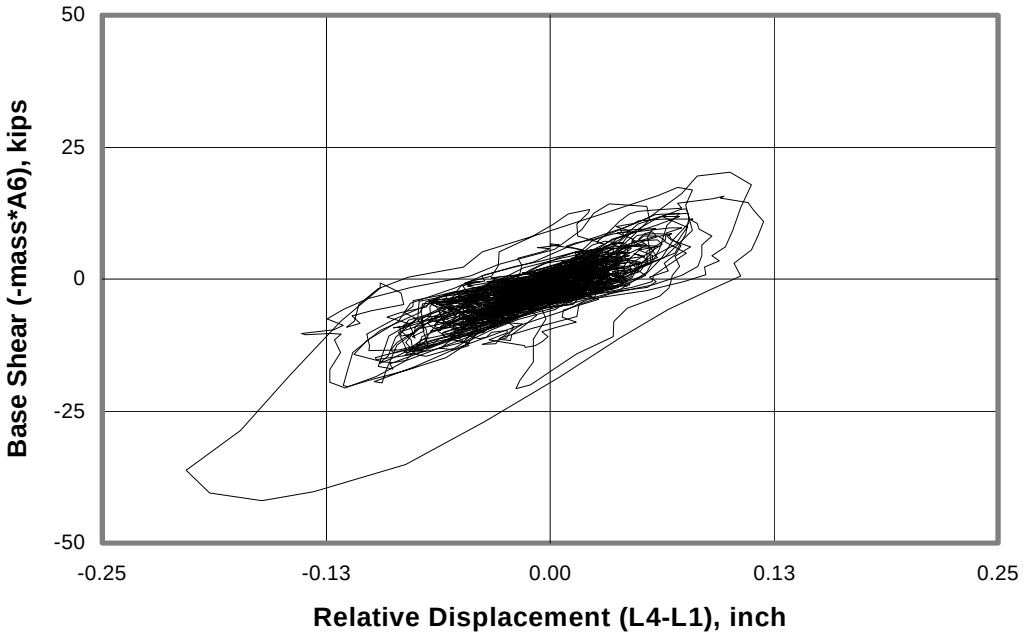

Figure 3.7 *Load-Displacement Response at Center of North Side of Slab, Model #2, Seismic Test #18*

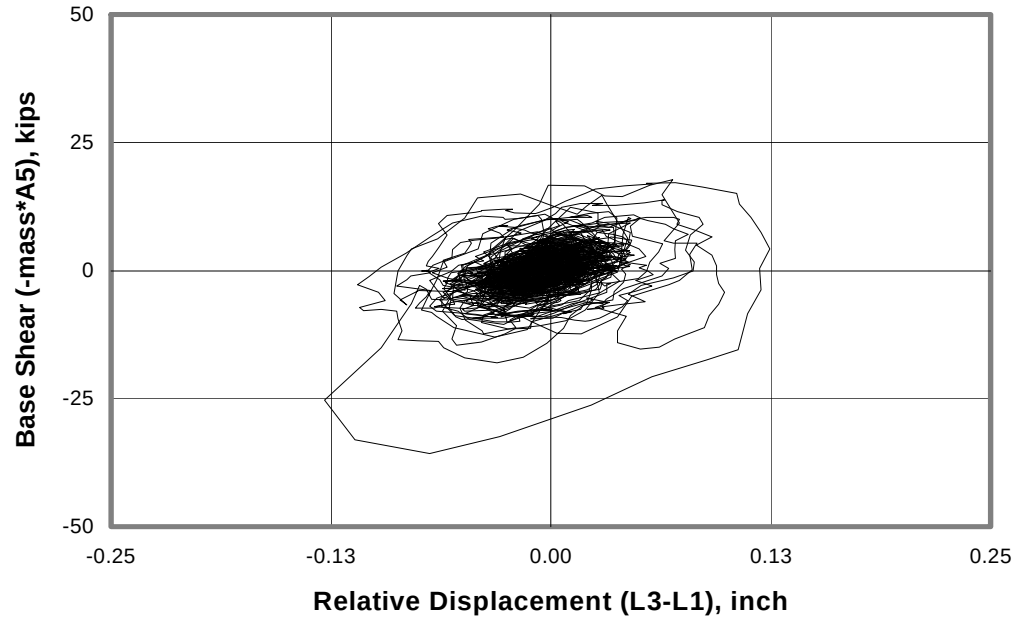

Figure 3.8 *Load-Displacement Response at Center of Top East Beam, Model #2, Seismic Test #18*

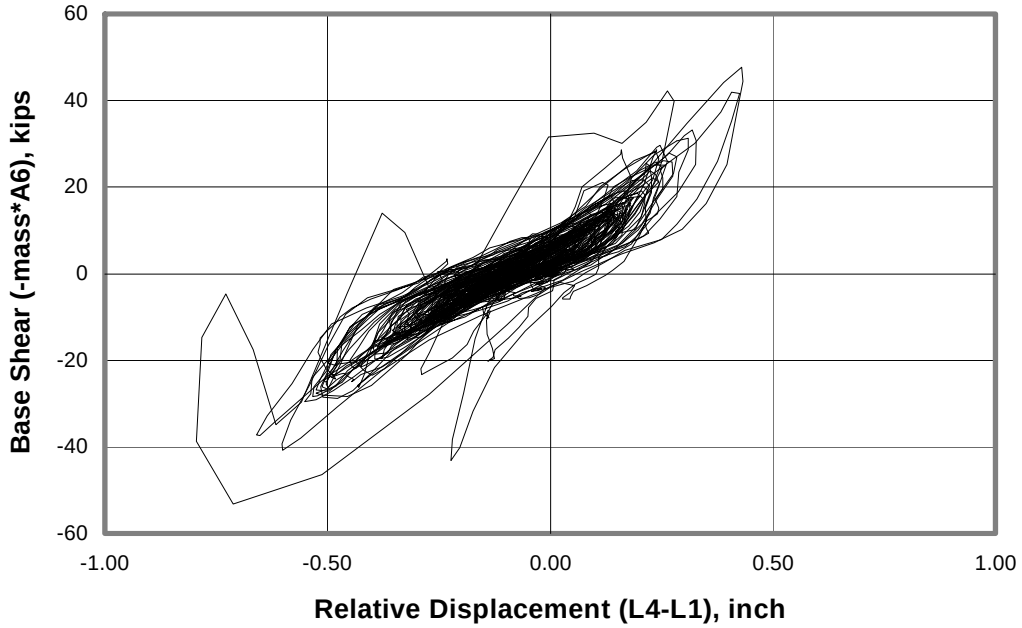

Figure 3.9 *Load-Displacement Response at Center of North Side of Slab, Model #2, Seismic Test #19*

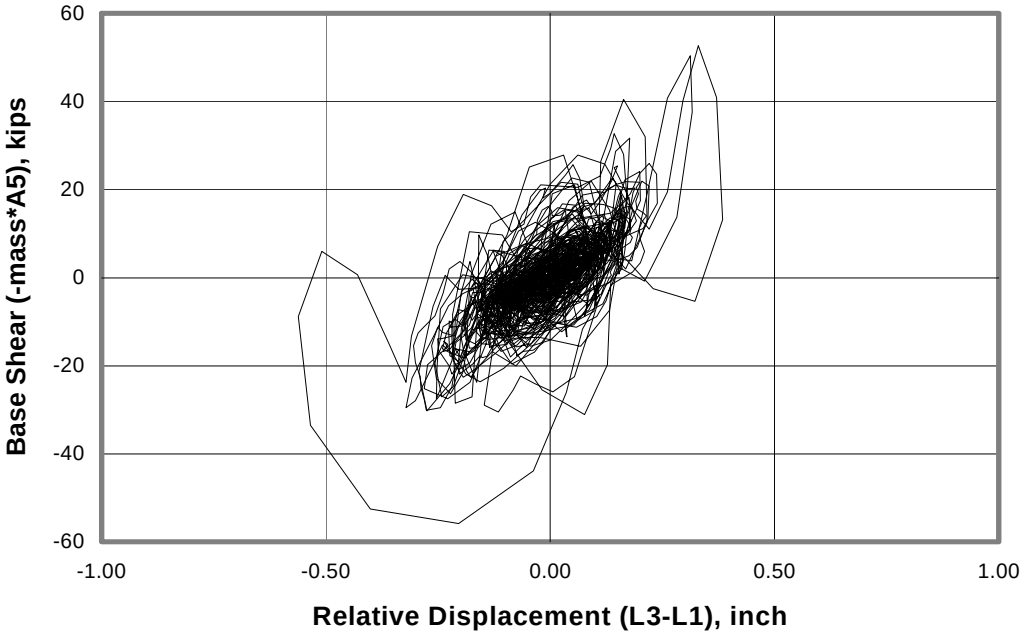

Figure 3.10 *Load-Displacement Response at Center of Top East Beam, Model #2, Seismic Test #19*

3.3.3. Synopsis of Overall Experimental Results for Model #3

This specimen consisted of the unrepaired north infilled frame of Model #2. The frame was rotated 90 degrees, and 6 out-of-plane seismic tests were conducted. Accelerations were recorded at the following locations:

- Base beam (Gage A13);
- At twelve points on the north infill (Gage A1 to A12);
- Mid-height of the northwest column (Gage A14);
- Top of the northwest column (Gage A15);
- Center of the top beam of north frame (Gage A16).

Displacements were recorded at the following locations:

- Base beam (Gage L1);
- Mid-height of the northwest column (Gage L2);
- West end of the top beam of the north frame (Gage L3);
- Center of the top beam of the north frame (Gage L4).

Figure 3.11 shows the locations of accelerometers and strain gages on the infill.

Since horizontal out-of-plane displacements of the infill were not measured, it is not possible to generate an out-of-plane load-displacement diagram for the infilled frame. Therefore, load-displacement diagrams were plotted only for the frame (at the center of the north beam and at the right beam-column joint), for each seismic test. However, these diagrams (not shown here) do not represent the real out-of-plane behavior of the infill because the tips of the frame columns were tied to the lab floor by cables as explained above.

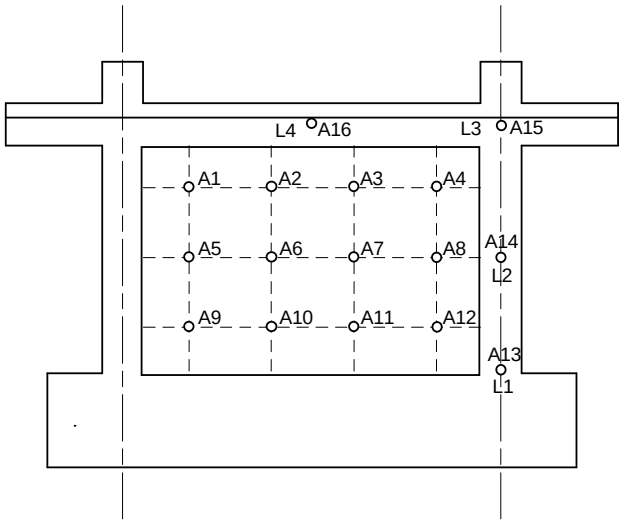

Figure 3.11 Accelerometer and Strain Gage Locations for Model #3

In spite of the lack of information on the infill deflections, their out-of-plane loads may be evaluated using the 12 accelerometers installed on their surface. Moreover, the relative lateral loads on different regions of the infill may be obtained, since the accelerometers were spaced uniformly on the infill surface.

Table 3.1 summarizes the maximum accelerations recorded for each accelerometer for all tests of this model. The recorded acceleration maxima are consistent over most of the infill surface, with a slight tendency to be higher at the top of the infill. The recorded acceleration peaks for the lower right corner invariably differ from the rest. This suggests a systematic problem with the accelerometer located in that region.

A maximum average acceleration of 6.0g was recorded on the infill for Seismic Tests #23 and #25. For these tests, maximum recorded base accelerations were 2.79g and 1.10g, respectively. Since the infill has a weight of about 0.20 kips (0.9 kN), the resulting out-of-plane load is estimated as 1.2 kips (5.3 kN). This force is a lower bound to the out-of-plane strength of the infill, since no collapse occurred during the test. A single random-vibration test was performed on this model before the seismic-test series was conducted. Results for Random Test #13 are shown in Figure B.2 of Appendix B. A fundamental frequency of 15 Hz was recorded, from which the initial uncracked stiffness of 4.5 kips/inch (0.8 kN/mm) was estimated.

Table 3.1 Peak Out-of-Plane Response Accelerations (g) for Model #3

Test	A_{base}	- - - - - TOP - - - - -				- - - - - MIDDLE - - - - -				- - - - - BOTTOM - - - - -			
#	A13	A1	A2	A3	A4	A5	A6	A7	A8	A9	A10	A11	A12
20	0.30	-0.42	-0.43	-0.43	-0.41	-0.42	-0.43	-0.43	-0.40	-0.39	0.41	-0.16	0.27
21	0.91	-0.77	0.75	0.76	0.76	-0.76	0.76	0.76	-0.78	-0.72	0.76	-0.18	0.89
22	1.83	-3.95	-4.11	-4.17	-4.12	-3.79	-3.93	-3.96	-3.84	-3.45	-3.58	-1.68	1.80
23	2.79	-5.44	-5.02	-5.01	-5.51	-6.06	-5.48	-5.61	-5.89	-5.98	-6.20	-1.60	2.70
24	-0.33	-1.87	-2.00	-1.97	-1.79	-1.67	-1.88	-1.82	-1.52	-1.23	-1.31	1.07	-0.27
25	-1.10	-5.86	-6.20	-6.23	-5.78	-4.87	-6.07	-5.90	-4.85	-4.13	-4.12	3.34	-0.84

3.3.4. Synopsis of Overall Experimental Results for Model #4

Using this strong repaired infilled frame, eight out-of-plane seismic tests were conducted. Accelerations were recorded at the following locations:

- Center of the base beam (Gage A15);
- At nine points on the infill (Gages A1 to A9 and A13);
- At mid-height of the columns (Gages A10 and A12);
- Center of the top beam of north frame (Gage A11).
- Right end of the top beam (joint) of north frame (Gages A11 and A14).

Displacements were recorded at the following locations:

- Base beam (Gage L7);
- At six points on the infill (Gages L1 to L5 and L9);
- Center of the top beam (Gage L6);
- Right beam-column joint of the north frame (Gage L8).

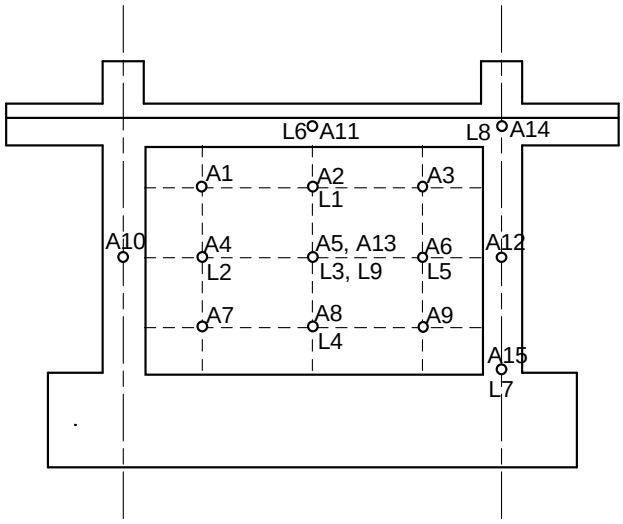

Figure 3.12 Accelerometer and Strain Gage Locations for Model #4

Figure 3.12 shows the locations of accelerometers and strain gages on the plane of the infill.

Load-displacement diagrams (not shown here) were plotted at the center of the top beam and at the right beam-column joint for each seismic test. Again, these do not represent the actual out-of-plane behavior of the specimen, due to the support given by the cables attached to the top of the frame.

As for Model #3, out-of-plane loads may be calculated using acceleration records. As before, a consistent pattern of accelerations was recorded, with a clear tendency toward higher accelerations at the top of the specimen. Table 3.2 summarizes the maximum accelerations recorded by each accelerometer for all tests of this model.

For Seismic Test #31, a maximum average acceleration of 10.0g was recorded on the infill, with a peak acceleration of 11.1g at the center of the infill. The maximum recorded base acceleration for this test was 8.60g.

The average out-of-plane lateral load is therefore estimated as 2.0 kips (8.9 kN), while the peak load at the center of the infill is 2.2 kips (9.8 kN). These forces, again, are only lower bounds to the out-of-plane strength of the infill, since no collapse occurred during the test.

Table 3.2 Peak Out-of-Plane Response Accelerations (g) for Model #4

Test	A_{base}	----- TOP -----			---- MIDDLE ----			--- BOTTOM ---		
#	A15	A1	A2	A3	A4	A5	A6	A7	A8	A9
26	-1.19	-1.32	-1.28	-1.43	-1.29	-1.32	-1.33	-0.46	-1.21	-1.24
27	-3.14	-3.78	-3.75	-3.89	-3.54	-3.64	-3.59	-3.17	-3.27	-3.28
28	-8.42	-8.82	-7.13	-8.77	-8.22	-7.88	-7.75	-5.44	-6.87	-7.19
29	-0.93	-1.30	-1.52	-1.75	-1.17	-1.36	-1.42	-0.99	-1.13	-1.13
30	-3.74	-5.62	-6.25	-6.42	-4.56	-5.03	-4.83	-3.67	-4.04	-4.07
31	-8.60	10.16	10.18	-9.39	9.46	11.10	9.60	-7.96	8.86	-8.60
33	-2.75	-5.01	-7.19	-5.44	-4.61	-5.45	-4.73	-4.68	-4.88	-4.53

In contrast to Model #3, for Model #4 out-of-plane displacements were measured at various locations on the infill. Hence, load-displacement diagrams were plotted at the center of the infill, for each of the Seismic Tests. In the following discussion, only Seismic Tests with base accelerations over 3.50g will be considered since load-displacement characteristics of tests with lower accelerations (seismic tests #26, #27, #29 and #33) are generally not useful for evaluating the overall response of the specimen. Seismic Test #32 was aborted.

- *Seismic Test #28:* The peak ground acceleration for this test was 8.42g. Figure 3.13 shows the load-displacement response of Model #4 for this test. Figure 3.13a was plotted using the out-of-plane displacement of the center of the infill relative to the base of the specimen while Figure 3.13b used the out-of-plane displacement relative to the average displacement of the surrounding frame ("L_{avg}"). Comparison of these two figures reveals a great difference between the two relative displacements.

- *Seismic Test #30:* The peak ground acceleration for this test was 3.74g. Figure 3.14 shows the load-displacement response of Model #4 for this test. As before, Figure 3.14a was plotted using the out-of-plane displacement of the center of the infill relative to the base of the specimen, and Figure 3.14b used the out-of-plane displacement relative to the average displacement of the surrounding frame. In this case, the two figures are almost identical, indicating that the frame motion is equal to the base input motion. However, load-displacement patterns imply unrealistic large displacements and low or zero stiffness.

- *Seismic Test #31:* The peak ground acceleration for this test was 8.60g. Figure 3.15 shows the load-displacement response of Model #4 for this test. Figure 3.15a was plotted using the out-of-plane displacement of the center of the infill relative to the base of the specimen, and Figure 3.15b used the out-of-plane displacement relative to the average displacement of the surrounding frame. As before, the two figures are almost identical, indicating that the frame motion is equal to the base input motion. Displacements are again very large.

Random Test #14 was conducted on this specimen before initiating the series of seismic tests. Results for this test are shown in Figure B.3 of Appendix B, from which a fundamental frequency of about 21 Hz is determined. Using this frequency, the initial stiffness of this model is estimated as 9.0 kips/inch (1.6 kN/mm). This stiffness is about two times the estimated initial stiffness for the unrepaired specimen (Model #3).

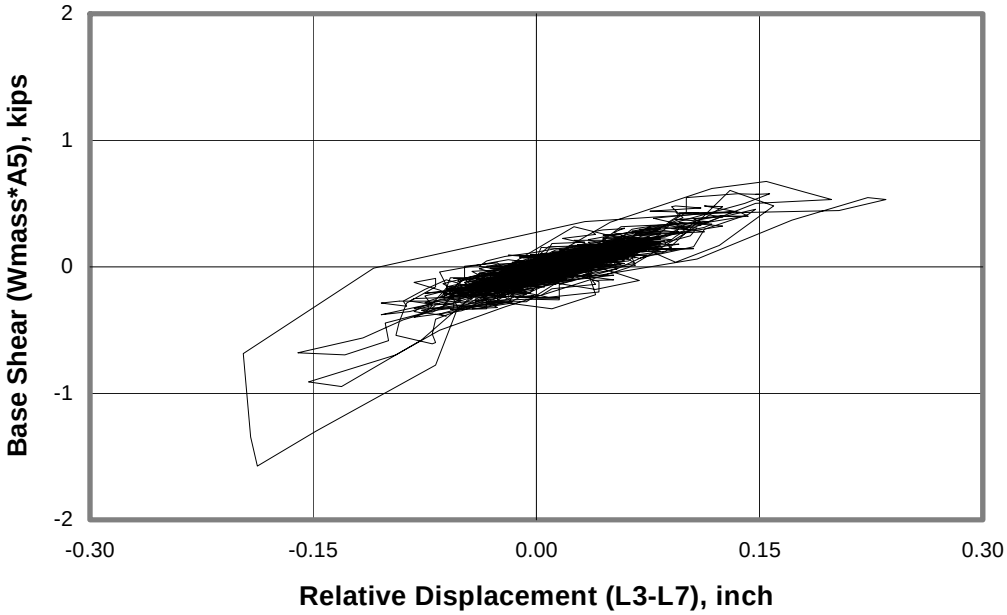

a) Relative to the base

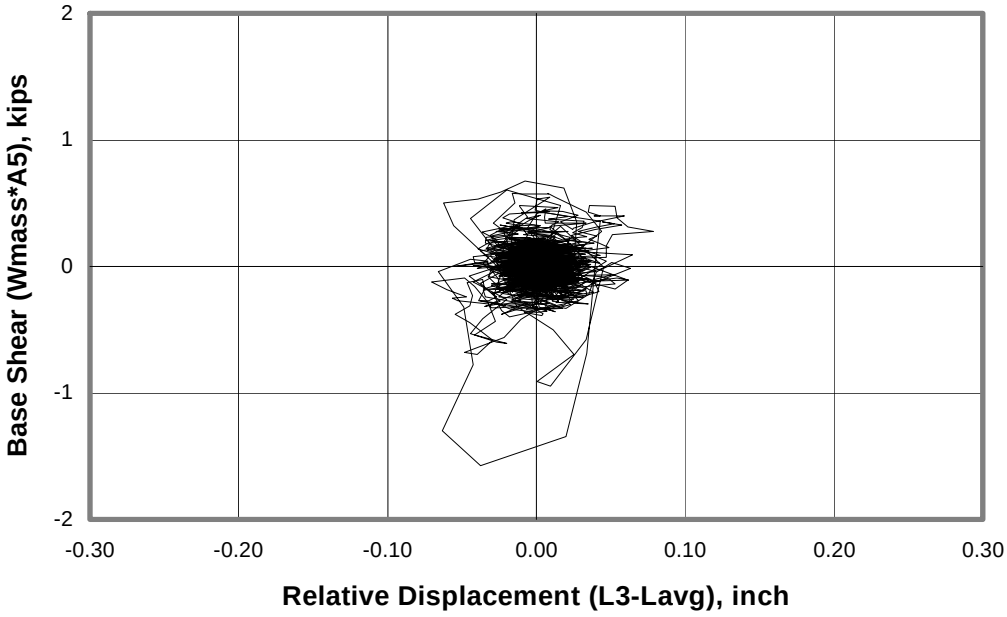

b) Relative to frame

Figure 3.13 Load-Displacement Response at Center of Infill, Model #4, Seismic Test #28

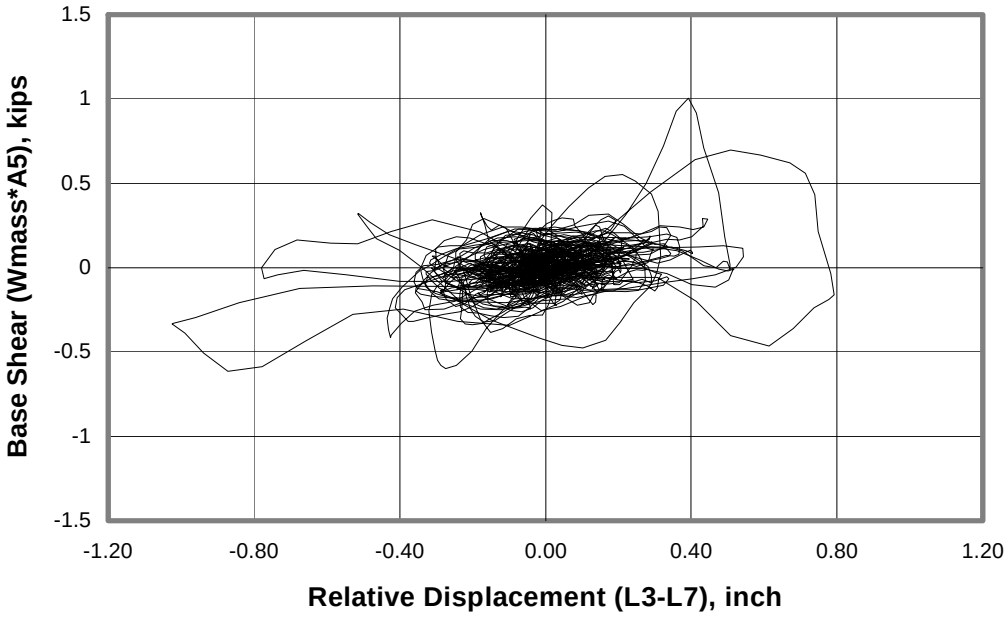

a) Relative to the base

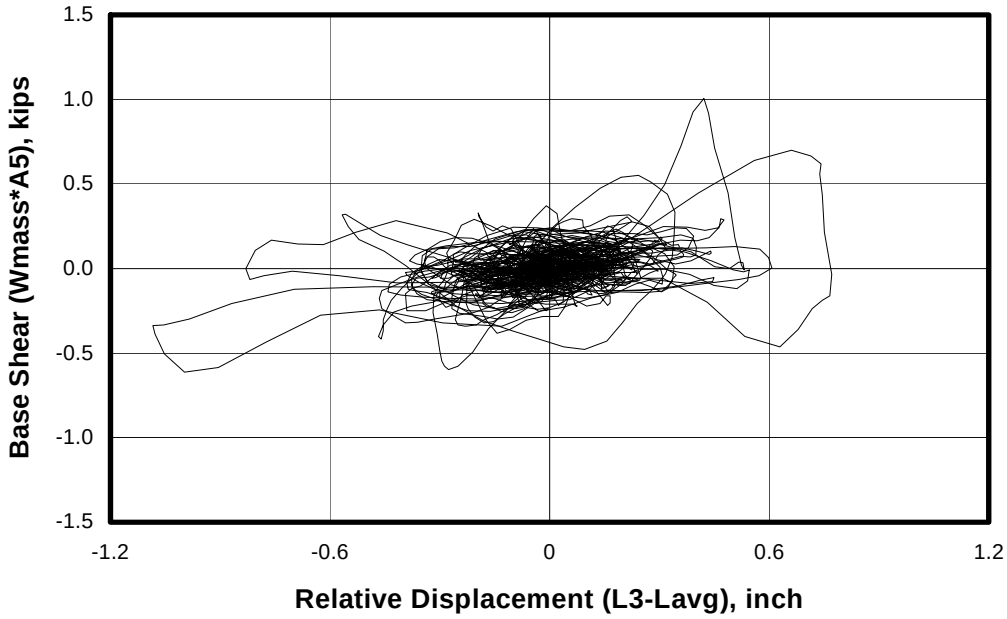

b) Relative to the frame

Figure 3.14 Load-Displacement Response at Center of Infill, Model #4, Seismic Test #30

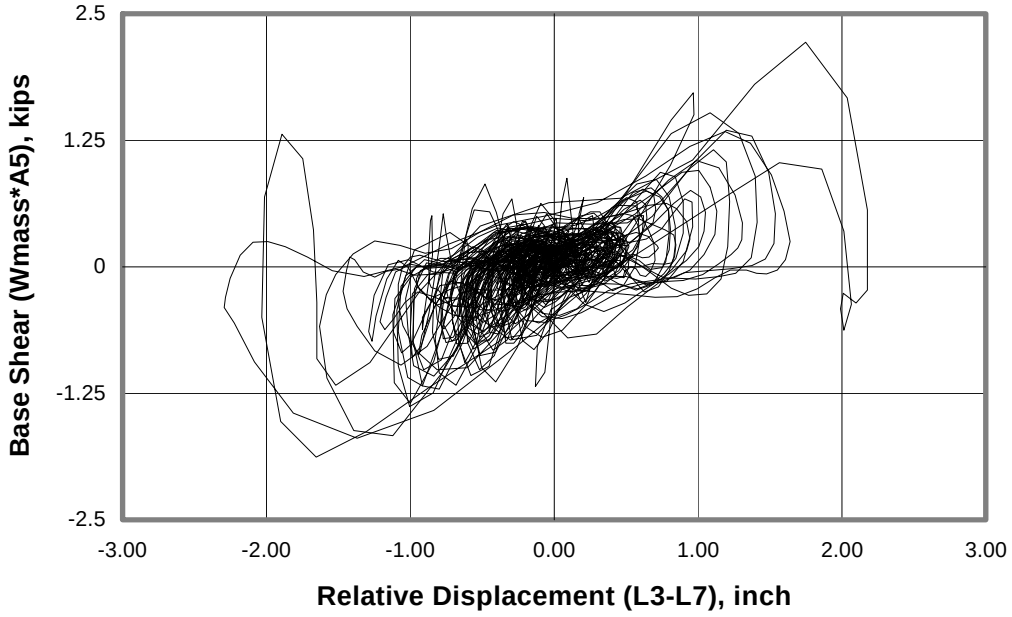

a) Relative to the base

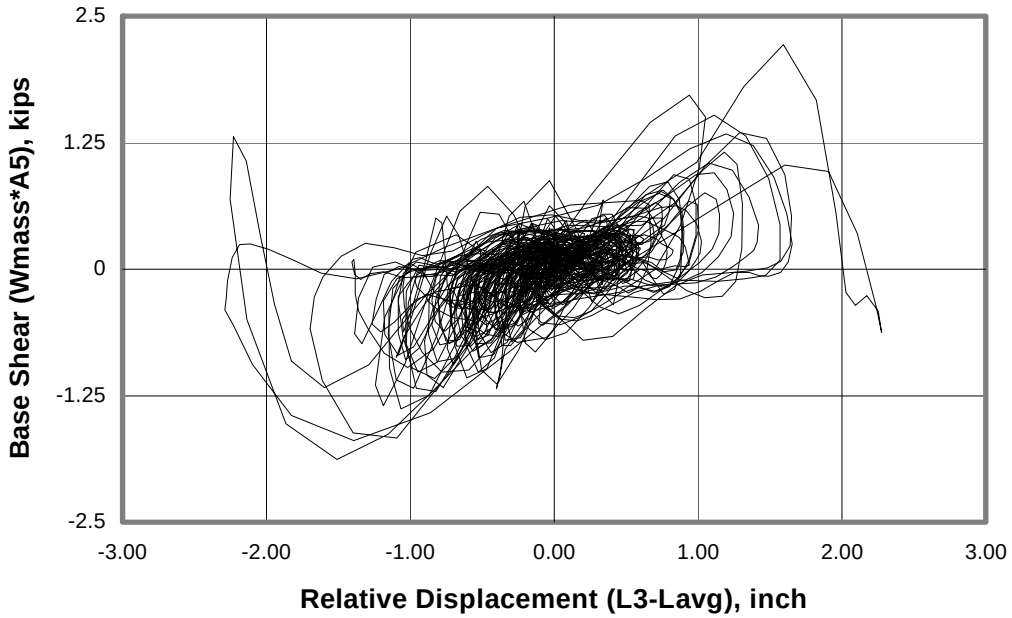

b) Relative to the frame

Figure 3.15 Load-Displacement Response at Center of Infill, Model #4, Seismic Test #31

3.3.5. Synopsis of Overall Experimental Results for Model #5

Using this virgin strong infilled frame, 7 seismic out-of-plane tests were conducted. Accelerations were recorded at the following locations:

- Base beam (Gage A16);
- At nine points on the infill (Gages A1 to A9 and A15);
- Mid-height of the columns (Gages A10 and A11);
- Center and ends (joints) of the top beam (Gages A12 through A14).

Displacements were recorded at the following locations:

- Base beam (Gages L3 and L6).);
- Beam-column joints (Gages L4 and L5)
- Center of the infill (L1 and L2

Figure 3.16 shows the locations of accelerometers and strain gages on the infill. Table 3.2 summarizes the maximum accelerations recorded for each accelerometer for all tests of this model. Out-of-plane response accelerations recorded on the infill were larger at the top than at the bottom.

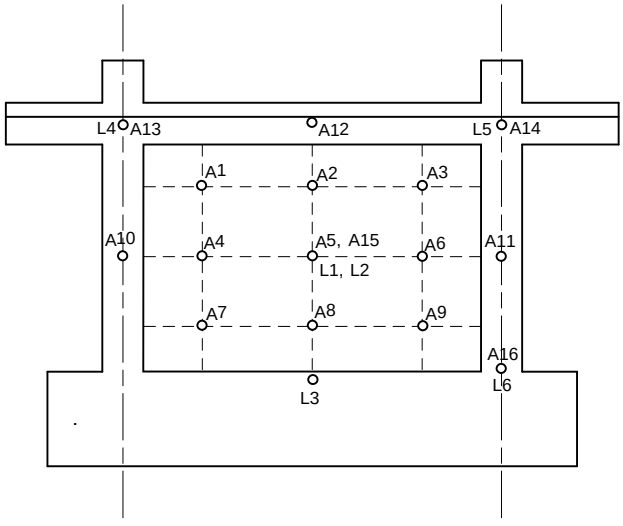

Figure 3.16 Accelerometer and Strain Gage Locations for Model #5

A maximum average acceleration of 5.0g was recorded on the infill during Seismic Tests #39 and #40, for which the maximum recorded base accelerations were 4.12g and 4.88g respectively. A lower bound to the average out-of-plane strength is therefore estimated as 1.0 kip (4.4 kN).

Table 3.3 Peak Out-of-Plane Response Accelerations (g) for Model #5

Test	A_{base}	--- TOP ---			--- MIDDLE ---			--- BOTTOM ---		
#	A16	A1	A2	A3	A4	A5	A6	A7	A8	A9
34	-0.58	-0.68	-0.67	-0.70	-0.63	-0.64	-0.62	-0.58	-0.59	-0.59
35	-1.56	-1.75	-1.83	-1.96	-1.68	-1.74	-1.74	-1.54	-1.60	-1.63
36	-3.47	-4.42	-4.52	-4.52	-3.57	-3.76	-3.65	-3.23	-3.36	-3.47
37	-0.46	-0.59	-0.60	-0.60	-0.55	-0.55	-0.53	-0.48	-0.50	-0.48
38	-3.91	-4.44	-4.55	-4.52	-3.81	-3.97	-4.09	-3.75	-3.79	-3.84
39	-4.12	-5.02	5.05	-4.94	4.68	4.79	4.63	4.16	4.14	4.22
40	4.88	5.18	4.35	-4.71	4.44	4.55	4.44	4.02	4.16	-4.23

Load-displacement diagrams were plotted at the center of the infill for each seismic test. In general, they show unrealistic patterns and inconsistent displacement levels. In the following discussions, only Seismic Tests #39 and #40 will be considered.

- *Seismic Test #39:* The peak ground acceleration for this test was 4.12g. Figure 3.17 shows the load-displacement response of Model #5 for this test. Figure 3.17a was plotted using the out-of-plane displacement at the center of the infill, measured with the "main" gage L2, relative to average displacement of the surrounding frame (L_{avg}). Figure 3.13b, on the other hand, was plotted using the "backup" gage L1. Both figures show a similarly unrealistic pattern.

- *Seismic Test #40:* The peak ground acceleration for this test was 4.88g. Figure 3.18 shows the load-displacement response of Model #5 for this test. As before, Figure 3.18a was plotted using the out-of-plane displacement at the center of the infill, measured with the "main" gage L2, relative to average displacement of the surrounding frame (L_{avg}), and Figure 3.13b was plotted using the "backup" gage L1. In this case,

the load-displacement pattern is consistent for both diagrams. However, some cycles exhibit very large displacements on only one side of the infill.

As for Models #3 and #4, a single random vibration test (Random Test #15) was performed before the series of seismic tests was initiated. Its results are presented in Figure B.4 of Appendix B from which a fundamental frequency of 24.5 Hz is obtained. Therefore, the initial stiffness for this specimen is estimated as 12 kips/inch (2.1 kN/mm). Notice that the initial stiffness for this "virgin" specimen is around three times larger than the initial stiffness of the previously in-plane damaged specimen (Model #3) and over 30% larger than that of the repaired specimen (Model #4).

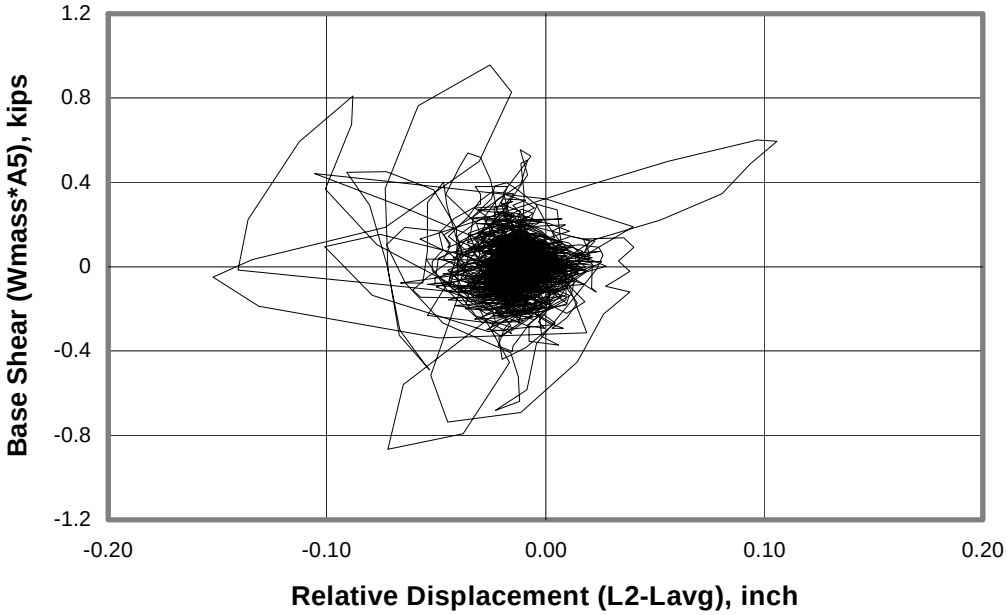

a) Using Main Displacement Gage

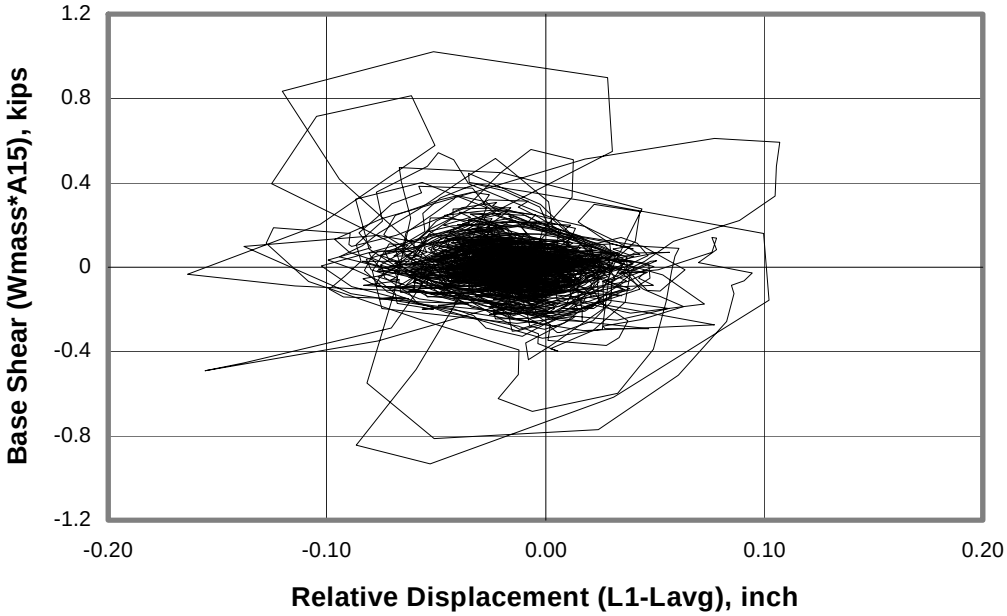

b) Using Backup Displacement Gage

Figure 3.17 Load-Displacement Response at Center of Infill (Backup), Model #5, Seismic Test #39

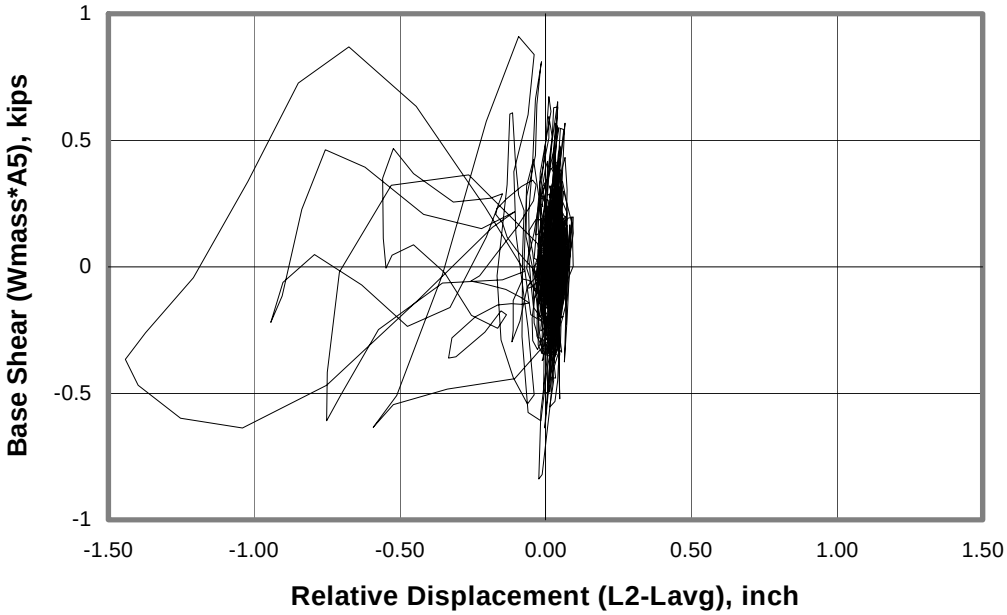

a) Using Main Displacement Gage

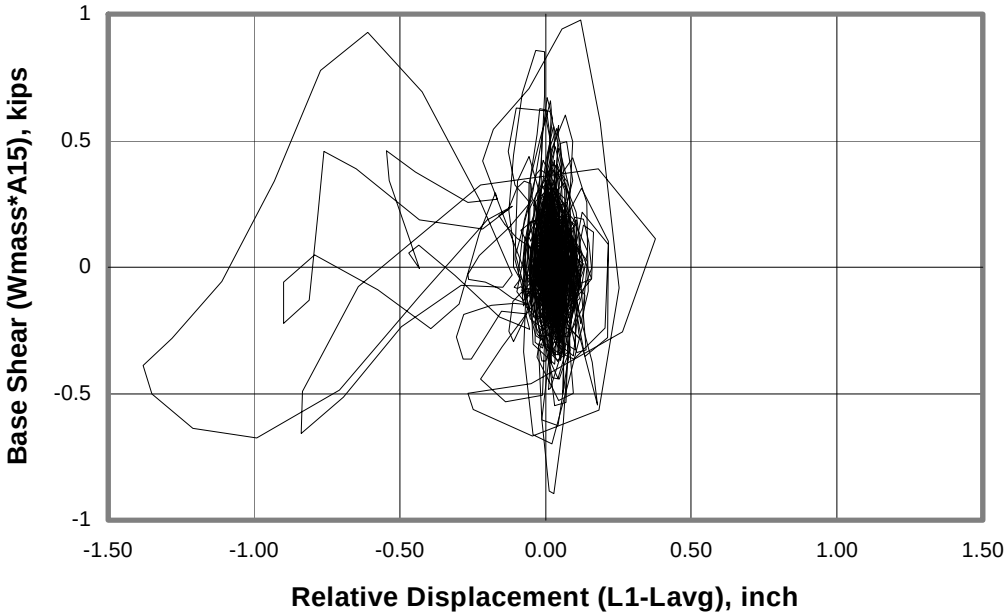

b) Using Backup Displacement Gage

Figure 3.18 Load-Displacement Response at Center of Infill (Backup), Model #5, Seismic Test #40

3.3.6. Synopsis of Overall Experimental Results for Model #6

Using this weak bare frame, 7 seismic in-plane tests were conducted. Accelerations were recorded at the following locations:

- Center of the east infill (Gage A1);
- East base beam (Gage A2);
- Mid-height of the north columns (Gages A3 and A4);
- Center of the east top beam (Gage A5);
- Center of the north face of the slab (Gage A6);
- Top of the steel mass (Gage A7).

Displacements were recorded at the following locations:

- East base beam (Gage D1);
- Mid-height of the northeast column (Gage D2);
- East and west top beams (Gages D3 and D5);
- Center of the north face of the slab (Gage D4);
- North face of the top steel mass (Gage D6).

Load-displacement diagrams, plotted at the center of the north side of the slab and at the top mass, are evaluated below for each seismic test:

- *Seismic Tests #41 to #44:* Tip displacements are very small (0.06 inches, 1.5 mm), accompanied by small base shears in an irregular pattern.

- *Seismic Test #45:* The peak ground acceleration for this test was 0.44g. Load-displacement diagrams for this test are shown in Figures 3.19 and 3.20. Base shears are low, and a linear elastic response of the frame is apparent.

- *Seismic Test #46:* The peak ground acceleration for this test was 1.12g. Load-displacement diagrams for this test, shown in Figures 3.21 and 3.22, exhibit an expected pattern, with a relatively low but consistent average stiffness of 47 kips/inch (8.2 kN/mm). The peak load was about 16 kips (71 kN), with a maximum displacement of 0.37 inches (9.4 mm) which corresponds to a drift of 1.1%. A linear elastic response of the frame is clear.

- *Seismic Test #47:* The peak ground acceleration for this test was 1.56g. Load-displacement diagrams, shown in Figures 3.23 and 3.24, display an initial stiffness consistent with that obtained in Seismic Test #46, followed by a degraded stiffness. The peak load for Test #47 was about 22 kips (98 kN), and the maximum displacement was 0.7 inches (18 mm) corresponding to 2.2% drift. As before, the response is generally linear elastic. In this case, however, some yielding of the frame is apparent near the peak load.

Random Tests #17 and #18 were conducted on this model immediately before and after the seismic-test series, respectively. Their results are shown in Figure B.5 of Appendix B. The initial fundamental frequency, obtained from Random Test #17, is about 12 Hz, while the final fundamental frequency, obtained from Random Test #18, is about 7 Hz. Using these measured frequencies, initial and final stiffness levels of 120 kips/inch (21 kN/mm) and 40 kips/inch (7 kN/mm), respectively, are estimated.

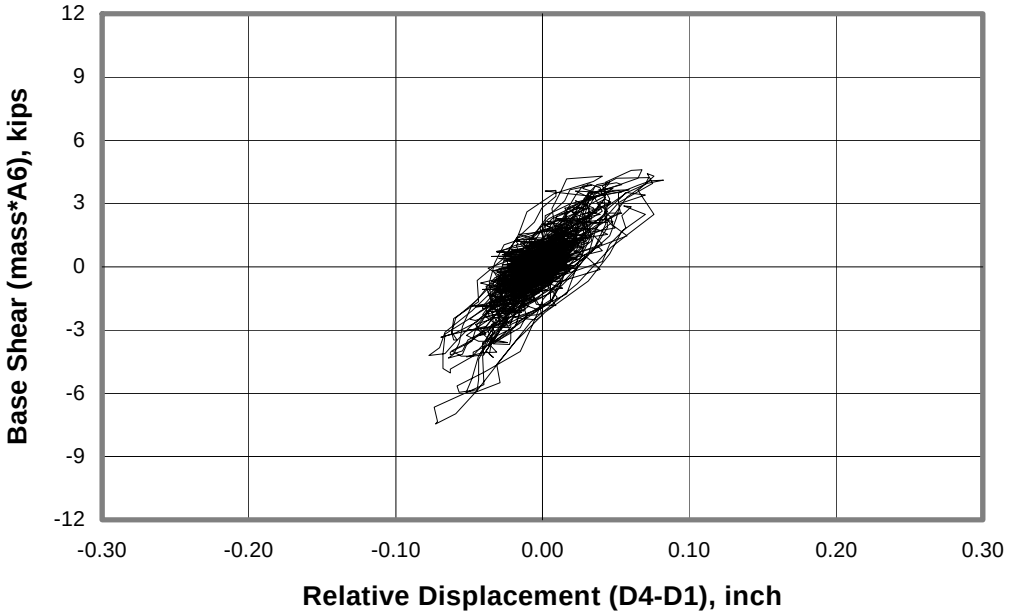

Figure 3.19 *Load-Displacement Response at Center of North side of Slab, Model #6, Seismic Test #45*

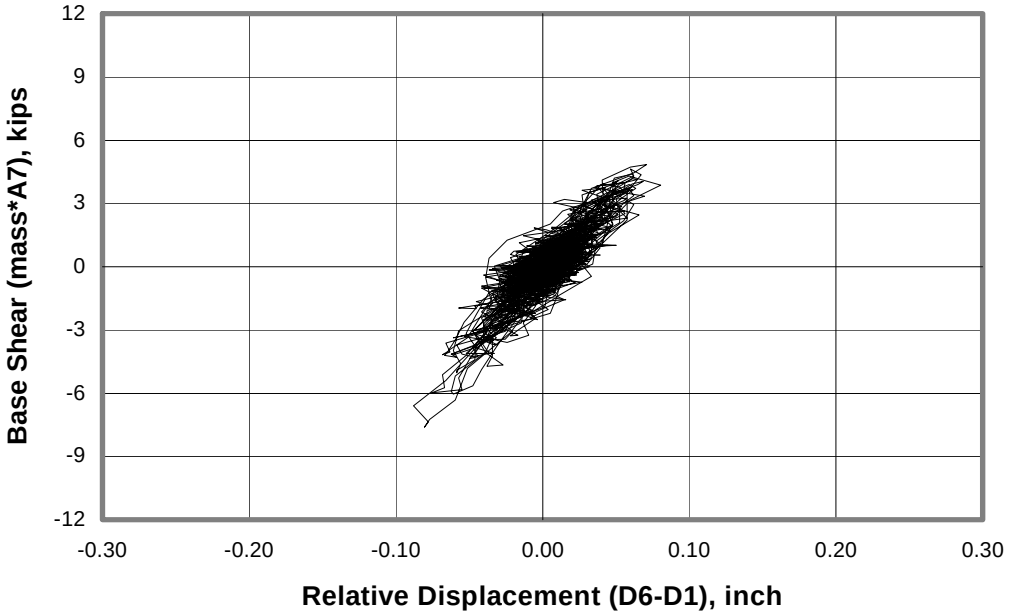

Figure 3.20 *Load-Displacement Response at Top Mass, Model #6, Seismic Test #45*

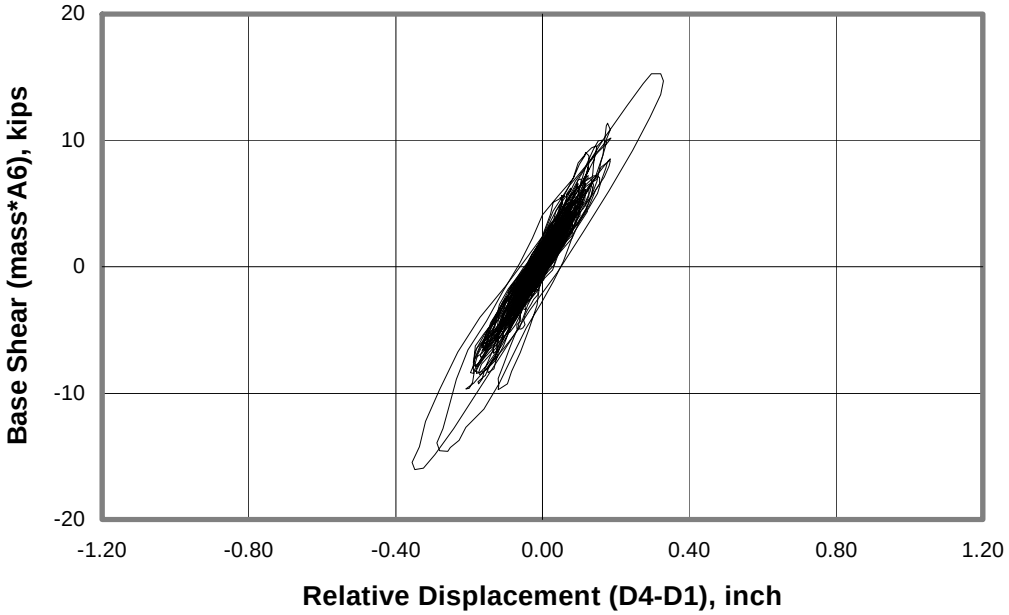

Figure 3.21 *Load-Displacement Response at Center of North Side of Slab, Model #6, Seismic Test #46*

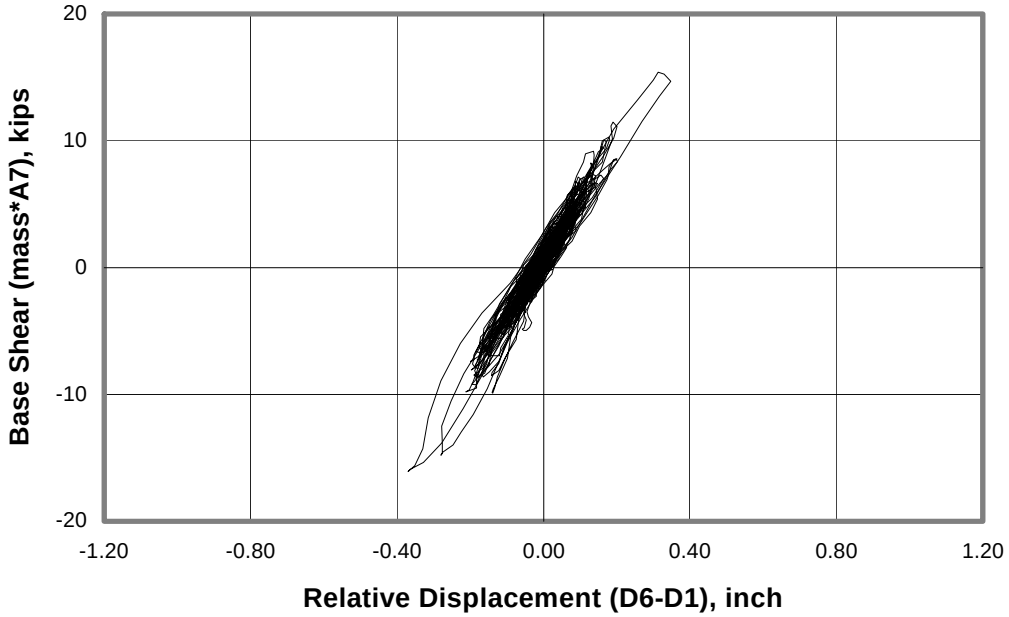

Figure 3.22 *Load-Displacement Response at the Top Mass, Model #6, Seismic Test #46*

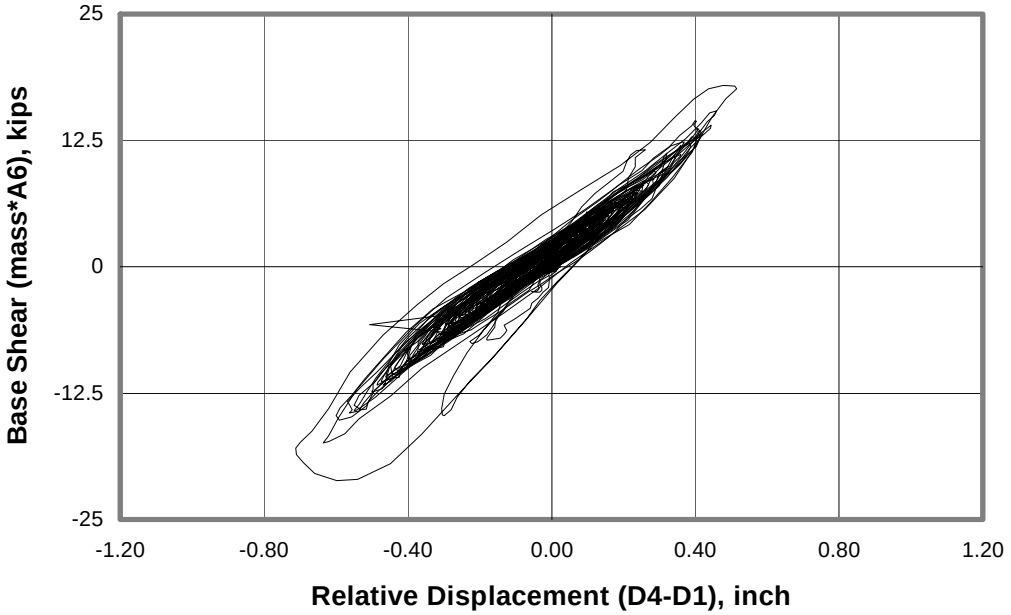

Figure 3.23 *Load-Displacement Response at Center of North side of Slab, Model #6, Seismic Test #47*

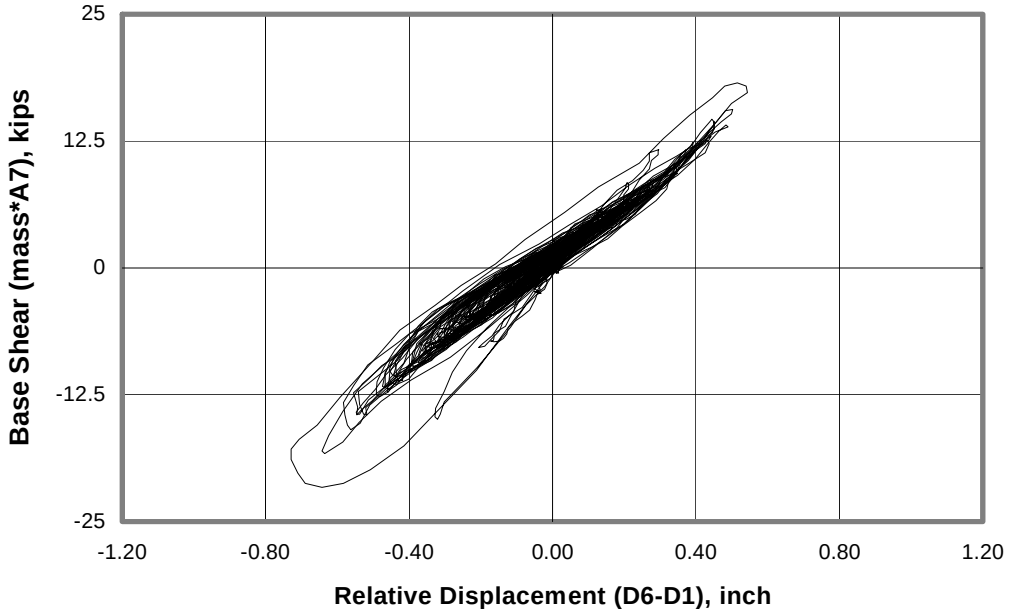

Figure 3.24 *Load-Displacement Response at Top Mass, Model #6, Seismic Test #47*

3.3.7. Synopsis of Overall Experimental Results for Model #7

Using this weak infilled frame, 5 seismic in-plane tests were conducted. Accelerations were recorded at the following locations:

- Center of the east infill (Gage A1);
- East base beam (Gage A2);
- Mid-height of the north columns (Gages A3 and A4);
- Center of the east top beam (Gage A5);
- Center of the north face of the slab (Gage A6);
- Top of the steel mass (Gage A7).

Displacements were recorded at the following locations:

- East base beam (Gage D1);
- Mid-height of the northeast column (Gage D2);
- East and west top beams (Gages D3 and D5);
- Center of the north face of the slab (Gage D4);
- North face of the top steel mass (D6).

Load-displacement diagrams, plotted at the top mass and at the north side of the slab, are evaluated below.

- *Seismic Tests #48 and 49:* Most cycles show low levels of base shear (under 10 kips, or 45 kN), with erratic behavior. Test #49 shows a single large hysteretic loop with a maximum base shear of about 20 kips (89 kN). However, its shape is not consistent with expected behavior.

- *Seismic test #50:* The peak ground acceleration for this test was 3.04g. Although the load-displacement diagram for the top mass is generally similar to that of the two previous tests, it has a large loop with a base shear of about 30 kips (133 kN) with an average stiffness under 300 kips/inch (53 kN/mm) and a maximum displacement of 0.12 inches (3.0 mm). This pattern is not evident in the diagram for the north side of the slab.

- *Seismic test #51:* The peak ground acceleration for this test was 6.38g. Load-displacement diagrams are shown in Figures 3.25 and 3.26. In this case, very similar patterns were obtained for both diagrams (top mass and north side of the slab). A single large loop with a maximum stiffness of about 200 kips/inch (35 kN/mm) and a peak base shear of about 50 kips (222 kN) is accompanied by small cycles with base shears under 25 kips (111 kN) and very low stiffness (under 100 kips/inch, or 18 kN/mm). Maximum displacements reach 0.4 inches (10 mm) corresponding to 1.2% drift. The frame apparently yielded at the peak load during this test.

- *Seismic test #52:* The peak ground acceleration for this test was 7.25g. Load-displacement diagrams, shown in Figures 3.27 and 3.28, display base shears generally under 30 kips (133 kN) and displacements under 0.6 inch (15 mm). However, a single large loop shows a maximum base shear over 50 kips (222 kN) and a displacement of about 0.90 inches (23 mm) corresponding to 2.8% drift. Average stiffness is 50 kips/inch (8.8 kN/mm) near the zero-load region. For large displacements, the stiffness increases to over 100 kips/inch (18 kN/mm). Some of the small cycles suggest an initial stiffness of 200 kips/inch (35 kN/mm) or more, consistent with previous tests. As for Seismic Test #51, yielding of the frame is apparent at peak load.

As for the previous model, random vibration tests were conducted on this specimen immediately before and after the series of seismic tests. Figure B.6 of Appendix B presents the results of Random Tests #19 and #20, from which fundamental frequencies of 38 and 21 Hz, respectively, were obtained. Using these frequencies, the initial stiffness of 1180 kips/inch (207 kN/mm) and the final stiffness of 360 kips/inch (63 kN/mm) were estimated.

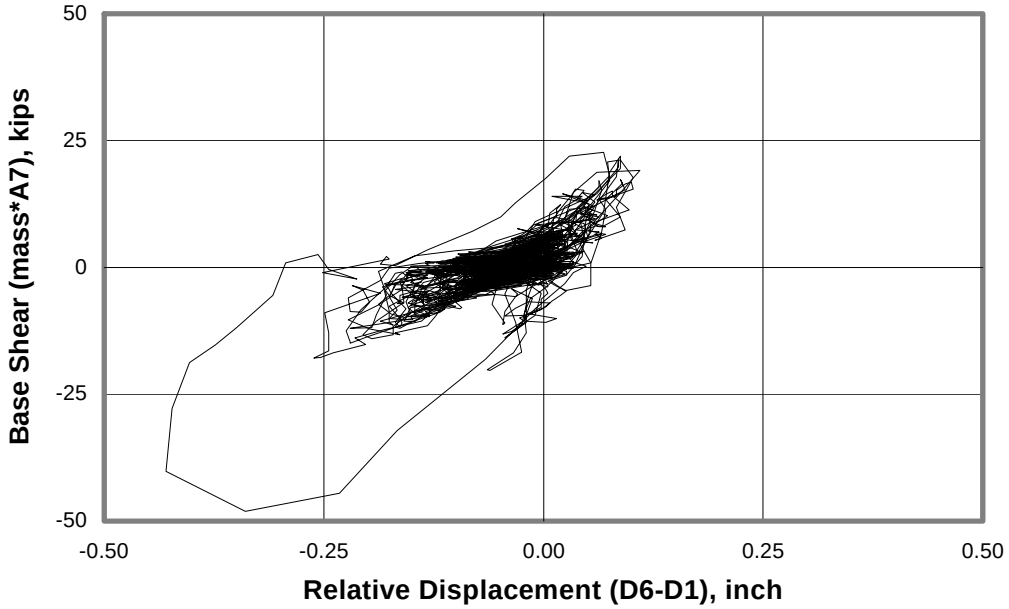

Figure 3.25 Load-Displacement Response at Top Mass, Model #7, Seismic Test #51

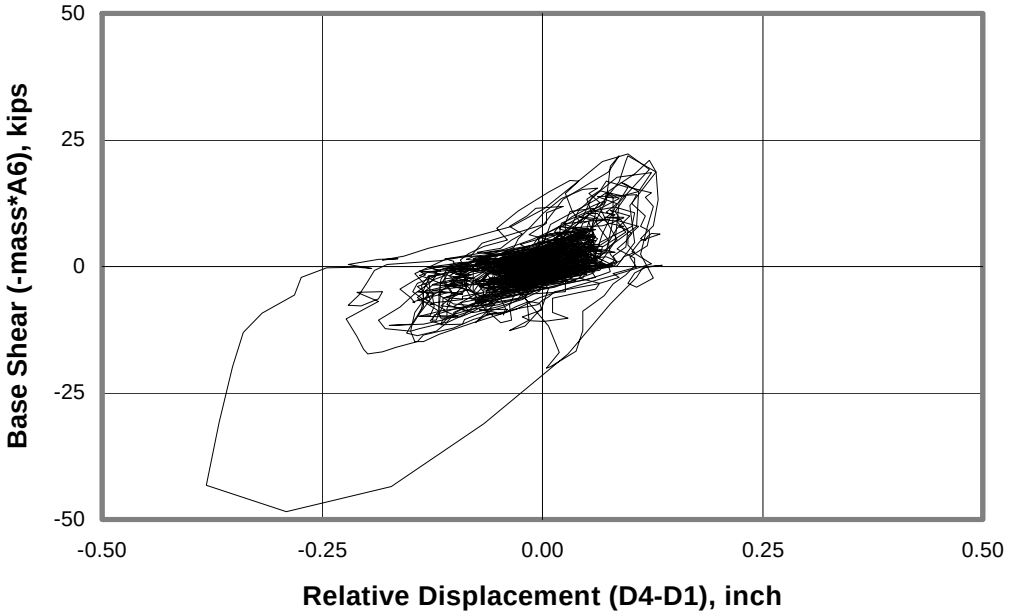

Figure 3.26 Load-Displacement Response at Center of North side of Slab, Model #7, Seismic Test #51

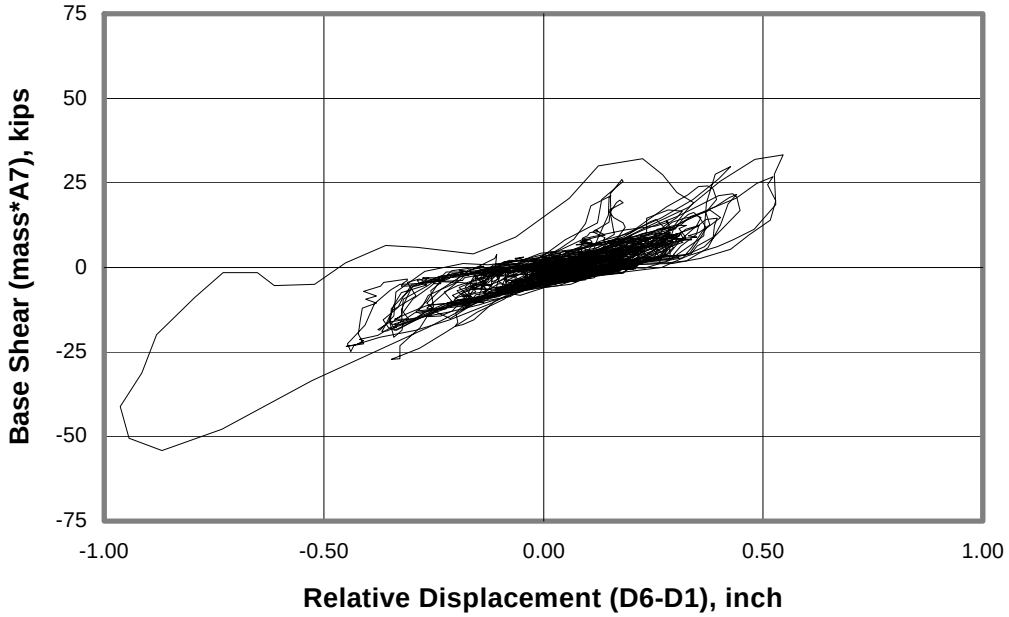

Figure 3.27 *Load-Displacement Response at Top Mass, Model #7, Seismic Test #52*

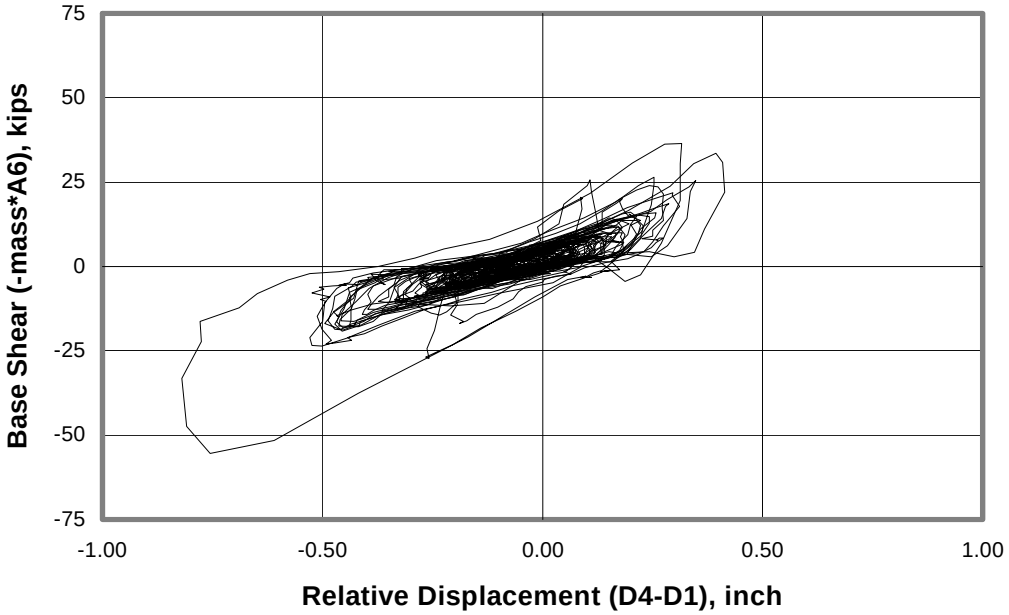

Figure 3.28 *Load-Displacement Response at Center of North Side of Slab, Model #7, Seismic Test #52*

3.3.8. Synopsis of Overall Experimental Results for Model #8

Using this unrepaired weak infilled frame, 6 seismic out-of-plane tests were conducted. Accelerations were recorded at the following locations:

- Center of the base beam (Gage A16);
- At 9 points on the infill (Gages A1 to A9 and A15);
- Mid-height of the columns (Gages A10 and A11);
- Center and ends (joints) of the top beam (Gages A12 to A14).

Displacements were recorded at the following locations:

- Base beam (Gages D2 and D5);
- Beam-column joints (Gages D3 and D4);
- Center of the infill (Gages D1 and D6)

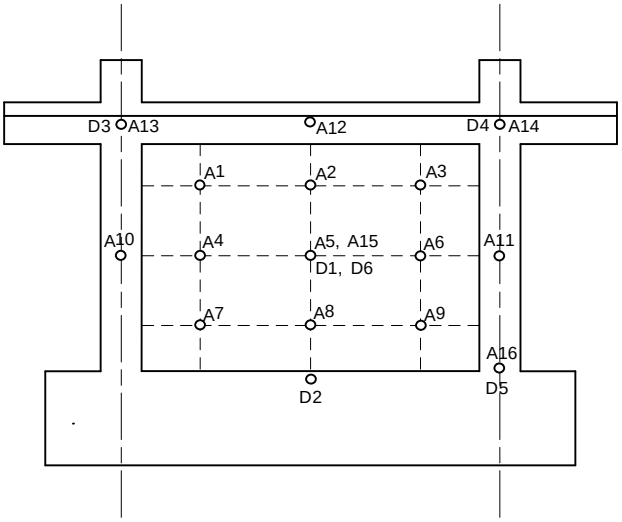

Figure 3.29 Accelerometer and Strain Gage Locations for Model #8

Figure 3.29 shows the location of the accelerometers and strain gages on the infill.

Load-displacement diagrams, plotted at the center of the infill, are evaluated below.

- *Seismic Tests #53 and #56:* Since very low levels of base acceleration were input to the specimen and most of the cycles showed erratic behavior, no further consideration was given to these tests.

- *Seismic Tests #54 and #55:* Peak ground accelerations for these tests were 7.02g and 6.62g respectively. Load-displacement diagrams for Seismic Test #54 and for Seismic Test #55 (Figure 3.30) are similar to each other, with several small hysteresis loops and a single large cycle. An average maximum response acceleration of about 8.0g was recorded. The maximum out-of-plane load was therefore estimated as 1.6 kips (7.1 kN). For these tests, the measured maximum lateral displacement at the center of the infill is about 0.3 in (7.6 mm). From the load-displacement diagrams, an average lateral stiffness of about 10 kips/inch (1.8 kN/mm) was obtained.

- *Seismic Test #57:* The peak ground accelerations for this test was 7.15g. The load-displacement diagram, shown in Figure 3.31, is similar to the diagrams obtained for Seismic Tests #54 and #55. In this case, however, several relatively large hysteresis cycles were recorded. A maximum average acceleration of about 8.50g was recorded. The maximum out-of-plane load is therefore estimated as 1.7 kips (7.5 kN). The measured maximum lateral displacement at the center of the infill, in this case, was about 0.35 inches (8.9 mm). From the load-displacement diagrams an average lateral stiffness of about 10 kips/inch (1.8 kN/mm) was again obtained.

- *Seismic Test #58:* The peak ground acceleration for this test was 7.99g. In this case, the load-displacement diagram, shown in Figure 3.32, displays several large cycles. The maximum recorded response acceleration was 10.0g corresponding to an out-of-plane applied load of 2.0 kips (8.9 kN). The maximum base acceleration was 8.0g. The maximum measured lateral displacement of the center of the infill was 0.6 inches (15 mm). The average lateral stiffness was estimated from the load-displacement diagram as 8.0 kips/inch (1.4 kN/mm).

Random Test #21 was conducted just before the initiation of the seismic-test series, while Random Tests #22 was performed at the end of it. Results from these two tests, presented in Figure B.7 of Appendix B, suggest an initial fundamental frequency of 24 Hz and a final fundamental frequency of 15 Hz. The initial and final stiffness were estimated as 12 kips/inch (2.1 kN/mm) and 4.5 kips/inch (0.8 kN/mm), respectively.

Table 3.4 Peak Out-of-Plane Response Accelerations (g) for Model #8

Test	A_{base}	----- TOP -----			--- MIDDLE --			--- BOTTOM ---		
#	A16	A1	A2	A3	A4	A5	A6	A7	A8	A9
53	-2.24	-2.83	-2.71	-2.80	-2.68	-2.84	-2.67	-2.36	-2.40	3.39
54	-7.02	-8.21	-7.27	-8.32	-7.52	-7.75	-6.77	-6.99	-7.02	-9.93
55	-6.62	-8.50	-7.93	-8.92	-7.67	-7.94	-6.90	-6.90	-7.07	9.63
56	-1.92	-3.17	-3.30	-3.22	-3.01	-3.18	-3.03	-2.09	-2.18	-2.22
57	-7.15	-8.78	-8.61	-9.32	-8.60	-8.09	-7.15	-7.63	-7.79	9.63
58	7.99	9.26	10.05	-9.37	-8.51	9.59	-8.70	8.33	-8.44	-8.98

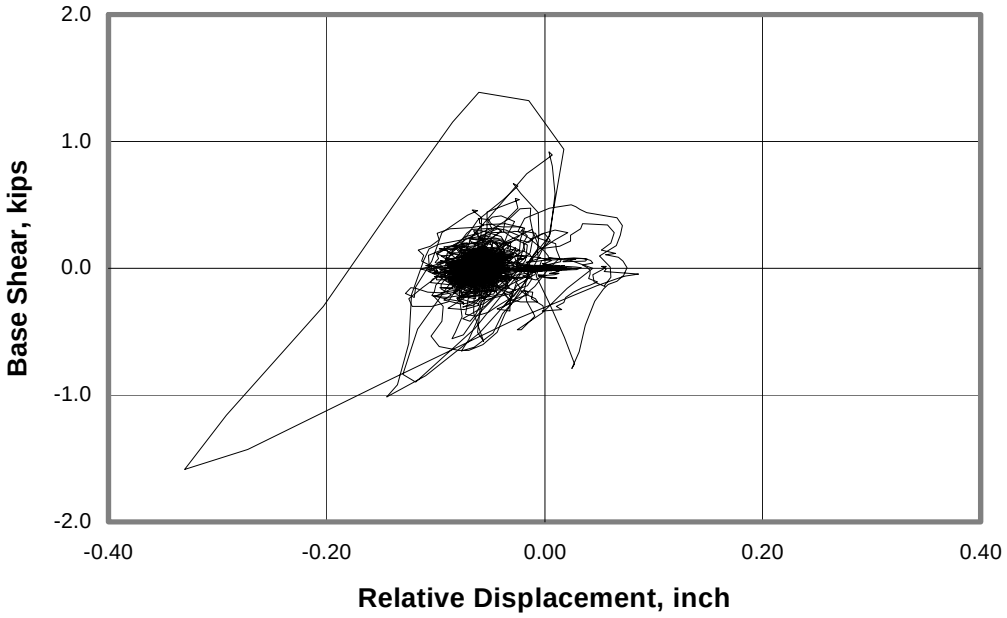

Figure 3.30 Load-Displacement Response at Center of Infill, Model #8, Seismic Test #55

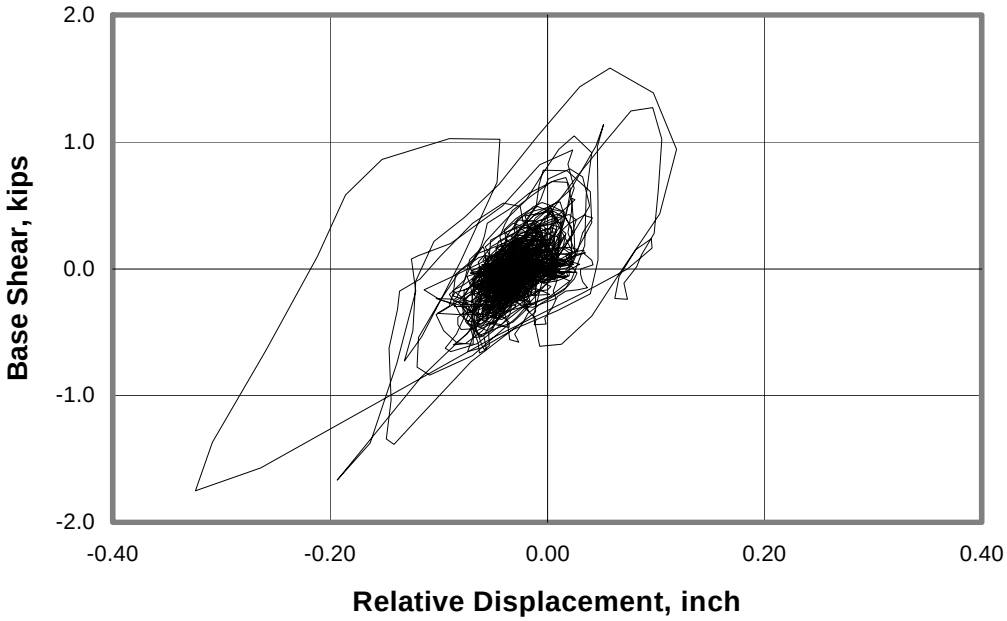

Figure 3.31 Load-Displacement Response at Center of Infill, Model #8, Seismic Test #57

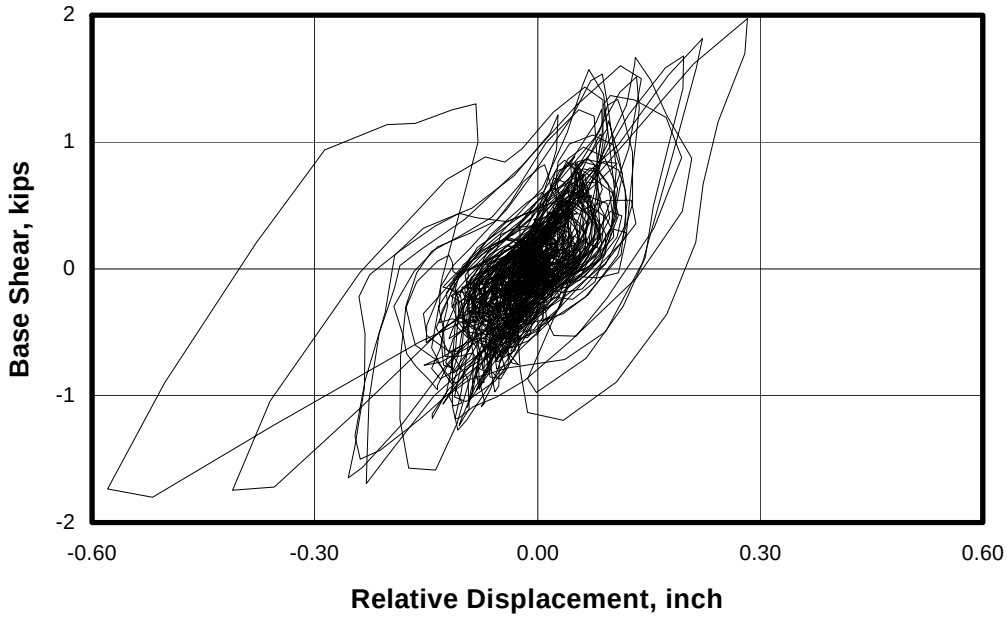

Figure 3.32 Load-Displacement Response at Center of Infill, Model #8, Seismic Test #58

CHAPTER 4

EVALUATION OF LOCAL EXPERIMENTAL RESULTS

4.1. General

The overall load-displacement response of the specimens was described in Chapter 3.0. In this chapter, local member response is examined. The individual structural members of the test specimen (beams, columns, and infills), were instrumented to record internal strains and relative deformations.

4.2. Maximum Reinforcement Strains for In-Plane Tests

Table 4.1 summarizes the maximum strains measured in the longitudinal bars of beam and columns of Model #1 for Seismic Tests #9, #10 and #11. No yielding was recorded in any bars for these tests. Strains are reported in micro-strain units ($\mu\in$), that is in millionths of inch/inch.

Table 4.1 Maximum Strains ($\mu\in$) in Longitudinal Reinforcement for Model #1

	Seismic Test #9		**Seismic Test #10**		**Seismic Test #11**	
Gage	**Tension**	**Compression**	**Tension**	**Compression**	**Tension**	**Compression**
S1	408	-215	728	-287	1072	-387
S2	206	-131	463	-241	1007	-336
S3	333	-161	663	-245	998	-404
S4	153	-98	364	-190	787	-317
S5	152	-90	294	-162	546	-292
S6	274	-60	492	-146	816	-284
S7	225	-160	454	-234	938	-351
S8	266	-81	587	-138	915	-238
S9	151	-154	411	-282	1323	-462
S10	137	-91	127	-141	375	-219
S11	290	-253	507	-441	1171	-576
S12	281	-143	693	-224	1114	-448
S13	220	-162	446	-278	1130	-401
S14	303	-165	678	-262	1108	-475
S15	184	-191	434	-329	1074	-465
S16	305	-144	644	-240	1076	-410

Table 4.2 summarizes the maximum tensile and compressive strains measured in the longitudinal bars of beam and columns of Model #2. In this case yielding was barely reached, since the maximum strain of 2250 $\mu\in$ at Gage S1 in Seismic Test #19 is very close to the yield strain of 2110 $\mu\in$.

Table 4.2 Maximum Strains ($\mu\in$) in Longitudinal Reinforcement for Model #2

	Seismic Test #18		**Seismic Test #19**	
Gage	**Tension**	**Compression**	**Tension**	**Compression**
S1	218	-154	2250	-2147
S2	129	-34	998	-52
S3	337	-26	1391	-180
S4	126	-36	843	-90
S5	58	-56	538	-79
S6	508	-45	1565	-36
S7	178	-88	192	-854
S8	37	-478	27	-1467
S9	267	-1553	275	-1532
S10	90	-177	334	-497
S11	87	-75	216	-967
S12	73	-116	462	-759
S13	133	-119	426	-910
S14	29	-296	202	-1339
S15	202	-63	496	-719
S16	28	-343	109	-1245

Table 4.3 summarizes the maximum strains measured in the longitudinal bars of beam and columns of Model #6. For Seismic Test #47 considerable yielding occurred in several locations.

Table 4.4 summarizes the maximum strains measured in the longitudinal bars of beam and columns of Model #7. In this case, yielding was again observed at several strain gages.

Table 4.3 Maximum Strains ($\mu\in$) in Longitudinal Reinforcement for Model #6

Gage	Seismic Test #45		Seismic Test #46		Seismic Test #47	
	Tension	**Compression**	**Tension**	**Compression**	**Tension**	**Compression**
S1	0	0	1568	-431	3272	-180
S2	218	-104	915	-628	3649	-425
S5	136	-74	1011	-349	1579	-482
S6	146	-67	802	-323	3584	-208
S9	33	-36	97	-182	468	-257
S11	21	-21	298	-20	500	-71
S15	21	-29	57	-62	48	-114
S17	14	-12	479	-13	582	-201
S14	11	-25	31	-57	29	-96

Table 4.4 Maximum Strains ($\mu\in$) in Longitudinal Reinforcement for Model #7

Gage	Seismic Test #51		Seismic Test #52	
	Tension	**Compression**	**Tension**	**Compression**
S1	0	0	0	0
S2	2495	-473	2664	-801
S5	976	-45	3362	-801
S6	18	-48	15	-29
S9	292	-83	389	-211
S11	199	-51	347	-24
S15	30	-38	35	-102
S16	479	-87	1218	-228
S14	89	-28	134	-14

CHAPTER 5

DISCUSSION OF EXPERIMENTAL RESULTS

5.1. Individual Specimen Response

In this section, the most significant observations regarding the individual seismic behavior of each Model based on its load-displacement response to simulated earthquakes are presented and discussed. Additionally, dynamic characteristics of each Model, measured by means of random vibration tests, are summarized.

1) Model #1 (in-plane, strong bare frame):
   a) Seismic Tests #1 to #8 and #12 to #15 were either aborted or had very low levels of base shear, showing irregular and inconsistent load-displacement response patterns. Therefore, they are not considered to represent well the behavior of this specimen.
   b) On the other hand, Seismic Tests #9, #10 and #11 show reasonable and consistent load-displacement patterns, as well as stiffness, strength and displacement values. An average backbone stiffness for the uncracked bare frame of 120 to 140 kips/inch (21 to 25 kN/mm) is obtained from these diagrams (within 20% of estimated cracked, transformed stiffness). Maximum measured base shear reached 20 kips (89 kN), while maximum displacement was 0.3 inches (7.6 mm) or 0.9% story drift.
   c) The initial uncracked measured stiffness (Random Test #3) was 150 kips/inch (26 kN/mm) and the measured cracked stiffness (Random Test #6) was 120 kips/inch (21 kN/mm). In both cases the stiffness closely agree with that obtained from the load-displacement diagrams of the seismic tests. The final measured stiffness (Random Test #8) was 80 kips/inch (14 kN/mm) and was almost half of the initial stiffness, suggesting a high level of damage (cracking) in the specimen.

2) Model #2 (in-plane, strong infilled frame):
   a) Seismic Tests #16 and #17 had low levels of input ground motion and showed very inconsistent response at various locations on the specimen accompanied by very low stiffness. Hence, these tests are not believed to represent the real behavior of this specimen.

b) The specimen reached story drifts as large as 2.2% during Seismic Tests #18 and #19. Measured load levels were 40 to 50 kips (178 to 222 kN). Hysteretic load-displacement histories seem reasonable, and are believed to represent the behavior of the strong infilled frame. Average secant stiffness for all loops of Seismic Test #18 is about 100 kips/inch (17.5 kN/mm). In the case of Seismic Test #19, it is about 50 kips/inch (8.7 kN/mm).

c) Measured initial stiffness (Random Tests #11 and #12) was 590 kips/inch (103 kN/mm), while the final stiffness was 120 kips/inch (21 kN/mm), implying a degradation of stiffness of about 80%. The initial stiffness is significantly higher than the average load-displacement stiffness obtained for Seismic Tests #18. On the other hand, the final stiffness is similar to such average value.

3) Model #3 (out-of-plane, strong infilled frame):

a) Out-of-plane displacements of the infill were not measured. Therefore, stiffness was not computed and load-displacement diagrams were not constructed. However, load levels, computed from the measured infill accelerations, were fairly constant over the surface with an average value of 1.2 kips (5.3 kN). This load may be considered a lower bound to the out-of-plane strength of the infill, since no collapse occurred during the Test.

b) The estimated initial stiffness of 4.5 kips/inch (0.8 kN/mm) was obtained from the results of Random test #13. Because no other random test was performed to this model after the seismic-test series, the effect of the ground motions on the stiffness of the specimen could not be assessed.

4) Model #4 (out-of-plane, strong repaired frame):

a) The out-of-plane load-displacement patterns obtained do not represent the behavior of the specimen well. Maximum lateral load levels imposed on the infill were over 2.0 kips (8.9 kN).

b) The repair technique, used during the test program, proved to be effective since load levels could be increased from 1.2 kips (5.3 kN) for Model #3 to 2.0 kips (8.9 kN) for this Model, that is, an increment of about 70%.

c) The test setup for out-of-plane excitation, using cables to tie the tip of the frame to the BSTM floor, was adequate since infill displacements measured relative to

the base of the specimen were practically identical to the infill displacements measured relative to the frame.

d) The estimated initial stiffness of 9.0 kips/inch (1.6 kN/mm) was obtained from the results of Random Test #14. Again for this model, no other random test was conducted; therefore, the effect of the ground motions on the stiffness of this specimen could not be assessed. However, comparing the initial stiffness of this model with that of Model #3 (unrepaired specimen), it is clear that the repair technique increased the initial stiffness of the specimen in about 100%.

5) Model #5 (out-of-plane, virgin strong infilled frame)

a) The out-of-plane load-displacement patterns obtained do not represent well the behavior of the specimen. Maximum lateral load levels imposed on the infill were about 1.0 kip (4.5 kN).

b) Using the results of Random Test #15, the initial stiffness of this model was estimated as 12 kips/inch (2.1 kN/mm). As in the case of Models #3 and #4, no other random test was performed on this specimen and therefore, the effect of the ground motions on the stiffness of this specimen could not be assessed.

6) Model #6 (in-plane, weak bare frame):

a) Seismic Tests #41 through #45 had low levels of input ground motion and unreliable load-displacement patterns. Consequently, these tests are not believed to represent the real behavior of this specimen.

b) Tests #46 and #47 show good load-displacement diagrams at the top slab. An average stiffness of 47 kips/inch (8.2 kN/mm) was measured. Maximum measured load and displacement were 22 kips (98 kN) and 0.7 inches (18 mm) respectively.

c) Random Test #17 implies an initial stiffness for this model of nearly 120 kips/inch (21 kN/mm). After the seismic-test series was completed, Random test #18 was conducted and from its results the final stiffness of this specimen was estimated as 40 kips/inch (7 kN/mm). Both stiffness levels were lower than the corresponding levels estimated for the strong frame (Model #1), as expected.

7) Model #7 (in-plane, weak infilled frame):
   a) Seismic Tests #48 and #49 had low levels of input ground motion and unreliable load-displacement patterns. Therefore, these tests do not represent the real behavior of this specimen.
   b) Seismic Test #50 suggests a stiffness value close to 300 kips/inch (53 kN/mm). These values were measured from a single hysteresis loop with maximum base shear of 30 kips (133 kN).
   c) Seismic Tests #51 and #52 show good load-displacement patterns at the top slab, with maximum loads reaching 60 kips (267 kN). Stiffness levels are generally under 200 kips/in, (35 kN/mm) suggesting a degrading behavior for this specimen. The maximum lateral displacement is 0.9 inches (23 mm).
   d) Using the results of Random Tests #19 and #20, the initial and final stiffness were estimated as 1180 kips/inch (207 kN/mm) and 360 kips/inch (63 kN/mm), respectively. Clearly the stiffness of this specimen decreased to less than one third of its initial (uncracked) level after the ground motions were applied.
   e) Stiffness levels obtained from the load-displacement diagrams greatly disagree with those estimated from the results of random tests. This further confirms that the displacements measured during the seismic tests were not correct for this model.

8) Model #8 (out-of-plane, weak infilled frame):
   a) Seismic Tests #53 and #56 had low levels of input ground motion and unreliable load-displacement patterns. Therefore, these tests are not believed to represent the real behavior of this specimen.
   b) Seismic Tests #54, #55, #57 and #58 show consistent and believable load-displacement patterns. The peak out-of-plane load was 2.0 kips (8.9 kN), and the maximum displacement was 0.6 inches (15 mm). Average stiffness was estimated as 10 kips/inch (1.8 kN/mm).
   c) The initial stiffness of this specimen was estimated from Random Test #21 as 12 kips/inch (2.1 kN/mm), while the estimate of the final stiffness from Random Test #22 is 4.5 kips/inch (0.8 kN/mm). This implies a reduction of the stiffness for this model due to the ground motions of about 70%.

5.2. Correlation between Local and Overall Response

In Section 5.1, it was concluded that little or no yielding occurred in the structural elements of the strong bare frame (Model #1). This is confirmed by the local response results shown in Section 4.2, since no yielding of the reinforcing bars occurred. In fact, for Seismic Test #11, the maximum strain in any reinforcing bar, which occurred in the beam, was only 63% of the yield strain. However, this implies significant damage to the specimen due to flexural cracking.

In the case of Model #2, the local response shows that no yielding occurred in any of the reinforcing bars during Seismic Test #18. Again, this corroborates the overall response results stated in section 5.1. For Seismic Test #19, on the other hand, local results show that some reinforcing bars yielded. However, this was not clear in the load-displacement diagrams shown in Section 3.3.2.

Overall load-displacement response for Model #6 shows that no yielding of the structure occurred during Seismic Tests #45 and #46, but that some yielding occurred during Seismic Test #47 (see Section 3.3.6). This behavior is confirmed by the local response results, shown in Section 4.2, since no yielding of the reinforcing bars occurred for the two first tests while some of the bars reached yield during the last test.

Finally, load-displacement response for Model #7 suggests that yielding of the specimen occurred for both Seismic Tests #51 and #52 (see Section 3.3.7). However, local response results show that no reinforcing bar yielded during Seismic Test #51, but that some did during Seismic Test #52.

In summary, it can be concluded that the local response results generally confirm the overall response findings and further explain the behavior of the specimens. For the strong-frame model, cracking began in the bare frame and yielding occurred after it was infilled. For the weak-frame model, yielding occurred in the bare frame and again in the infilled frame.

5.3. Conclusions Regarding In-Plane Response of Bare Frames

1) In-plane, bare-frame tests involving very low levels of base acceleration (under 0.5g) clearly show load-displacement characteristics that are inconsistent with each other, and not useful for evaluating specimen behavior. These “poor” load-displacement patterns are apparently due to the precision of the instruments.

2) Seismic tests with higher levels of ground input acceleration were useful. The average in-plane stiffness for these tests was about 130 kips/inch (23 kN/mm) in the case of the strong-frame specimen, and about 50 kips/inch (9 kN/mm) for the weak-frame specimen. The maximum base shear in both cases was about 20 kips (89 kN).

3) The values of stiffness for the strong frame, obtained from the results of random tests, varied from 150 kips/inch (26 kN/mm) to 80 kips/inch (14 kN/mm).

4) The values of stiffness for the weak frame, obtained from the results of random tests, varied from 120 kips/inch (21 kN/mm) to 40 kips/inch (7 kN/mm).

5.4. Conclusions Regarding In-Plane Response of Infilled Frames

1) Again in this case, tests involving low levels of base acceleration (under 2.0g) show "poor" load-displacement characteristics.

2) Seismic tests with higher levels of ground input acceleration were useful. An initial stiffness of about 300 kips/inch (53 kN/mm) was measured for the weak infilled frame. For subsequent tests, a degraded stiffness of less than 200 kips/inch (35 kN/mm) was measured. Maximum base shear was about 60 kips (267 kN). For the strong infilled frame, inconsistencies in measured displacements made it difficult to estimate the stiffness with confidence. Maximum base shear was about 50 kips (220 kN).

3) The results of random tests were used to estimate the in-plane stiffness of the infilled frames. In the case of the weak infilled frame, the initial stiffness is about 1180 kips/inch (207 kN/mm) while the final stiffness is about 360 kips/inch (63 kN/mm). From these results, it can be concluded that after a series of "moderate" ground motions, the in-plane stiffness of the infilled frame was reduced to less than one third of its initial value.

4) The initial and final values of stiffness for the strong infilled frame, obtained from the results of random tests, were 590 kips/inch (103 kN/mm) and 120 kips/inch (21 kN/mm), respectively. These values of stiffness are inconsistent with those obtained for

the weak infilled frame and therefore, they are not believed to represent the actual levels of stiffness of this specimen.

5.5. Conclusions Regarding Out-of-Plane Response of Infilled Frames

1) Seismic tests with low levels of ground input acceleration (generally under 4.0g) show load-displacement characteristics that are inconsistent with each other, and not useful for evaluating specimen behavior.

2) Seismic tests with higher levels of ground input acceleration were useful. Maximum out-of-plane shears reached 2.0 kips (8.9 kN), corresponding to an equivalent uniform load of 190 lb/ft^2 (9.1 kPa). A maximum out-of-plane displacement at the middle center of the infill was 0.60 inches (15 mm). The average stiffness was then estimated as 10 kips/inch (1.8 kN/mm).
3) The results of random tests were used to estimate the out-of-plane stiffness of the infilled frames. In the case of the strong infilled frame, which was previously loaded in-plane, the initial stiffness is about 4.5 kips/inch (0.8 kN/mm). After loaded in the out-of-plane direction and repaired, its stiffness was increased to about 9.0 kips/inch (1.6 kN/mm). That is, the result of the repair technique was to upgrade the stiffness of the infill to twice its original stiffness (before the out-of-plane excitation).
4) The initial stiffness of an undamaged ("virgin") strong-frame specimen was estimated as 12 kips/inch (2.1 kN/mm). If this stiffness is compared to that of the previously in-plane loaded strong-frame specimen (4.5 kips/inch or 0.8 kN/mm), it is clear that in-plane damage reduced the stiffness to about one third the initial value.
5) For the weak infilled frame, the out-of-plane stiffness decreased from 12 kips/inch (2.1 kN/mm) to 4.5 kips/inch (0.8 kN/mm), that is about 63%, due to the out-of-plane ground motions. It is concluded that the stiffness was reduced, in this case, to about 30% of the original after "moderate" ground motions.

CHAPTER 6

ANALYTICAL IDEALIZATIONS FOR IN-PLANE LOADING

6.1. General Remarks

In this chapter, the specimens whose in-plane experimental behavior was described in Chapters 4 and 5 are analyzed using several theoretical approaches. Four computer programs were used to set up mathematical models of the specimens, and to predict their response under both static and dynamic loading. The main assumptions and the procedures used in the computer programs and in the preparation of the analytical idealizations are summarized in the next section. Finally, Sections 6.3 and 6.4 present the predicted response obtained from the computer model, and compare it to the experimental response.

6.2. Computer Programs Used for Analytical Idealizations

The computer programs RCCOLA (Mahin and Bertero, 1977, Farahany 1983) and DRAIN-2DX (Kanaan and Powell, 1975) were used to idealize the bare frames; the programs FEM/I (Ewing et al., 1987) and LPM/I (Kariotis et al., 1992) were used to idealize the infilled frames. The following sections describe each program and the characteristics of its corresponding idealization.

6.2.1. RCCOLA (Mahin and Bertero, 1977, Farahany 1983)

This program analyzes reinforced concrete beam-column sections. It was used to calculate the moment-curvature behavior of beams and columns for both the strong (Model #1) and the weak (Model #6) bare frames, for subsequent input into DRAIN-2DX. The stress-strain relationship proposed by Kent and Park (1971) was used for the concrete, assuming f'_c =5000 psi. The steel yield strength was assumed to be 62.5 ksi. The analysis considered the side slab in the beam. For both the column and the beam, the initial section only was analyzed. Confinement of sections was not considered since the level of loading was much lower than that causing cover spalling.

6.2.2. DRAIN-2DX (Kanaan and Powell, 1975, Allahabadi and Powell, 1988)

This general purpose computer program for inelastic static and dynamic analysis of plane structures was used to analyze the response of both weak and strong bare frames (Models #1 and #6, respectively), subjected to the ground accelerations used for the shaking table tests. The beam-column element used to model columns and beams is composed of elastic and inelastic components

in parallel, with both axial and flexural stiffness and shear deformation. Yielding is restricted to concentrated plastic hinges at the element ends where strain hardening is simulated by allowing the inelastic component to yield under constant moment, while the elastic component continues to take load. No bond slip of longitudinal bars is accounted for.

Yield moments for beams and interaction diagrams for columns were obtained from RCCOLA output. Since the beams are L-shaped, the yield moments were given different values for positive and negative bending. Masses were assumed to be concentrated at beam-column joints. Rotational mass was computed using the self-weight of beams and columns only, assuming a cubic deflected shape for the elements. Translational mass was computed using the self-weight of the frame and slab, and the concentrated mass on top of the slab. Viscous damping was taken as 5% of critical. Rayleigh damping was used, for which values of mass- and stiffness-proportional damping were computed using the fundamental period obtained from an initial run in which viscous damping was neglected.

6.2.3. FEM/I (Ewing et al., 1987)

This is a finite-element program for the nonlinear static analysis of masonry walls. It was used to calculate the static push-over response of the infilled concrete frame. The material constitutive law considers biaxial states of stress and pre- and post-cracking behavior. The program uses an initial stiffness formulation with an incremental solution method that is reliably convergent for softening systems when prescribed displacements are used as primary excitation. Masonry behavior is supposed to be dominated by material nonlinearity; while geometric nonlinearities are assumed negligible. Effects of cracking are accounted for in the model. Tension cracks are smeared over the integration points of each finite-element and the compressive strength is reduced after tensile cracking occurs in orthogonal directions. Masonry and concrete strengths of 5 ksi and a steel yield strength of be 62.5 ksi were assumed.

6.2.4. LPM/I (Kariotis et al., 1992)

This program was used to compute the nonlinear dynamic response of the weak and strong infilled frames, idealized as lumped-parameter models, excited by the ground accelerations used during the shaking table tests. The infilled frame was modeled using a nonlinear, hysteretic, degrading spring element (Element 11, Figure 6.9), originally formulated for masonry cantilever walls. The behavior of this element is defined by force-deformation relations based on analysis and results of cyclic experiments of reinforced masonry walls. The envelope of its hysteretic response is

defined by the initial stiffness; stiffness softening to a peak strength; deformation at peak strength; and strength degradation after peak strength. Additionally, the hysteretic behavior is defined by the degrading unloading stiffness, rules for reloading, and pinch force. The values of these parameters were obtained from the output of the FEM/I push-over analysis. Viscous damping was neglected, since it is usually negligible compared to hysteretic damping and the nonlinear model was calibrated neglecting viscous damping.

6.3. Analytical Idealization for Bare Frame Specimens

6.3.1. Idealization for Model #1

The idealization for Model #1 (strong bare frame, excited in-plane) had a calculated fundamental period of 0.097 seconds, and a calculated initial lateral stiffness of 110 kips/inch (19.3 kN/mm), close to that obtained using test data (120 kips/inch or 21.0 kN/mm). The calculated load-displacement response for one of the seismic tests is compared in Figure 6.1 with that observed experimentally. Nearly linear elastic load-displacement patterns with no significant yielding were predicted, while actual test data showed wider hysteretic loops, implying more energy dissipation than predicted. Maximum predicted base shears were within 15% of those found experimentally. Differences between maximum predicted and experimental tip displacements were more significant (within 25%). A single response peak was observed in some cases, due to spikes in the excitation. However, actual test data show that such spikes had less effect on the response of the actual structure.

6.3.2. Idealization for Model #6

The idealization for Model #6 (weak bare frame, excited in-plane) had a calculated fundamental period of 0.133 seconds and an initial lateral stiffness of 45 kips/inch (7.9 kN/mm), very close to the values obtained from the actual test data (47 kips/inch, or 8.2 kN/mm). The computed load-displacement history for one of the seismic tests is compared in Figure 6.2 with that observed experimentally. Larger levels of yielding, and therefore greater displacements (as much as 300%) than those obtained experimentally were predicted. The effect of ground acceleration spikes was greater with increased yielding, causing several large hysteretic loops in the analytical response. Hence, energy dissipation was not well predicted by the computer idealizations as for Model #1. Maximum predicted base shears were very close to the experimental ones for some of the tests (within 5%).

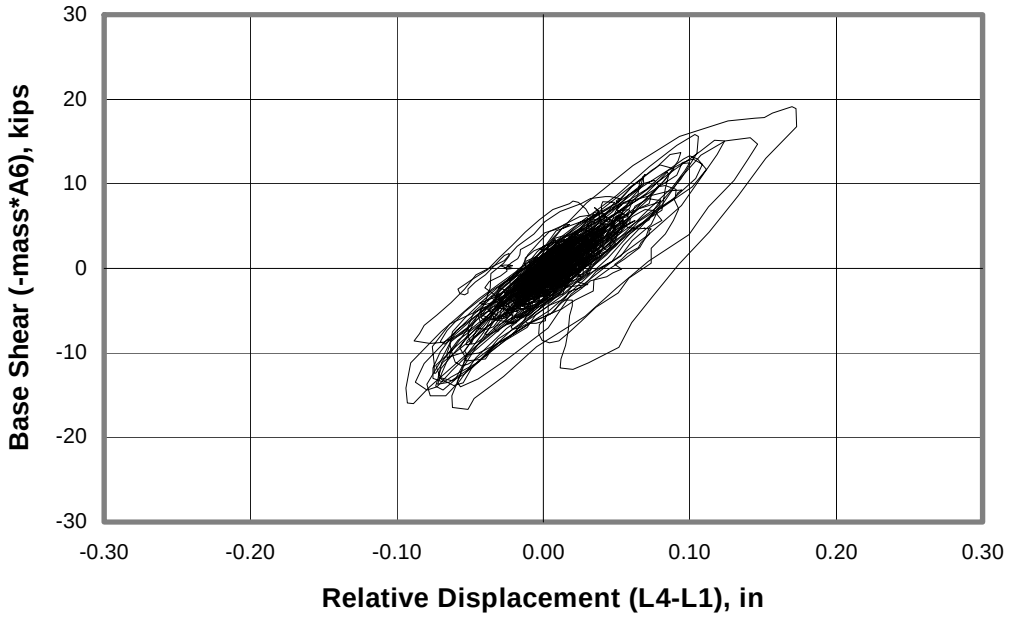

(a) Measured Load-Displacement

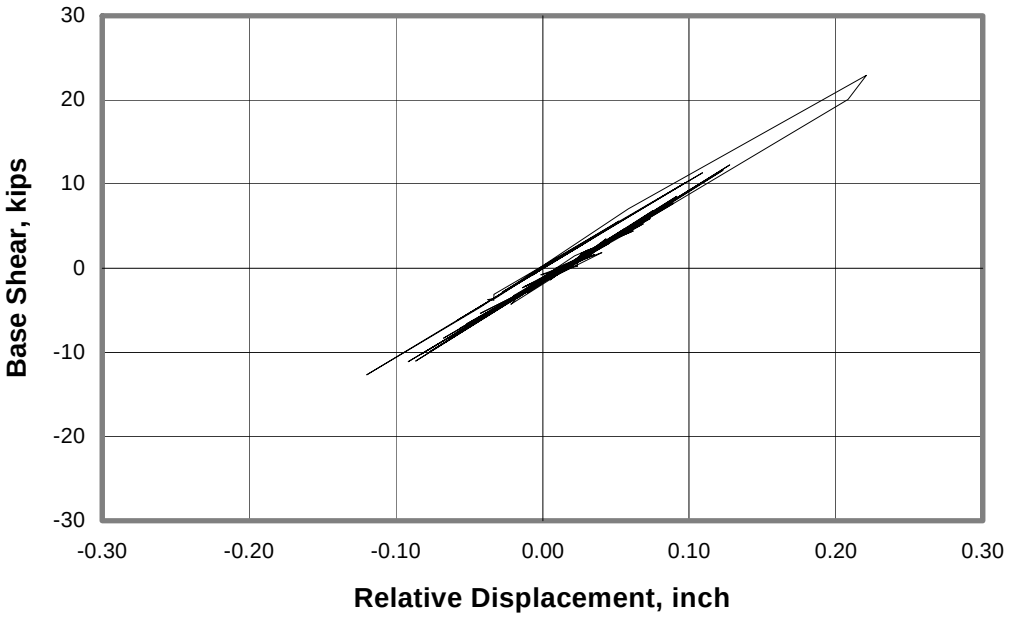

(b) Predicted Load-Displacement Behavior

Figure 6.1 Measured vs. Predicted Load-Displacement Behavior, Model #1, Seismic Test #10

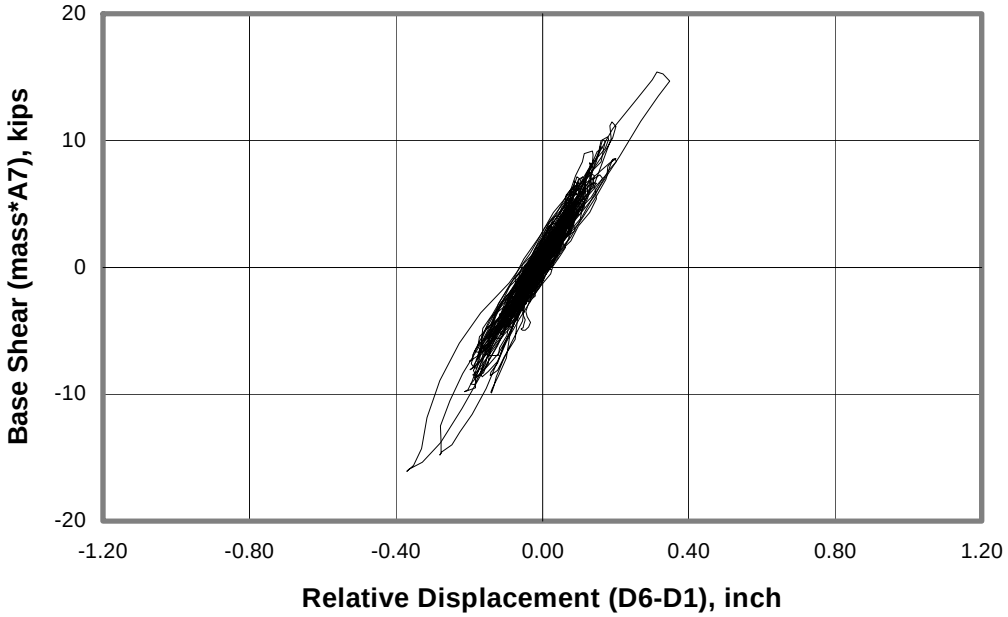

(a) Measured Load-Displacement Response

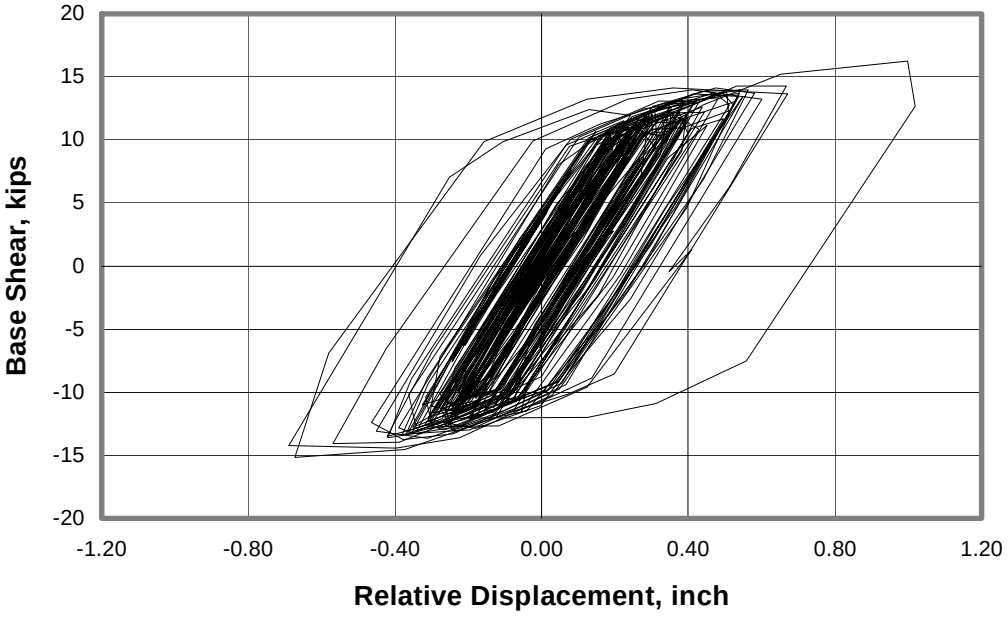

(b) Predicted Load-Displacement Behavior

Figure 6.2 Measured vs. Predicted Load-Displacement Behavior, Model #6, Seismic Test #46

6.3.3. Conclusions Regarding Analytical Idealization of Bare Frames

In general, results from DRAIN-2DX adequately predict the stiffness and strength of bare frames. Predicted values of backbone stiffness and maximum base shear were within 10% of the values obtained experimentally. However, displacement predictions were as much as 30% higher than the experimental values for the strong frame, and as much as 300% for the weak frame. Furthermore, the effect of ground acceleration spikes on base shear is generally overestimated by over 20%. Additionally, load-displacement predictions for tests with low excitation did not compare well with the measured response. This is probably due to inaccuracies caused by signal noise, gage sensitivity, and/or accuracy of data measurement and acquisition equipment. Finally, analysis considering bond slip or anchorage failure and strength and stiffness degradation will probably give more accurate results.

6.4. Analytical Idealization for Infilled Frames Loaded In-Plane

6.4.1. Idealization for Model #2

The results of the pushover analysis on the idealization for Model #2 (strong infilled frame, excited in-plane), performed using FEM/I, are shown in Figure 6.3. The finite-element mesh used for analysis is shown in Figure 6.4. From the pushover results, the spring parameters for LPM/I were obtained. Figure 6.5 shows the force-displacement characteristics of Element 11 of LPM/I, and how it relates to the FEM/I output. The idealization had a calculated initial fundamental period of 0.023 seconds and an average lateral stiffness of 1820 kips/inch (320.3 kN/mm). Calculated load-displacement histories are compared in Figure 6.6 with those observed experimentally.

The predicted load-displacement pattern was almost linear elastic, showing no significant yielding or energy dissipation. Corresponding diagrams plotted using actual test data showed wider hysteretic loops, implying more energy dissipation. One exaggerated loop, caused by a ground acceleration spike, was recorded both analytically and experimentally with almost twice the average displacement and base shear. The maximum predicted base shear was close to that obtained from actual test data (within 10%). However, the predicted maximum displacement was only 15% of that obtained from test data.

Experimental displacements are as high as 0.7 inches, corresponding to drift ratios over 2%. Such displacements are considerably large for masonry walls and therefore, are believed to be invalid. Consequently, predicted lateral stiffness cannot be compared to that obtained experimentally. Stiffness obtained experimentally using random tests for this model is also believed to be invalid, as mentioned in Section 4.3.

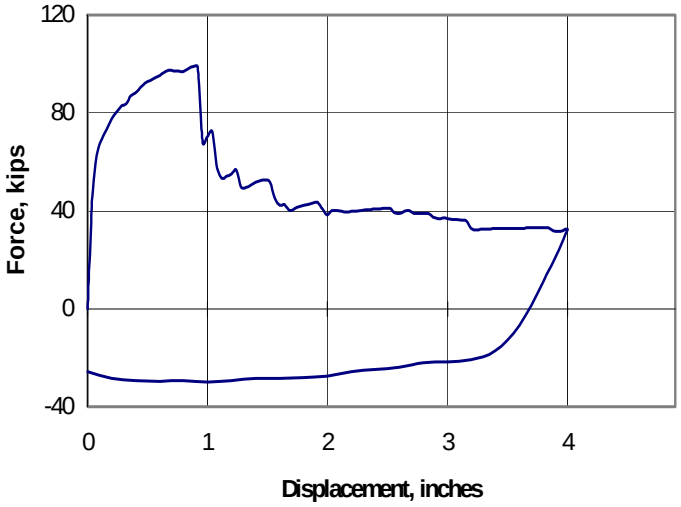

(a) Strong Infilled Frame (Model #2)

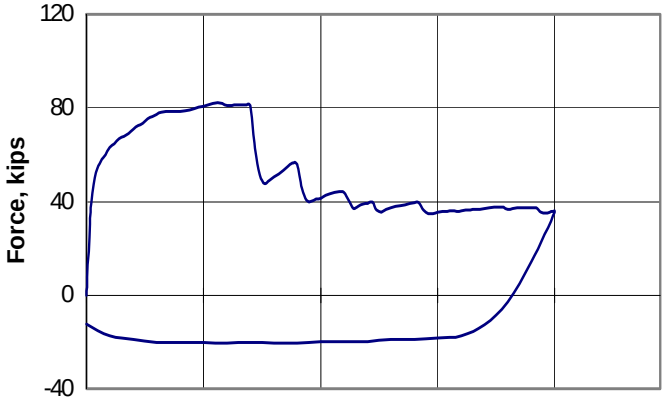

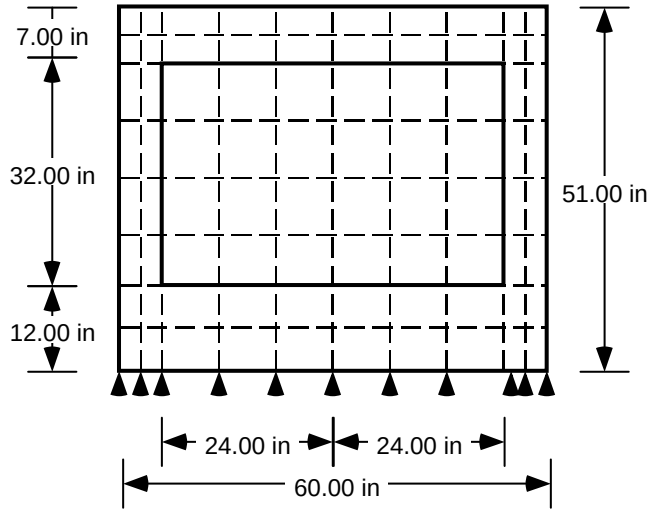

Figure 6.4 Finite Element Mesh used for FEM/I Analysis

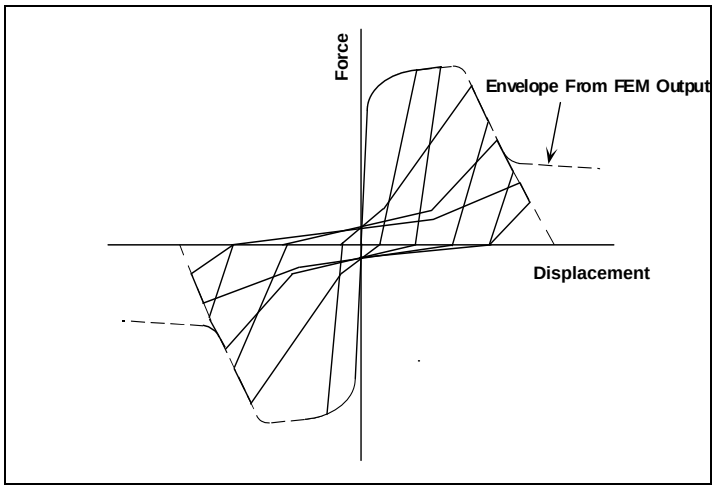

Figure 6.5 Force-Displacement characteristics of LPM/I Element 11 (Kariotis 1992)

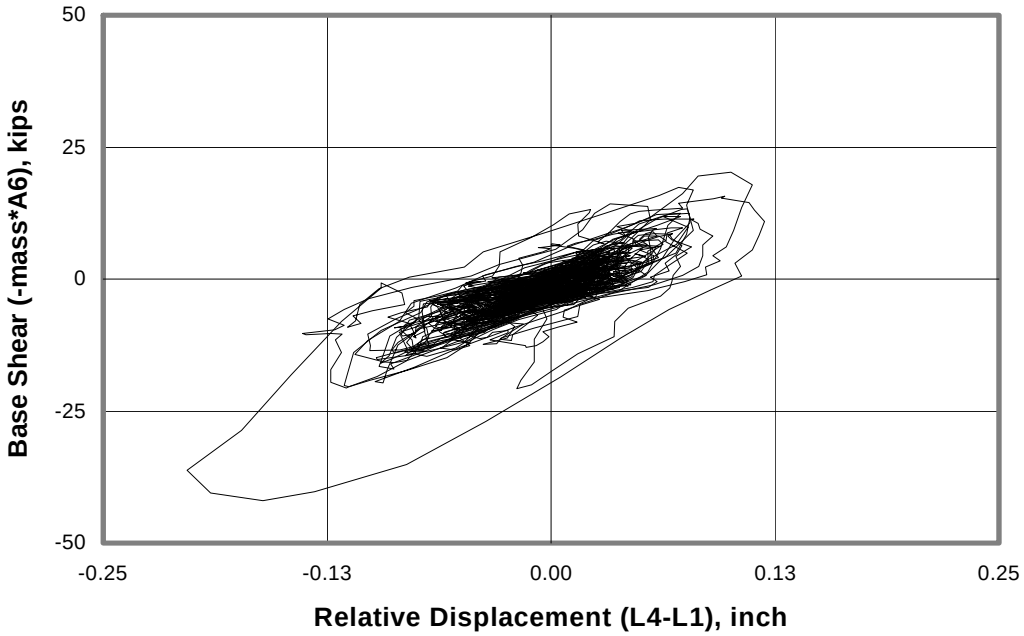

(a) Measured Load-Displacement Response

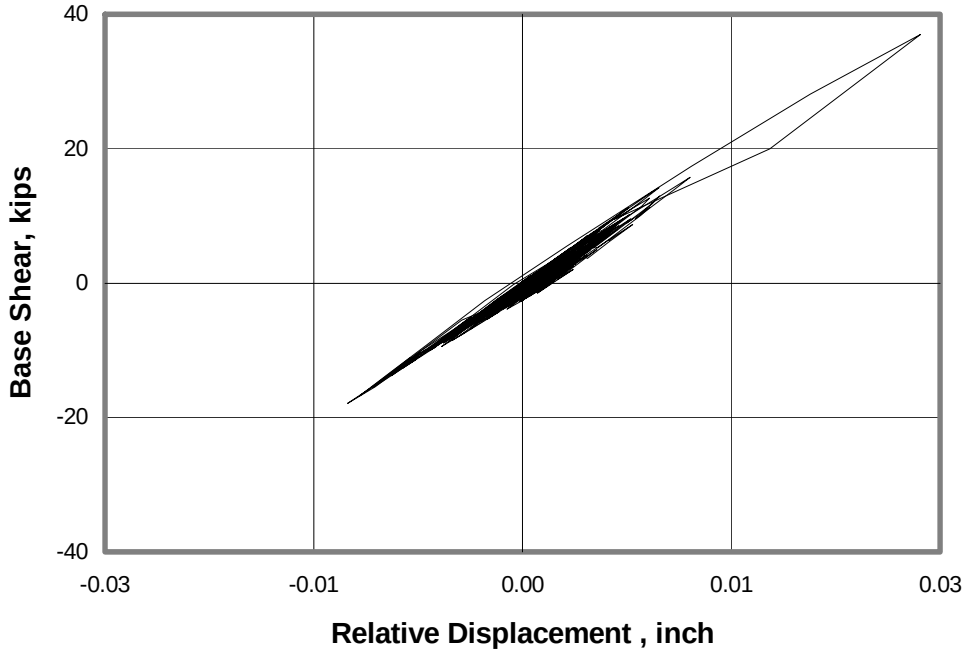

(b) Predicted Load-Displacement Behavior

Figure 6.6 Measured vs. Predicted Load-Displacement Behavior, Model #2, Seismic Test #18

6.4.2. Idealization for Model #7

The idealization for Model #7 (weak infilled frame, excited in-plane) had a calculated initial fundamental period of 0.023 seconds, and an average lateral stiffness of 1000 kips/inch (175 kN/mm), 15% less than the initial stiffness obtained by Random Test #19 (Section 3.3.7). Although the predicted initial stiffness of this idealization is close to that of Model #2 (1550 kips/inch, or 271.3 kN/mm versus 1820 kips/inch or 318.5 kN/mm), the calculated average stiffness is much lower, probably because of the degradation that occurred due to crushing of the infill. Calculated load-displacement histories are compared in Figure 6.7 with those observed experimentally.

Both predicted and measured load-displacement diagrams showed wide loops implying significant energy dissipation. A single peak (with about double the average maximum base shear) was noticed in both cases. The maximum predicted base shear was close to that obtained from the actual test data. However, the predicted maximum displacement was much lower than that obtained from the test data. For the same reasons discussed in Section 6.4.1, the displacement values obtained experimentally are believed to be invalid, and the predicted lateral stiffness will not be compared to that obtained experimentally.

6.4.3. Conclusions Regarding Analytical Idealization of Infilled Frames Loaded In-Plane

The predicted initial stiffness for Model #2 was higher than that for Model #7 (1820 kips/inch, or 318.5 kN/mm versus 1550 kips/inch, or 271.3 kN/mm), although both models had the same infill. This suggests that the stiffness of the confining frame has a significant effect on the behavior of infilled frames. The computer idealization for infilled frames predicts the effect of spikes in ground accelerations to within 15% of the experimental value. Patterns for the tip displacement-base shear diagrams plotted using experimental data are were similar to patterns plotted using predicted response. However, values of displacements are very high (implying a 2.3% drift). Because of these inconsistencies in measured displacements, it is difficult to draw firm conclusions regarding measured stiffness.

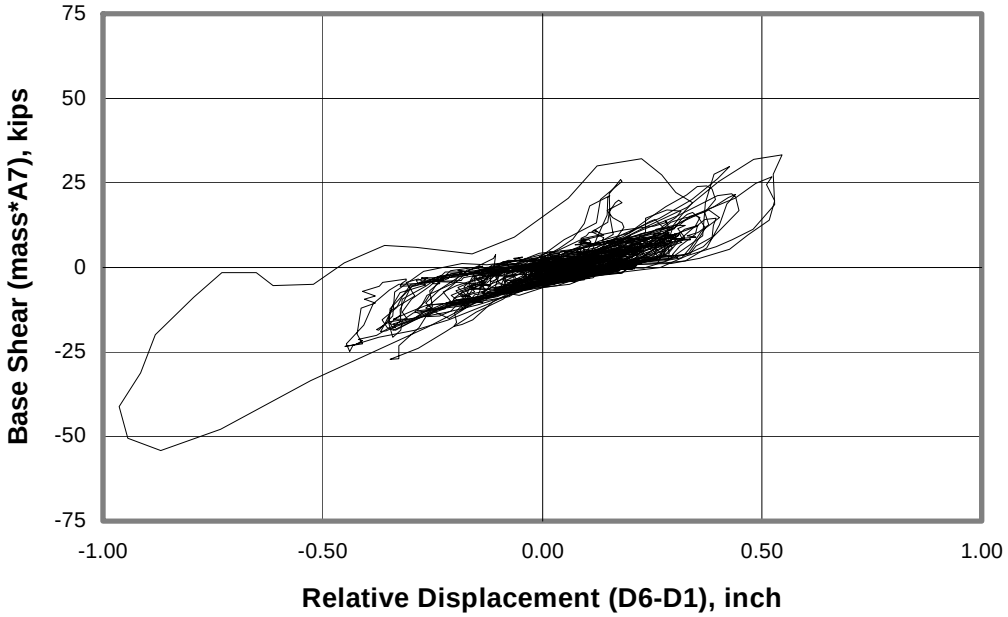

(a) Measured Load-Displacement Response

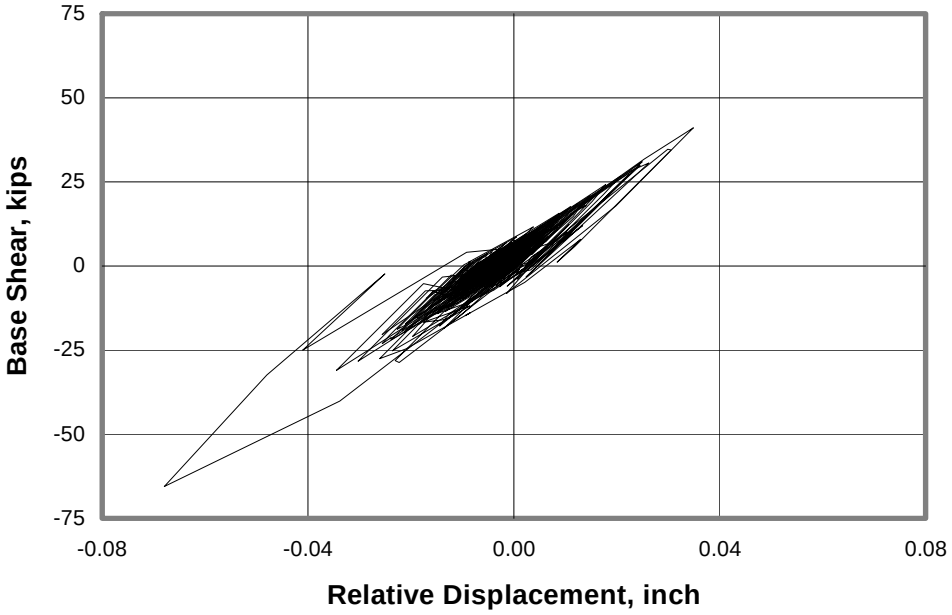

(b) Predicted Load-Displacement Behavior

Figure 6.7 Measured vs. Predicted Load-Displacement Behavior, Model #7, Seismic Test #52

CHAPTER 7

SIMPLIFIED ENGINEERING IDEALIZATIONS FOR IN-PLANE AND OUT-OF-PLANE BEHAVIOR

7.1. General Remarks

Studies of the behavior and strength of masonry infills excited in- and out-of-plane have been of interest to researchers for the last several decades. Previous experimental and analytical research has led to the development of several methods to predict the lateral stiffness and strength of infilled frames.

The purposes of this chapter are:

- to review different analytical approaches for the analysis and design of infilled frames for in-plane actions;
- to present equivalent-strut methods for predicting the lateral in-plane stiffness and strength of infilled frames, modify these methods if required, and recommend one method on the basis of accuracy and ease of use;
- to present a method for determining out-of-plane strength of cracked masonry infills.

7.2. Simplified Analytical Idealization of the In-Plane Behavior of Infilled Frames

The in-plane structural action of an infilled frame may be idealized in various ways:

1) As a shear wall;
2) As an equivalent diagonal strut; and
3) As equivalent multiple struts.

Each one of these approaches is discussed below.

7.2.1. Shear Wall Idealization

In this case, the infilled frame is considered an isolated shear wall whose in-plane strength is due to vertical diaphragm action. However, this idealization neglects the interaction between the infill panel and the frame, and therefore, greatly underestimates the infilled frame strength and

stiffness (Thomas and Klingner, 1990). Previous research (Thomas and Klingner, 1990) showed that the in-plane lateral stiffness and strength of an infilled frame is greater than the sum of the individual contributions of the frame and the infill, mainly because of the difference between the flexural deformation pattern of the frame, and the shearing deformation pattern of the infill (See Figure 7.3).

7.2.2. Equivalent Strut Idealizations

In the equivalent strut idealization, the infilled frame is replaced by a bare frame braced by compression diagonals (Stafford Smith, 1966). This is a reasonable simplification since in-plane lateral deflection of the infilled frame causes a separation along part of the frame-infill interface and contact is maintained only at opposite corners (See Figure 7.3), where load is transferred diagonally through a compression zone in the panel that can be idealized as a strut. It is an oversimplified approximation of the load transfer between frame and infill since such transfer actually takes place over an extended contact length, and not just at one point at a corner of the infill (Stafford Smith, 1962). But, application of the theory is still justified in most practical structures, in which the frame is very flexible compared to the infill, and any discrepancy caused by this simplification is insignificant (Stafford Smith, 1962).

As part of the study reported by Bashandy et al. (1995), the effect of the equivalent strut simplification was investigated, by constructing three different finite-element idealizations for the infilled frame using FEM/I. In the first case, the actual properties of masonry were used to represent the whole infill wall. For the second case, finite elements were used to idealize the masonry forming a diagonal strut only. In the third case, the tensile strength of the elements representing masonry units at the boundary of the infill was specified to be 10% of the actual masonry tensile strength, in order to model the separation at the frame-infill interface. The results from a push-over analysis for the three idealizations are almost identical. This implies that the equivalent strut idealization accurately represents the behavior of infilled frames.

7.2.3. Equivalent Multiple Struts Idealization

In this method, proposed by Thiruvengadam (1985), the infills are replaced by multiple pin-jointed vertical and diagonal struts. For the elastic behavior range, when no separation of the infill-frame interface occurs, the vertical struts model the axial stiffness of the infill, while the diagonal struts model its lateral in-plane stiffness. At a certain load level, separation along a predetermined length (Stafford Smith and Carter, 1969) is assumed to occur, and the struts in that region are removed.

Natural frequencies of multi-story frames obtained using this idealization compared well with those obtained experimentally and analytically using the finite element method (Thiruvengadam, 1985). Moreover, modeling of the frame-infill interaction and reciprocal stiffening effect is a clear improvement over the single-strut idealization. Finally, by suitably selecting the location and characteristics of the struts, openings on the wall can be also modeled.

7.2.4. Equivalent-Strut Methods for In-Plane Stiffness

Previous research (Thomas and Klingner, 1990) recommended the use of a method developed by Stafford Smith (1966) for the prediction of the lateral in-plane stiffness of infilled frames because of its relative accuracy, consistency and simplicity. Furthermore, that method was preferred because of the availability of design graphs. Recent research (Angel et al., 1994) endorsed the use of a different method developed by Holmes (1961, 1963). In this section two Stafford Smith methods (called "SS1" and "SS2") and the Holmes method are discussed. Results from each method are compared to results from finite element analysis, for both the strong and weak infilled frames (analytical idealizations of Models #2 and #7).

a) Method SS1 (Stafford Smith, 1966):

Although this method is dimensionally consistent, only U.S. customary units are used here, to match the methods' original form, and to make comparison with other methods easier. According to Stafford Smith, the stiffness of an infill panel is affected not only by the size, thickness proportions, and material of the panel, but also by the length and distribution of the applied load on the corner. As the frame stiffness increases, the contact length and consequently the effective stiffness also increases. The method also considers the possibility of rigid and pinned connections, even though the difference between calculated stiffness for both cases was presumed to be small in most structures (Stafford Smith, 1966).

For a rigid frame, this method combines the strain energies of the tension in the windward column, A, the compression in the equivalent strut, B, and the frame bending, C. The lateral in-plane stiffness of the infilled frame can then be determined from the equivalent structure, as reviewed below (Stafford Smith, 1962).

The lateral stiffness of the infilled frame is given by

$$K = \frac{A + B + C}{C(A + B)} \tag{7.1}$$

where:

$$A = \frac{h \tan 2\theta}{A_c E_f} \tag{7.2}$$

$$B = \frac{d}{w t E_i (\cos 2\theta)} \tag{7.3}$$

$$C = \frac{h^3 (3 I_b h + 2 I_c L)}{12 E_f I_c (6 I_b h + I_c L)} \tag{7.4}$$

h	=	height of column (inches)
θ	=	angle of diagonal to horizontal (degrees)
A_c	=	cross-sectional area of the column (inch^2)
E_f	=	elastic modulus of frame (ksi)
d	=	diagonal length of the infill panel (inches)
w	=	width of the equivalent strut (inches)
t	=	thickness of the infill panel (inches)
E_i	=	elastic modulus of infill panel (ksi)
I_b	=	moment of inertia of the beam (inch^4)
I_c	=	moment of inertia of column (inch^4)
L	=	length of beam (inches)

b) Method SS2:

This method is not dimensionally consistent, and was formulated for U.S. customary units. The effect of the stiffness of the frame members in flexure compared to that of the infill panel in compression was considered by Stafford Smith in later studies (Stafford Smith, 1966, 1967a, 1967b, 1969, 1978; Carter and Stafford Smith, 1969; Riddington and Stafford Smith, 1977). The stiffer the frame compared to the infill panel, the greater the contact length, and consequently the stiffer the infilled frame. To indicate the relative stiffness between infill panel and frame, Stafford Smith therefore defines a non-dimensional parameter, λ, analogous to that used in elastic foundation theory to express the stiffness of the foundation relative to an overlaying beam (Stafford Smith, 1966):

$$\lambda = \sqrt[4]{\frac{E_i \, t \sin\theta}{4 E_f \, I_c \, L}} \tag{7.5}$$

where

E_i	=	elastic modulus of infill panel (ksi)
E_f	=	elastic modulus of frame (ksi)
t	=	thickness of infill panel (inches)
θ	=	angle between the diagonal and the horizontal (degrees)
I_c	=	moment of inertia of the column ($inch^4$)
L	=	Length of beam (inches)

Given an expression for relative stiffness, λL, a relationship can be derived for α, the length of contact between infill and frame after lateral load has been applied:

$$\frac{\alpha}{L} = \frac{\pi}{2\lambda L} \tag{7.6}$$

where

α = contact length between frame and panel during loading (inches)

L = length of the infill panel (inches)

This relationship, which was adapted from the case of a beam on elastic foundation under a concentrated load; compares very closely with more complex relationships derived considering triangular and parabolic stress distributions over the contact length, and also agrees with experimental results (Stafford Smith, 1966). However, theoretical predictions of the strut effective width based on the contact length expression were consistently higher than experimental values. Therefore, a set of curves for design (shown in Figure 7.1), based on experimental results, was adopted. The equivalent width of the compression diagonal can be found by entering the charts with a computed relative stiffness. The area of the equivalent strut is then the product of the width and thickness of the infill panel:

$$A_{strut} = w \cdot t \tag{7.7}$$

Once the area of the equivalent strut has been determined, the lateral deflection of the resulting braced frame can be calculated by conventional methods.

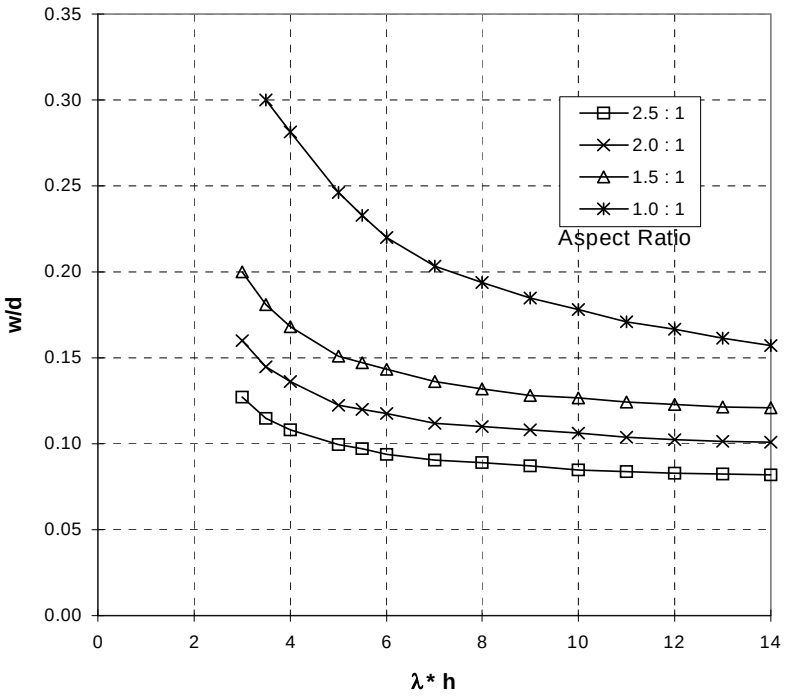

Figure 7.1 w/d as a Function of λh for Different Aspect Ratios (Stafford Smith 1966)

c) Holmes' Method (1961, 1963):

This method is presented in U.S. customary units (although it is dimensionally consistent), to match the method's original form and to make comparison with other methods easier. Holmes considered a single-panel specimen subjected to a horizontal shear force P which produces a compressive resultant, H/cosθ in the infill, as illustrated in Figure 7.3. By considering the forces in the frame and the infill panel separately, the horizontal force causing failure may be determined by evaluating the shortening of the equivalent strut. The expression proposed to evaluate the horizontal stiffness of the specimen is given by Equation 7.8.

$$K = \frac{24 E I_c}{h^3 \left[1 + \left(\frac{I_c}{I_b} \right) \cot \theta \right]} + \frac{t f_c'}{3 \varepsilon_c} \tag{7.8}$$

where

E_f = elastic modulus of frame (ksi)

I_c = moment of inertia of column (inch^4)

I_b = moment of inertia of the beam (inch^4)

θ = angle between the diagonal and the horizontal (degrees)

ε_c = strain in infill at failure

h = height of the frame (inches)

A = cross-sectional area of the equivalent strut (inch^2)

f'_c = diagonal compressive strength of the infill panel (ksi)

Equation 7.8 suggests that the in-plane stiffness depends primarily on the relative geometry of the frame, the infill thickness, and the mechanical properties of both the masonry panel and the frame. The compressive area of the equivalent strut was found to depend primarily on the infill thickness and aspect ratio. Finally, the method assumes an idealized linear force-deflection relationship up to crushing of the masonry at which failure of the system occurs.

The lateral in-plane stiffness of the strong and weak infilled frames was calculated using both Stafford Smith methods and Holmes' method. In Table 7.1, results are compared with the secant stiffness computed at half the strength using program FEM/I (Ewing et al., 1987). The FEM/I secant stiffness results were matched by method SS2, and by Holmes' method. However, method SS2 is recommended, because it considers the relative stiffness of the frame and infill to estimate the contact length of their interface and therefore, predicting a more accurate value for the strut effective width. In contrast, Holmes' method uses a constant value for the width of the equivalent strut, which may lead to inaccurate results in some cases. Previous research shows that the stiffness of infilled frames exposed to cyclic loads eventually degrades to about half this initial value (Angel et al., 1994).

Table 7.1 Predicted Specimen Stiffness, kips/inch

Model	**Predicted Stiffness**			
	Finite Element Method	**Simplified Methods**		
		SS1	**SS2**	**Holmes**
Strong frame	1486	776	1380	1268
Weak frame	1306	670	1160	1234

7.2.5. Equivalent-Strut Methods for In-Plane Strength

The method by Liauw and Kwan's (Liauw and Kwan, 1982, 1983a, 1983b, 1985) for determining the lateral in-plane strength has been recommended previously (Thomas and Klingner, 1990). Strength predictions using this method were in some cases rather low and therefore, conservative. However, they were also very consistent (Thomas and Klingner, 1990). In this section Liauw and Kwan's method, as well as an older method proposed by Holmes (Holmes, 1963), will be discussed. Their results will be compared to those obtained from the push-over analyses, performed using FEM/I, for both the strong and weak infilled frames (Models #2 and #7). The predicted lateral strength will not be compared to results from the dynamic tests, as the infilled frames tested in-plane were not excited up to their lateral strength.

a) Liauw and Kwan's Method:

Liauw and Kwan combined plasticity theory with nonlinear finite element analyses to estimate collapse loads for infilled frames. They addressed issues ignored in previous (Wood,

1978) studies like multi-story design and distinction between integral and non-integral infill panels. “Integral” infilled frames have mechanical connectors between frame and infill, while “Non-integral” infilled frames have no such connectors. According to Liauw and Kwan, failure to differentiate between integral and non-integral frames led to wide discrepancies between previous theoretical predictions and experimental results (Liauw and Kwan, 1983).

Wood (1978) included a penalty factor to lower the effective crushing stress of the infill panel to account for its lack of plasticity. However, according to Liauw and Kwan, Wood’s over-estimation of the collapse shear is due to the assumption of excessive friction at the interface between the infill panel and the frame, and to neglect of separation between infill panel and frame in the composite shear mode. According to Liauw and Kwan, friction has an insignificant effect, and should be considered only as reserve strength. Therefore, only three failure modes exist for the non-integral infilled frame, as shown in Figure 7.2.

1) Corner crushing with failure in columns
2) Corner crushing with failure in beams
3) Diagonal crushing

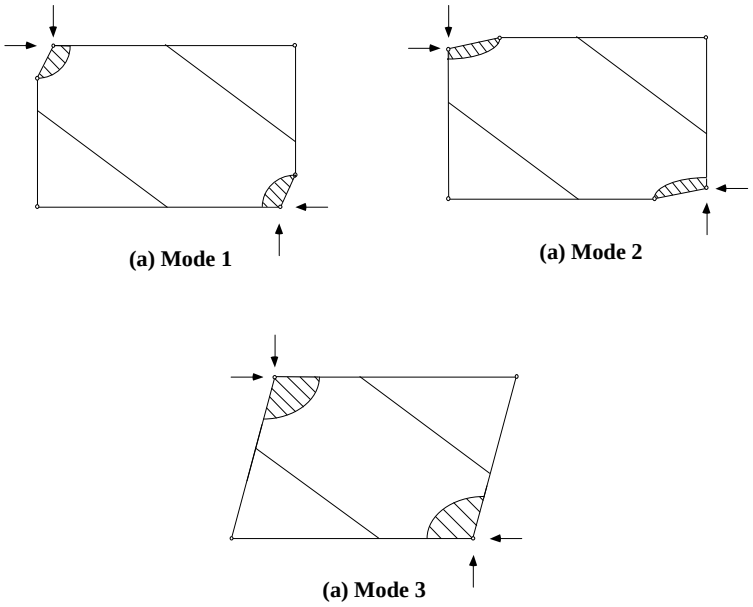

Figure 7.2 Collapse modes for infilled frames (Liauw and Kwan)

The collapse shears for each failure mode in single-story, non-integral infilled frames are expressed by Equations 7.9 to 7.11: The maximum collapse shear is the minimum value of these three equations.

Mode 1: $$H_u = \sigma_c t\, h \sqrt{\frac{2\left(M_{pj} + M_{pc}\right)}{\sigma_c\ t\, h^2}} \tag{7.9}$$

Mode 2: $$H_u = \frac{\sigma_c t\, h}{\tan\theta} \sqrt{\frac{2\left(M_{pj} + M_{pc}\right)}{\sigma_c\ t\, h^2}} \tag{7.10}$$

Mode 3: $$H_u = \frac{4 M_p}{h} + \frac{\sigma_c\ t h}{6} \tag{7.11}$$

where

H_u = in-plane design strength of infill panel (kips)

h = story height (inches)

M_{pb} = plastic moment of the beam (inch-kip)

M_{pc} = plastic moment of the columns (inch-kip)

M_p = the smaller of M_{pb} and M_{pc} (inch-kip)

Plasticity theory can be applied not only to single-story frames but also to multi-story ones, since the collapse modes in both cases are basically the same. However, many different combinations of failure modes are possible, and estimating the strength can be difficult. For that reason, a simplified procedure was developed by Liauw and Kwan for story-by-story design of multi-story infilled frames. Equations 7.12 to 7.14 predict the collapse shear in lower stories (that is, all stories except the uppermost) for integral and non integral construction:

Mode 1: $$H_u = \sigma_c\ t\ h \sqrt{\frac{4\ M_{pc}}{\sigma_c\ t\, h^2}} \tag{7.12}$$

Mode 2: $$H_u = \frac{\sigma_c\, t\, h}{\tan\theta}\sqrt{\frac{4M_{pb}}{\sigma_c\, t\, h^2}} \tag{7.13}$$

Mode 3: $$H_u = \frac{4M_{pc}}{h} + \frac{\sigma_c\, t\, h}{6} \tag{7.14}$$

The lateral strength of both the strong and the weak infilled frames were calculated using Liauw's methods for both single and multi-story frames, and were compared with the results from FEM/I (Table 7.2). As expected, the predictions of this method were low.

b) Holmes' Method (Holmes, 1963):

This method is based on the analysis of the results of small-scale and full-scale tests of steel infilled frames. As in Holmes' stiffness method, the infill has been replaced by an equivalent strut, as shown in Figure 7.3. The load causing failure, given by Equation 7.15, is found by matching the change in the length of the diagonal AC of the frame to the shortening of the diagonal strut.

$$H = \frac{24 E I_c\, \varepsilon'_c\, d}{h^3\left[1+\left(\frac{I_c}{I_b}\right)\cot\theta\right]}\cos\theta + \frac{t\, d\, f'_c}{3}\cos\theta \tag{7.15}$$

where

E_f = elastic modulus of frame (ksi)

I_c = moment of inertia of column (inch^4)

I_b = moment of inertia of the beam (inch^4)

d = diagonal length of the infill panel (inches)

θ = angle between the diagonal and the horizontal (degrees)

ε'_c = strain in infill at failure

h = height of the frame (inches)

A = cross-sectional area of the equivalent strut (inch^2)

f'_c = diagonal compressive strength of the infill panel (ksi)

The first term on the right-hand side of the Equation 7.15 represents the load carried by the frame alone, calculated on an elastic basis. However, this value should be limited by the peak strength of the bare frame, which is given by the lesser of $\frac{4M_{pc}}{h}$ or $\frac{4M_{pb}}{h}$, where M_{pc} and M_{pb} are the fully plastic moments of the columns and the beams respectively, and h is the height of the frame. The value of the lateral strength obtained by this method, shown in Table 7.2, is much higher than that predicted by FEM/I.

Table 7.2 Predicted Specimen In-Plane Strength, kips

Model	**Predicted Strength**			
	Finite Element Method	**Simplified Methods**		
		Liauw	**Holmes**	**CERL**
Strong Frame	192	128	311	196
Weak Frame	164	97	30.5	162

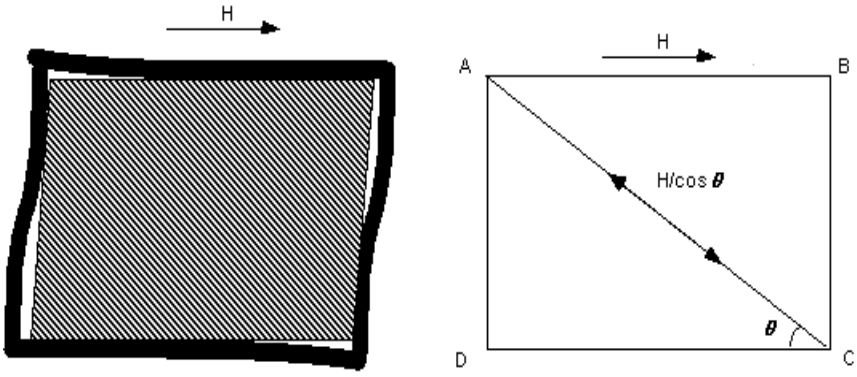

Figure 7.3 Structural Action of an Infilled Frame with a Horizontal Shear Force, H

The main reason for the high estimated collapse load using Holmes' method is that the area of the equivalent strut is overestimated since the its width is fixed to one-third of the length of the infill diagonal, irrespective of the relative stiffness of the frame and infill. A modification to Holmes' expression is presented in Equation 7.16 in order to account for the effect of relative frame-infill stiffness on the width of the equivalent diagonal strut.

$$H = \frac{24 E I_c \, \varepsilon_c' \, d}{h^3 \left[1 + \left(\frac{I_c}{I_b} \right) \cot\theta \right]} \cos\theta + A \, f_c' \, \cos\theta \qquad (7.16)$$

A is the area of the diagonal strut obtained using the curves of method SS2 described in Section 7.2.3. This modification will be referred to here as the "CERL Method." As shown in Table 7.2, predictions of CERL method are very close to those obtained by FEM/I. Consequently, the CERL Method is recommended for the estimation of the lateral in-plane strength of infilled frames.

7.3. Simplified Analytical Predictions of the Out-of-Plane Strength of Infills

7.3.1. Effect of Arching Action

Extensive experimental work has shown that masonry infills are capable of resisting much larger lateral loads than would be predicted using conventional bending analysis. In early tests, fixed-end brick beams developed 3 to 6 times the load-carrying capacity of simply supported beams, due mainly to arching action (McDowell et al., 1956).

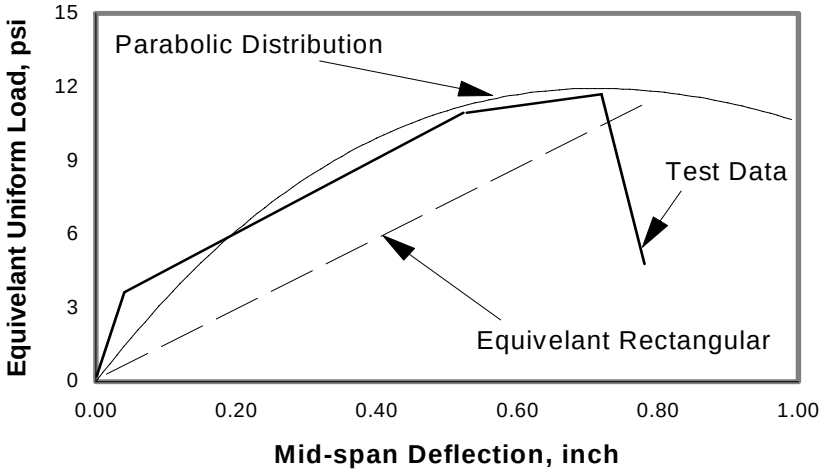

Figure 7.4 Comparison of Resistance Functions Using Different Stress Distributions with Test Data

The compressive stress-strain properties of masonry are important when considering arching action. In previous research, different stress distributions were assumed. Some workers have assumed a triangular stress distribution; others, rectangular (Dawe and Seah, 1990); and still others, elasto-plastic (McDowell et al., 1956). In the method presented here, an equivalent rectangular stress block based on Cohen's theory (McDowell et al., 1956) was used. Cohen assumed a uniform compressive stress equal to the maximum compressive stress for masonry over the whole compression area, thus overestimating the compressive force and the effect of arching action. The equivalent stress block used in this study considers the difference between the assumed and the actual stress distributions.

Figure 7.4 compares the out-of-plane strength predicted using an equivalent rectangular stress block and a parabolic stress distribution with test data (Bashandy et al., 1995). The rectangular stress block resistance function assumes a uniform stress equal to $0.85f'_{c,}$ over a portion of the contact length, and a linear load-deflection relationship up to the peak strength. The ratio between the length of the stress block and the contact length does not affect the strength because the contact length was chosen so that the lateral strength would be maximum.

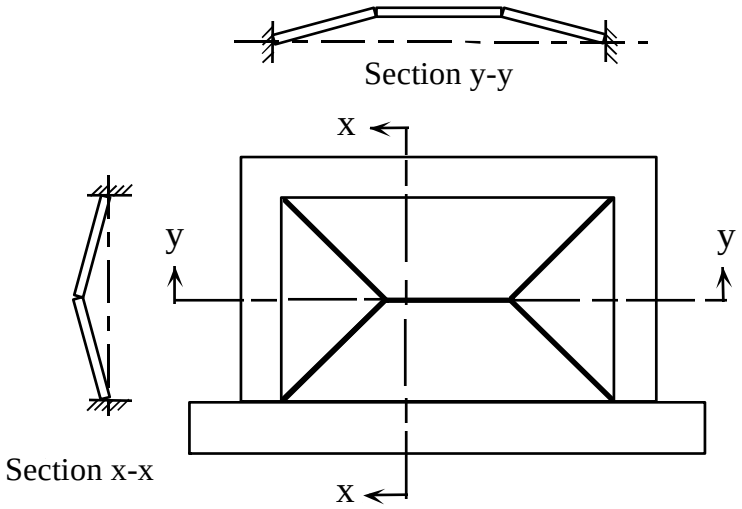

Figure 7.5 Deflected Shape of a Typical Infill During Out-of-Plane test

Both strength and displacement obtained using a parabolic stress strain distribution are very close to test results (within 2%) except in the initial range. On the other hand, the equivalent rectangular stress block method is less accurate. However, maximum strength and deflection are still close to the test results (within 6%). This inaccuracy results from assuming a linear load-deflection relationship. Because the contribution of the lateral resistance of a masonry infill is mostly from segments reaching the deflection at maximum strength, and because the equivalent stress block method simplifies the estimation of the total lateral strength of an infill with an "X" yield line pattern (as described in Section 7.3), the method is considered acceptable.

Figure 7.5 shows the idealized yield-line pattern and deflected shape of an infill loaded out-of-plane to collapse (Angel et al., 1994), while Figure 7.9 shows the actual typical infill crack pattern. This cracking (and yield) pattern shows that arching action exists in both vertical and horizontal directions. The strength prediction method presented in this section considers both arching and two-way action and is based on such yield-line pattern.

7.3.2. Proposed Method for Predicting the Out-of-Plane Strength of Infills

In this section the development of the method proposed by Bashandy et al. (1995) is outlined. Details of the derivations are given by Bashandy (1995) and Bashandy et al. (1995).

A typical deflected masonry segment is shown in Figure 7.6. According to Cohen (McDowell et al., 1956b), the out-of-plane strength is obtained at a deflection, x_y, at which a compressive stress f'_c (the ultimate compressive strength of the mortar or the masonry, whichever is weaker) exists at points m, n and o. The deflection is given by

$$x_y = \frac{t\, f_c'}{E\, \varepsilon_m} = \frac{t\, f_c'}{E \dfrac{L' - \dfrac{h}{2}}{L'}} \tag{7.17}$$

where ε_m is the strain and L' is the length of the diagonal shown in Figure 7.6.

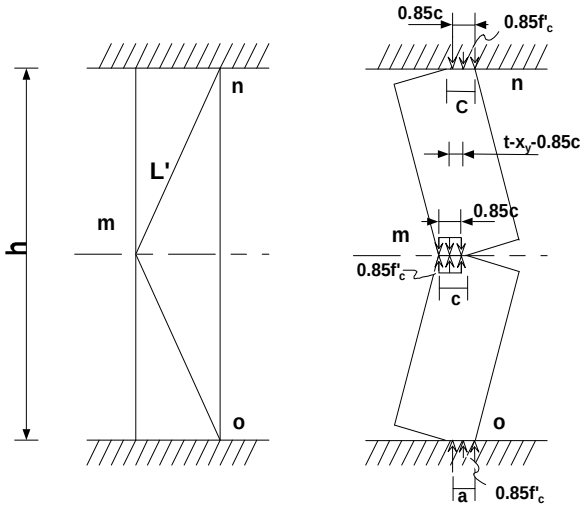

Figure 7.6 Stresses in Masonry Segments with Out-of-Plane Deflection

The resisting moment associated with the deflection, x_y, is given by Equation 7.18, in which the bearing width, c, is chosen so that the moment, M_y, is a maximum.

$$M_y = \frac{0.85 f_c'}{4}\left(t - x_y\right)^2 \tag{7.18}$$

Figure 7.6 corresponds to the deflection pattern of Figures 7.8a. However, according to the yield line pattern shown in Figure 7.7, there is another shape for the deflected segment (shown in Figure 7.8b). The corresponding moment for this segment will also be given by Equation 7.18.

The lateral strength of a segment is obtained by equating the external work to the internal work done when the segment is subjected to a virtual deflection δ. For the segment shown in Figure 7.8(a), the strength is given by Equation 7.19, and for the segment shown in Figure 7.8(b), the strength is given by Equation 7.20.

$$w = \frac{8 M_y}{h^2} \tag{7.19}$$

$$w = \frac{2 M_y}{hx - x^2} \tag{7.20}$$

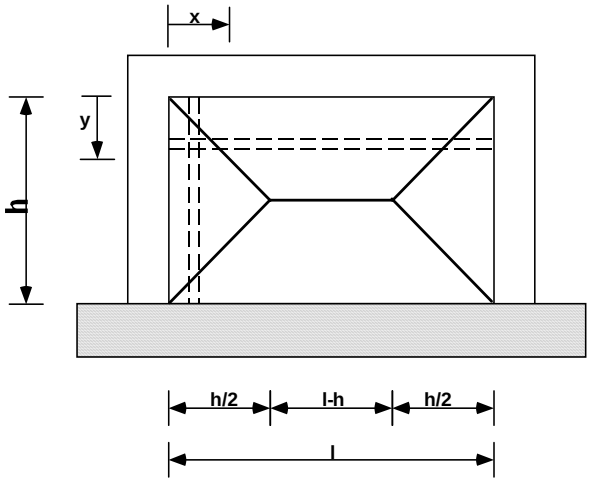

Figure 7.7 Yield Line Pattern of an Infill

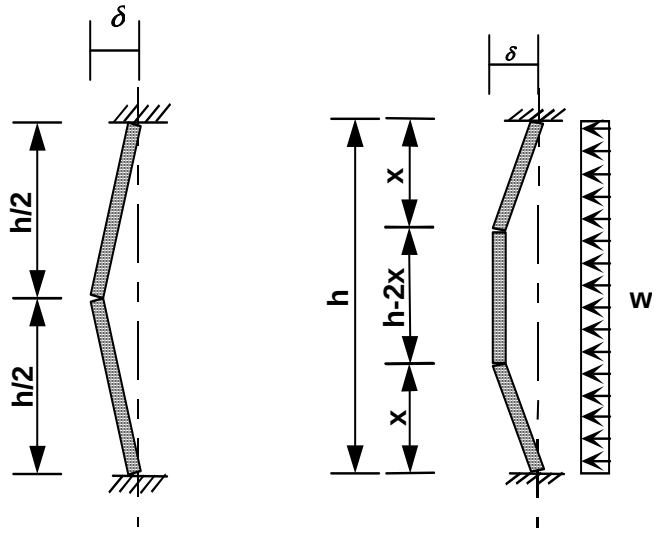

Not all horizontal and vertical strips experience the deflection x_y associated with the maximum moment M_y. According to Cohen, the resisting moment is directly proportional to the out-

of-plane deflection, up to x_y. The resisting moment at any place with out-of-plane deflection, $\delta(x)$, less than x_y, is given by $M(x) = \frac{\delta(x)}{x_y} M_y$.

From the yield line pattern shown in Figure 7.7, for vertical strips

$$\delta(x) = \frac{x}{h/2} x_{yv} = \frac{2x}{h} x_{yv} \tag{7.21}$$

and for horizontal strips,

$$\delta(y) = \frac{y}{h/2} x_{yh} = \frac{2y}{h} x_{yh} \tag{7.22}$$

where x_{yv} and x_{yh} are obtained from Equation 7.17, substituting h as the height of the infill and the length of the infill respectively. Using these expressions, out-of-plane strength for horizontal and vertical strips can be computed.

The resistance of horizontal segments is associated with the maximum out-of-plane deflection for a horizontal strip. In rectangular panels, the maximum out-of-plane deflection (at the center of the panel) is governed by the crushing of masonry in the center vertical strips. Failure will occur before horizontal strips can reach the lateral deflection required to develop a moment equal to M_{yh}.

The total force resisted by the infill, W, is given by Equation 7.23 and was obtained from the summation of the forces resisted by the horizontal and vertical strips

$$W = 8\frac{M_{yv}}{h}(l-h) + 8M_{yv}\ln(2) + 8\frac{M_{yh}}{h}\left(\frac{x_{yv}}{x_{yh}}\right)\ln\left(\frac{l}{l-h/2}\right)l \tag{7.23}$$

7.3.3. Effect of Previous In-Plane Damage, Frame Stiffness, and Yield-Line Pattern

Significant reduction in out-of-plane strength occurs when the infill has sustained severe in-plane damage (Angel et al., 1994). Since Equation 7.23 is consistent with moderate in-plane x-shaped damage, a reduction factor that depends on the panel slenderness ratio and the magnitude of

existing in-plane damage (evaluated visually according to Figure 7.9) proposed by Angel et al. (1994) may be applied. Values for such reduction factor, R, are presented in Table 7.3. R should be used for severe in-plane damage as a multiplier of the out-of-plane strength.

Out-of-plane behavior also depends on the stiffness of the confining frame (Angel et al. 1994). Another reduction factor, given by Equation 7.24, was proposed to account for the flexibility of the confining frame for panels at edge locations (for the cases of exterior bays). However, this factor causes no significant reductions for the case of reinforced concrete confining frames for most practical dimensions.

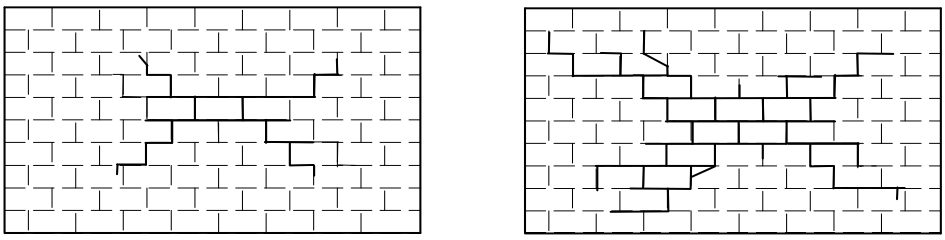

Moderate Damage Severe damage

Figure 7.9 Degrees of Infill Cracking Damage (adapted from Angel et al. 1994)

Table 7.3 Reduction factors for severe in-plane damage (based on Angel et al., 1994)

h/t	R
5	0.997
10	0.945
15	0.889
20	0.830
25	0.776
30	0.735

$$R_2 = 0.357 + 7.14 \times 10^{-8} EI \qquad \text{For } 2\times10^6 \text{ kip-inch} \le \text{EI} \le 9\times10^6 \text{ kip-inch} \quad (7.24a)$$

$R_2 = 1$ For EI > 9×10^6 kip-inch (7.24b)

This reduction factor cannot be used directly with the scaled specimen because it does not consider the effect of the confining member's length on its stiffness. If the reduction factor computed using the above equations is multiplied by the cube of the ratio between the column height of this specimen and the column height of real buildings (33 inches, or 838 mm versus 120 inches or 3048 mm), it will give no reduction in the out-of-plane strength due to the confining frame stiffness.

Angel et al. (1994) suggest that the lowest predicted strength is obtained using vertical one-way strips cracked horizontally. However, experimental results have shown that previous in-plane loading cracks the panels in an "X" pattern, and therefore the case cited by Angel et al. does not appear to be the worst case. Using the approach presented in this thesis, which assumes an "X" yield line pattern and includes two way action, the out-of-plane strength was 17% lower than that calculated assuming a horizontal crack at mid-height. This result can be explained since in an "X" yield line pattern, only the center vertical strips reach the displacement corresponding to the strength due to arching action. Vertical strips at a horizontal distance h/2 from the confining frame will have less lateral deformation, and thus less arching action and less lateral strength, causing a decrease in the total lateral strength for the infill. Additionally, the contribution of horizontal strips to the total strength is usually small since they have higher displacement capacities (due to their length) and the lateral displacement at maximum strength (governed by the shorter vertical strips) usually develops low strains, and thus low compression and a little arching action in these strips.

7.3.4. Comparison between Experimental Data and Proposed Arching Theory

The maximum experimental out-of-plane lateral strength of infilled frames is compared in Table 7.4 to the strength predicted using the arching theory presented in this thesis and to that predicted using Angel et al. proposal. The lateral strength as predicted by both methods is significantly higher than that obtained experimentally.

Table 7.4 Predicted versus Observed Out-of-Plane Strength of Infills, psf

	Test results	**Arching theory**	**Angel's Theory**
Lateral Strength	190	1775	1787

According to a test observer (Sweeney), the infilled frames were excited out-of-plane up to their lateral strength. However, another test description (Al-Chaar et al., 1994) states that the infilled frames were loaded out-of-plane up to cracking of the panel only. According to Al-Chaar et al., the difference between the test results and the estimated out-of-plane strength is due to the fact that, in the dynamic tests, the panels were excited only up to cracking while theoretical expressions estimate ultimate out-of-plane strength. A second reason, and probable most important, slight relative displacements were observed between panel segments defined by the "X" yield pattern. Such relative displacements increase the effective slenderness ratio of the infill and decrease the contact surface between segments along cracks, therefore decreasing the out-of-plane strength.

7.3.5. Comparison among Proposed Approaches for Predicting Out-Of-Plane Strength of Infills

In this section, predicted out-of-plane strength of infills for different geometries are compared using three different theoretical approaches, for a slenderness ratio (*h/t*) range from 0 to 50. Figure 7.10 shows strength estimates for three aspect ratios (*l/h*) as predicted by Dawe and Seah (1990).

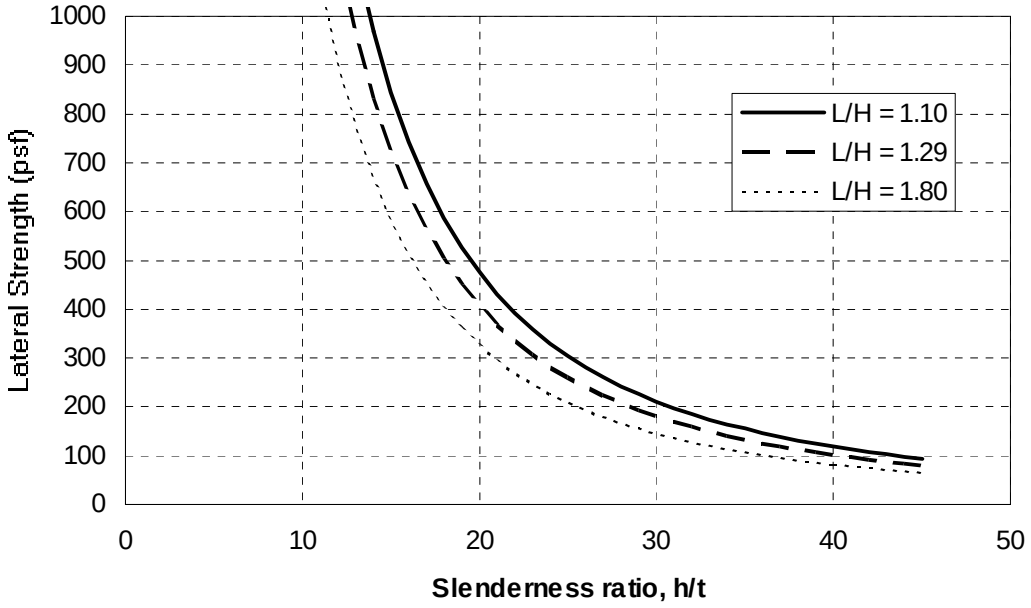

Figure 7.10 Predicted Out-Of-Plane Strength of Infills (Dawe and Seah, 1990)

Figure 7.11 shows the estimated cracking and crushing strength of infills using the method proposed by Angel et al. (1994). That approach does not account for the aspect ratio of the panel. Finally, Figure 7.12 shows the results of the method proposed by Bashandy et al. (1995), which is also presented in the Section 7.3.2 of this thesis, for three aspect ratios of the frame.

The three approaches give similar results for slenderness ratios under 40 for ultimate out-of-plane strength. The effect of aspect ratios between 1 and 2 are negligible according to Dawe and Seah (1990), and Bashandy et al. (1995) approaches, thus justifying Angel's approach. However, the approach proposed by Bashandy et al. (Equation 7.23) is the simplest of the three, and therefore is recommended to predict the out of plane strength of infilled frames.

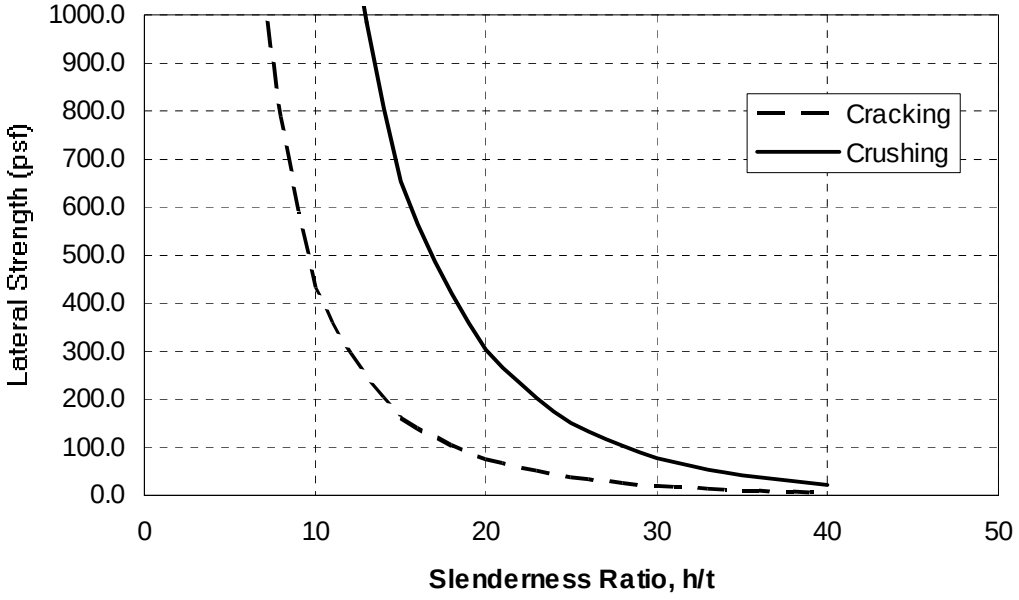

Figure 7.11 Predicted Out-Of-Plane Strength of Infills (Angel et al., 1994)

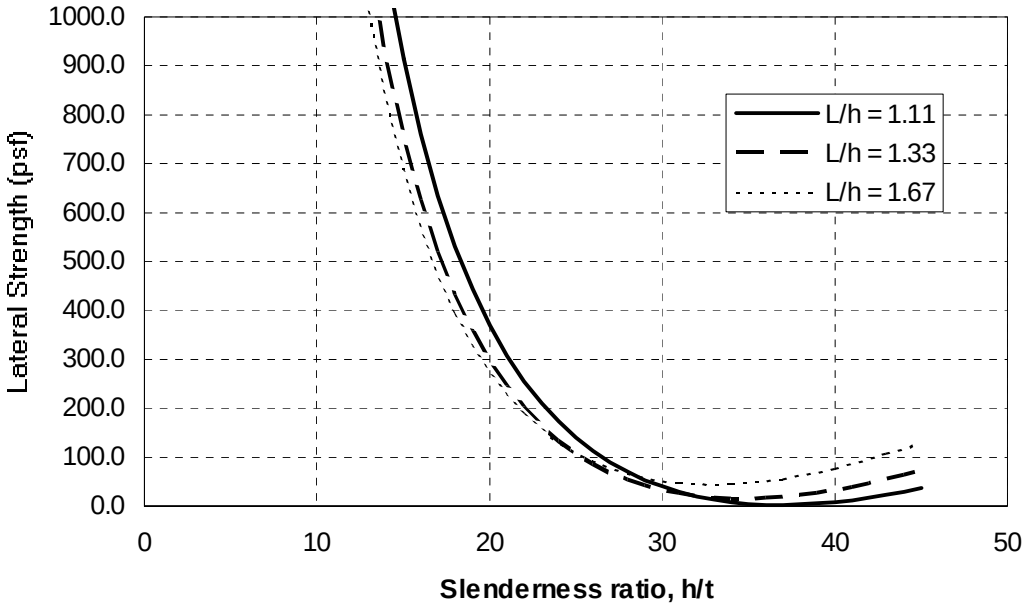

Figure 7.12 Predicted Out-Of-Plane Strength of Infills (Bashandy et al., 1995)

CHAPTER 8

SUMMARY, CONCLUSIONS AND RECOMMENDATIONS

8.1. Summary

A recent survey of U. S. Army buildings showed that a considerable percentage of them can be classified as reinforced concrete frames with infill masonry walls. In order to evaluate the strength and seismic behavior of such structures, the U. S. Army Construction Engineering Laboratory (USACERL) carried out an experimental program on several half-scale infilled frame specimens subjected to dynamic loading. Using a shaking table, both in-plane and out-of-plane simulated earthquake motions were applied to virgin, previously damaged, and repaired specimens. The experimental data obtained from this test series were then analyzed at the University of Texas at Austin. The objective of this work was to develop reliable analysis tools to predict the real strength and the dynamic response of infilled frames. Evaluation of in-plane and out-of-plane behavior of the infilled frames was performed using their load-displacement response. Maximum base shears, deflections, and internal strains were measured and assessed. Using various mathematical idealizations, the dynamic response of the specimens was predicted analytically. Finally, simplified analytical idealizations were developed to predict the strength and stiffness of infilled frames, and several design procedures were reviewed.

8.2. Conclusions

8.2.1. General Conclusions Regarding Experimental Behavior of Specimens

Results from tests with low levels of base acceleration were not useful for evaluating the strength and stiffness of the specimens. Moreover, the forces generated in the specimens during such tests were usually just a fraction of the yielding and failure loads, and they induced generally minor damage in the specimens.

On the other hand, results from tests with higher base shears were generally useful for evaluating the strength and stiffness of the specimens. For some tests, however, measured displacements were unrealistically large, and stiffness could not be evaluated accurately.

8.2.2. Conclusions Regarding the Behavior of Bare-Frame Specimens

1) The measured average backbone stiffness of the strong bare frame obtained from the load-displacement diagrams (using seismic tests) was 120 to 140 kip/inch (21.0 to 24.5 kN/mm). Maximum measured load and displacement were 20 kips (89.0 kN) and 0.3 inches (7.6 mm) respectively. From the results of random tests, the stiffness varied from 80 kips/inch (14 kN/mm) to 150 kips/inch (26 kN/mm).

2) The measured average backbone stiffness from seismic tests of the weak bare frame was 47 kips/inch (8.2 kN/mm). Maximum measured load and displacement were 22 kips (97.9 kN) and 0.7 inches (17.8 mm) respectively. From the results of random tests, the stiffness varied from 40 kips/inch (7 kN/mm) to 120 kips/inch (21 kN/mm).

3) The weak bare frame was excited up to yield; the strong bare frame was not.

4) Computer idealizations using DRAIN-2DX gave acceptable predictions of stiffness and maximum base shear (within 10%). Maximum tip displacement was less accurately predicted, since they generally exceeded the experimental values by 30%. In some cases of post-yielding behavior predicted displacements were as much as 300% higher than the measured displacements.

5) The computer idealizations exaggerate the effect of spikes in ground acceleration, especially if the structure is yielding. Predicted displacements and base shears resulting from spikes were generally higher than those measured by about 20%. Spikes in excitation while the structure was yielding caused an overestimation of tip displacement by about 50%.

8.2.3. Conclusions Regarding the In-Plane Behavior of Infilled-Frame Specimens

1) For the strong infilled frame, average stiffness evaluated from seismic tests is not reliable because of the unrealistic measured tip displacement. Measured base shear levels were 30 to 40 kips (130 to 180 kN). Levels of stiffness obtained from random tests varied from 530 kips/inch (103 kN/mm) down to 120 kips/inch (21

kN/mm). However, these values are believed to be invalid since they are lower than those obtained for the weak infilled frame.

2) For the weak infilled frame, very low values of stiffness were obtained from seismic tests, ranging from 200 to 300 kip/inch (35 to 53 kN/mm). Base shears had values of 30 to 60 kips (133 to 267 kN). From the results of random tests, an initial stiffness of 1180 kips/inch (207 kN/mm) and a final stiffness of 360 kips/inch (63 kN/mm) were obtained. These values suggest a degradation of the stiffness to about one-third of its initial value as a result of the seismic excitation.

3) Measured displacements from in-plane tests of infilled frames are unreasonable (drifts exceeding 2%). This is probably due to inaccuracies caused by signal noise, gauge sensitivity, and/or accuracy of the data measurement and acquisition equipment.

4) Infilled frames under in-plane excitation were not excited up to failure; however, some damage was induced in them.

5) The stiffness of the confining frame significantly affects the response of the infilled frames. Finite element analysis showed that the infill in the strong frame would crack at higher lateral loads than the infill in the weak frame, because the contact length between the frame and the infill is higher for the strong frame than for the weak one.

6) Nonlinear response predictions using the FEM/I followed by the LPM/I computer idealizations had a similar pattern to experimental test data. Maximum predicted base shear was close to that obtained experimentally (within 10%).

7) Computer idealization predicts the effects of spikes of shaking table acceleration on the response accurately (within 15%). Energy dissipation was predicted fairly well in one case, but not in another.

8.2.4. Conclusions Regarding the Out-Of-Plane Behavior of Infilled-Frame Specimens

1) Measured response accelerations were fairly uniform over the surface of the infills, with a slight tendency to increase with height.

2) No collapse occurred in any test. Therefore, measured load levels are only lower bounds to the strength of the specimens.

3) Strong-frame specimen results are as follows: the maximum base shear for the previously damaged specimen was about 1.2 kips (5.3 kN); the maximum base shear for the repaired infill was over 2.0 kips (8.9 kN); and the maximum base shear for the virgin infill was about 1.0 kip (4.4 kN).

4) For the weak infilled-frame specimen, the maximum out-of-plane base shear was 2.0 kips (8.9 kN), and the maximum displacement was 0.6 inches (15.2 mm). The average stiffness was estimated as 10 kips/inch (1.8 kN/mm).

5) Maximum lateral pressure levels (transverse inertia force per unit area) on the repaired specimen were almost twice those of the unrepaired panel for similar levels of damage.

6) The level of lateral pressure reached in the damaged infill was higher than in the virgin specimen. However, this may be due to the fact that the specimens were not excited up to their ultimate strength. Therefore, it is not possible to assess the real effect of prior in-plane excitation on the out-of-plane strength of the panels.

7) The cracking pattern in the infill was X-shaped, similar to that obtained for corresponding static tests.

8) Predicting the out-of-plane strength of infill panels using one-way strips cracked at mid-span is not conservative.

8.3. Recommendations for Implementation

1) Dynamic analysis of infilled frames excited in-plane can be performed accurately using equivalent (single degree of freedom) idealizations in conjunction with the computer program LPM/I, as described in Appendix B. Peak shears are predicted to within 5%; predictive accuracy of peak displacements cannot be assessed, due to inconsistencies in measured displacements. However, shapes of hysteresis loops are predicted reasonably well.

2) The initial lateral stiffness of infilled frames excited in-plane is most accurately predicted using Stafford Smith's second method "SS2" (as explained in Section 7.2.3). Under cyclic loads the stiffness will eventually degrade to about half of this initial value.

3) The lateral strength of infilled frames excited in-plane is most accurately predicted using the "CERL" Method (as explained in Section 7.2.4)

4) The out-of-plane strength of infills can be predicted using the yield line-arching theory (as explained in Section 7.3).

8.4. Recommendations for Further Research

1) Further experimental research is required to determine the effect of in-plane damage on the out-of-plane strength of infilled frames. Similarly, the effect of previous damage due to out-of-plane shaking on the in-plane strength must also be assessed.

2) Further experimental research is required to idealize the effect of the relative displacements between the cracked segments of an infill panel on that panel's out-of-plane strength.

CHAPTER 9

REFERENCES

Al-Chaar, G., Angel, R., and Abrams, D. P. (1994), "Dynamic Testing of Unreinforced Brick Masonry Infills," Proceedings of the Symposium on Advances in Engineering for Concrete and Masonry Structures, April 24-28, 1994.

Allahabadi, R. and Powell, G. H. (1988), "DRAIN-2DX User Guide, " EERC Report No. 88/06, University of California, Berkeley.

Angel, R., Abrams, D., Shapiro, D., Uzarski, J. and Webster, M. (1994), "Behavior of Reinforced Concrete Frames with Masonry Infills," Civil Engineering Studies, Structural Research Report No. 589, University of Illinois, Urbana, March 1994.

Anderson, C. (1984), "Arching Action in Transverse Laterally Loaded Masonry Wall Panels," The Structural Engineer, Vol. 62B, pp. 12-23.

Bashandy, T. R. (1995), "Behavior of Reinforced Concrete Infilled Frames under Dynamic Loading: Part 1," MS Thesis, The University of Texas at Austin.

Bashandy, T., Rubiano, N. R., and Klingner, R. E. (1995), "Evaluation and Analytical Verification of Infilled Frame Test Data," PMSFEL Report No.95-1, The University of Texas at Austin.

Beavers, J.E., Bennett, R. M., and Flanagan, R. D. (1992) "Research on Unreinforced Hollow Clay Tile Walls and Development of Computational Mechanics," Mechanics in Structural Engineering, Elsevier, London.

Carter, C. and Stafford Smith, B. (1969), "Structural Behavior of Masonry Infilled Frames Subjected to Racking Loads," Designing, Engineering, and Constructing with Masonry Products, F. B. Johnson, ed., pp. 226-233.

Dawe, J. L. and Seah, C. K. (1990), "Out-of-Plane Resistance of Concrete Masonry Infilled Panels," Journal of the Canadian Society of Civil Engineering, January 1990, pp. 854-864.

Eremin, A. A. (1956), "Discussion of Arching Action Theory of Masonry Walls," Journal of the Structural Division of the American Society of Civil Engineers, Vol. 82, pp. 1067-27 - 1067-40.

Ewing, R. D., El-Mustapha, A., and Kariotis, J. C. (1987), "FEM/I: A Finite Element Computer Program for the Nonlinear Static Analysis of Reinforced Masonry Building Components," Report No. 2.2-1 EKEH (Revised 1990).

Farahany, M. M. (1983), "Computer Analysis of Reinforced Concrete Cross-Sections," MS Thesis, The University of Texas at Austin, December 1983.

Holmes, M. (1961), "Steel Frames with Brickwork and Concrete Infilling," Proceedings of the Institution of Civil Engineers, Vol. 19, No. 6501, August 1961, pp. 473-475.

Holmes, M. (1963), "Combined Loading on Infilled Frames," Proceedings of the Institution of Civil Engineers (25), pp. 31-38.

Kanaan, A. E. and Powell, G. H. (1975), "DRAIN-2D," EERC Report No. 73-6 and 3-22, University of California, Berkeley.

Kariotis, J. C., Rahman, A. M. D., Wafqi, O. M., and Ewing, R. D. (1992), "LPM/I Version 1.03 A, Computer Program for the Nonlinear, Dynamic Analysis of Lumped Parameter Models," Report No. 2.3-4, EKEH.

Kent, D. C. and Park, R. (1971), "Flexural Members with Confined Concrete," Journal of the Structural Division, ASCE, Vol. 97, No. ST7, July 1971, pp. 1969-1990.

Kwan, A. K. H. and Xia, Q. (1995), "Shake-Table Tests of Large-Scale Shear Wall and Infilled Frame Models," Proceedings of the Institution of Civil Engineers, Structures and Buildings, Vol. 110, No. 1, pp. 66-77.

Liauw, T. C. and Kwan, K. H (1982), "Nonlinear Analysis of Multistory Infilled Frames," Proceedings of the Institution of Civil Engineers, Part 2, No. 73, pp. 441-454.

Liauw, T. C. and Kwan, K. H (1983a), "Plastic Theory of Non-Integral Infilled Frames," Proceedings of the Institution of Civil Engineers, Vol. 75, September, pp. 707-723.

Liauw, T. C. and Kwan, K. H (1983b), "Plastic Theory of Infilled Frames with Finite Interface Shear Strength," Proceedings of the Institution of Civil Engineers, Vol. 75, December , pp. 707-723.

Liauw, T. C. and Kwan, K. H (1985), "Unified Plastic Analysis of Infilled Frames," Journal of Structural Engineering, ASCE, Vol. 111, No. 7, July 1985.

Mahin, S. A. and Bertero, V. V. (1977), "RCCOLA: A Computer Program for Reinforced Concrete Column Analysis, User's Manual and Documentation," Department of Civil Engineering, University of California, Berkeley, August 1977.

McDowell, E. L., McKee, K. E., and Sevin, E. (1956), "Arching Action Theory of Masonry Walls," Journal of the Structural Division of the American Society of Civil Engineers, Vol. 82, Paper 915, pp. 915-1 - 915-18.

Page, A. W. (1978), "Finite Element Model for Masonry," ," Journal of the Structural Division, ASCE, Vol. 104, No. ST8, August 1978, pp. 1267-1285.

Riddington, J. R. and Stafford Smith, B. (1977), "Analysis of Infilled Frames Subjected to Racking with Design Recommendations," The Structural Engineer, Vol. 55, No. 6, pp. 263-268.

Saneinejad, A. and Hobbs, B. (1995), "Inelastic Design of Infilled Frames," Journal of Structural Engineering, ASCE, Vol. 121, No. 4, pp. 634-649.

Stafford Smith, B. (1962), "Lateral Stiffness of Infilled Frames," Proceedings of the Institution of Civil Engineers, Vol. 88, No. 3355, December 1962, pp. 183-199.

Stafford Smith, B. (1966), "Behavior of Square Infilled Frames," Journal of the Structural Division, ASCE, Vol. 92, No. ST1, February 1966, pp. 381-403.

Stafford Smith, B. (1967a), "The Composite Behavior of Infilled Frames," Tall Buildings, A. Coull and B. Stafford Smith, eds., Pergamon Press, London, 1967, pp. 481-495.

Stafford Smith, B. (1967b), "Methods for Predicting the Lateral Stiffness and Strength of Multi-Storey Infilled Frames," Building Science, Pergamon Press, Vol. 2, November 1967, pp. 247-257.

Stafford Smith, B. and Carter, C. (1969), "A Method of Analysis of Infilled Frames," Proceedings of the Institution of Civil Engineer, Vol. 44, No. 7218, September 1969, pp. 31-48.

Stafford Smith, B. and Riddington, J. R. (1978), "The Design of Masonry Infilled Steel Frames for Bracing Structures," The Structural Engineer, Vol. 56B, No. 1, March 1978, pp. 1-7.

Thiruvengadam, V. (1985), "On the Natural Frequencies of Infilled Frames," Earthquake Engineering and Structural Dynamics, Vol. 13, John Wiley & Sons Ltd., pp. 401-419.

Thomas, R. D. and Klingner, R. E. (1990), "Behavior of Infilled Frames," Chapter 4 in Limit States of Masonry. The Masonry Society, Boulder, Colorado.

Wood, R. H. (1978), "Plasticity, Composite Action and Collapse Design of Unreinforced Shear Wall Panels in Frames," Proceedings of the Institution of Civil Engineer, Vol. 65, No. 8110, June 1978, pp. 381-411.

APPENDIX A:

DESCRIPTION OF DATA REDUCTION PROCESS

The accelerations, displacements and strains recorded during the tests were translated into engineering units and saved in computer files with five channels per files. Figure A.1 shows the first lines of a typical shaking table data file.

Because the instrument setup and the recording channels were different for all the tests, the data reduction process was carried out using one computer program per model. The following shows the listing of the computer program DACO1.FOR, written in the FORTRAN language, which was used to reduce the data of Model #1. Similar programs were written for the other models.

FIRST LINES OF A SHAKING TABLE DATA FILE

Sweeney Model #1, Seismic Test #9
Sample Frequency = 200 hz

S15 IN/IN*10-6	S16 IN/IN*10-6	D1 IN	D2 IN	D3 IN
-5.981445	1.525879	0.000038	0.000040	0.000098
-5.737305	3.051758	0.000040	0.000041	0.000101
-5.737305	3.967285	0.000035	0.000041	0.000099
-6.347656	0.915527	0.000037	0.000041	0.000090
-8.056641	0.610352	0.000038	0.000038	0.000095
-8.056641	1.220703	0.000037	0.000040	0.000096
-7.568359	1.831055	0.000031	0.000044	0.000102
-5.493164	2.441406	0.000038	0.000040	0.000093
-6.103516	1.831055	0.000040	0.000040	0.000092
-6.469727	1.525879	0.000038	0.000035	0.000087
-6.835938	1.525879	0.000034	0.000035	0.000095
-5.859375	2.136230	0.000037	0.000032	0.000093
-5.737305	0.305176	0.000035	0.000037	0.000093
-6.713867	2.441406	0.000037	0.000035	0.000096
-7.202148	0.915527	0.000037	0.000040	0.000093
-6.958008	0.915527	0.000035	0.000038	0.000095
-6.469727	3.051758	0.000027	0.000038	0.000090
-6.835938	0.610352	0.000037	0.000041	0.000093
-7.324219	0.000000	0.000040	0.000041	0.000093
-7.446289	0.610352	0.000035	0.000040	0.000101
-5.493164	2.441406	0.000040	0.000043	0.000098
-4.150391	2.441406	0.000038	0.000041	0.000101
-4.638672	2.746582	0.000038	0.000038	0.000104
-8.666992	0.000000	0.000037	0.000038	0.000098
-6.713867	0.915527	0.000037	0.000034	0.000093
-6.713867	1.220703	0.000038	0.000038	0.000095
-6.835938	1.525879	0.000041	0.000040	0.000099
-6.713867	2.441406	0.000037	0.000040	0.000096
-6.347656	2.441406	0.000037	0.000044	0.000099
-5.737305	2.746582	0.000041	0.000041	0.000090
-6.835938	1.831055	0.000038	0.000040	0.000093

LISTING OF THE COMPUTER PROGRAM DACO1.FOR

```
      *234567890123456789012345678901234567890123456789012345678901234567890*
     *    &   1         2         3         4         5         6         7 **
      *             USACERL - EVALUATION OF INFILL FRAME TESTS               *
      *             DACO1: DAta COnversion program FOR mODEL #1              *
      *             Developed by Nestor Rubiano at UT Austin (June 1994)     *
C
IMPLICIT REAL*8(A-H,O-Y)
    IMPLICIT CHARACTER*5 (Z)
    COMMON /FILES/ FILIN1,FILOUT,IFIN1,IFOUT
    COMMON /PARAM/ NAVEDAT,NTOTDAT,ICHAN
    CHARACTER*12 CHAN1, CHAN2
    CHARACTER*5 TEST
    CHARACTER*15 FILIN1, FILIN2
    CHARACTER*15 FILOUT
    DIMENSION DATA(5)
    AMASS=10.
    SAMFREQ=200.
    NTOTDAT=50.*SAMFREQ
    NAVEDAT=3.*SAMFREQ
C
 1000 WRITE (*,2000)
    WRITE (*,2001)
    WRITE (*,2002)
    READ (*,1100) TEST
 1100 FORMAT (A)
 1200 WRITE (*,2010)
    WRITE (*,2011)
    WRITE (*,2012)
    WRITE (*,2013)
    WRITE (*,2014)
    WRITE (*,2015)
    WRITE (*,2016)
    WRITE (*,2017)
    WRITE (*,2018)
    WRITE (*,2019)
    WRITE (*,2020)
    WRITE (*,2021)
    WRITE (*,2022)
    WRITE (*,2025)
    READ (*,*) NOPT
    IF (NOPT .EQ. 11) GO TO 1000
    IF (NOPT .EQ. 12) GO TO 3000
    IF (NOPT .EQ. 1) THEN
      FILIN1=TEST // '11.TXT'
      FILIN2=TEST // '02.TXT'
      FILOUT=TEST // 'LDC.PRN'
      CHAN1=' REL. DISPL.'
      CHAN2=' BASE SHEAR '
      ICHAN1=1
      ICHAN2=4
ICHAN3=1
ELSE IF (NOPT .EQ. 2) THEN
  FILIN1=TEST // '11.TXT'
  FILIN2=TEST // '01.TXT'
  FILOUT=TEST // 'LDE.PRN'
  CHAN1=' REL. DISPL.'
  CHAN2=' BASE SHEAR '
  ICHAN1=1
  ICHAN2=3
  ICHAN3=5
ELSE IF (NOPT .EQ. 3) THEN
  FILIN1=TEST // '01.TXT'
  FILOUT=TEST // 'ACB.PRN'
  CHAN1='    TIME    '
  CHAN2=' ABS. ACCEL.'
  ICHAN=1
ELSE IF (NOPT .EQ. 4) THEN
  FILIN1=TEST // '01.TXT'
  FILOUT=TEST // 'ACC.PRN'
  CHAN1='    TIME    '
  CHAN2=' ABS. ACCEL.'
  ICHAN=1
ELSE IF (NOPT .EQ. 5) THEN
  FILIN1=TEST // '02.TXT'
  FILOUT=TEST // 'ACE.PRN'
  CHAN1='    TIME    '
  CHAN2=' ABS. ACCEL.'
  ICHAN=5
ELSE IF (NOPT .EQ. 6) THEN
  FILIN1=TEST // '11.TXT'
  FILOUT='TEST // 'DIB.PRN'
  CHAN1='    TIME    '
  CHAN2=' ABS. DISPL.'
  ICHAN=1
ELSE IF (NOPT .EQ. 7) THEN
  FILIN1=TEST // '11.TXT'
  FILOUT=TEST // 'DIC.PRN'
  CHAN1='    TIME    '
  CHAN2=' REL. DISPL.'
  ICHAN1=1
  ICHAN2=4
ELSE IF (NOPT .EQ. 8) THEN
  FILIN1=TEST // '11.TXT'
  FILOUT=TEST // 'DIE.PRN'
  CHAN1='    TIME    '
  CHAN2=' REL. DISPL.'
```

```
      ICHAN1=1
      ICHAN2=3
     ELSE IF (NOPT .EQ. 9) THEN
      FILOUT=TEST // 'STM.PRN'
      IFIN1=4
      IFOUT=6
      NSTR=0
      FILIN1=TEST // '03.TXT'
      ICHAN=2
CALL STRAINMAX(NSTR)
      FILIN1=TEST // '03.TXT'
      ICHAN=3
      CALL STRAINMAX(NSTR)
      FILIN1=TEST // '03.TXT'
      ICHAN=4
      CALL STRAINMAX(NSTR)
      FILIN1=TEST // '03.TXT'
      ICHAN=5
      CALL STRAINMAX(NSTR)
      FILIN1=TEST // '04.TXT'
      ICHAN=1
      CALL STRAINMAX(NSTR)
      FILIN1=TEST // '04.TXT'
      ICHAN=2
      CALL STRAINMAX(NSTR)
      FILIN1=TEST // '04.TXT'
      ICHAN=3
      CALL STRAINMAX(NSTR)
      FILIN1=TEST // '04.TXT'
      ICHAN=4
      CALL STRAINMAX(NSTR)
      FILIN1=TEST // '04.TXT'
      ICHAN=5
      CALL STRAINMAX(NSTR)
      FILIN1=TEST // '05.TXT'
      ICHAN=1
      CALL STRAINMAX(NSTR)
      FILIN1=TEST // '05.TXT'
      ICHAN=2
      CALL STRAINMAX(NSTR)
      FILIN1=TEST // '05.TXT'
      ICHAN=3
      CALL STRAINMAX(NSTR)
      FILIN1=TEST // '05.TXT'
      ICHAN=4
      CALL STRAINMAX(NSTR)
      FILIN1=TEST // '05.TXT'
      ICHAN=5
      CALL STRAINMAX(NSTR)
      FILIN1=TEST // '06.TXT'
      ICHAN=1
      CALL STRAINMAX(NSTR)
      FILIN1=TEST // '06.TXT'
      ICHAN=2
      CALL STRAINMAX(NSTR)
      CLOSE(IFOUT)
       GO TO 2500
      END IF
C
      IFIN1=4
      OPEN (IFIN1,FILE=FILIN1,STATUS='OLD')
      DO 5 I=1,4
    5 READ (IFIN1,*)
      IF (NOPT .LE. 2) THEN
IFIN2=5
       OPEN (IFIN2,FILE=FILIN2,STATUS='OLD')
       DO 6 I=1,4
    6  READ (IFIN2,*)
      END IF
      IFOUT=6
      OPEN (IFOUT,FILE=FILOUT,STATUS='UNKNOWN')
      WRITE (IFOUT, 2030) CHAN1, CHAN2
C
      IF (NOPT .LE. 2) THEN
       AVE1=0.
       AVE2=0.
       AVE3=0.
       DO 20 I=1,1000
        READ (IFIN1,*) (DATA(J),J=1,4)
        AVE1=AVE1+DATA(ICHAN1)
        AVE2=AVE2+DATA(ICHAN2)
        READ (IFIN2,*) (DATA(J),J=1,5)
   20   AVE3=AVE3+DATA(ICHAN3)
       AVE1=AVE1/1000.
       AVE2=AVE2/1000.
       AVE3=AVE3/1000.
       REWIND IFIN1
       REWIND IFIN2
       DO 21 I=1,4
   21   READ (IFIN1,*)
       DO 22 I=1,4
   22   READ (IFIN2,*)
       DO 30 I=1,10000
        READ (IFIN1,*) (DATA(J),J=1,4)
        DATA1=(DATA(ICHAN2)-AVE2)-(DATA(ICHAN1)-AVE1)
        READ (IFIN2,*) (DATA(J),J=1,5)
        DATA2=-AMASS*(DATA(ICHAN3)-AVE3)
   30   WRITE (IFOUT, 2040) DATA1, DATA2
       CLOSE(IFIN2)
      ELSE
       NCOL=5
       IF (NOPT .GE. 6) NCOL=4
       AVE=0.
       DO 40 I=1,1000
        READ (IFIN1,*) (DATA(J),J=1,NCOL)
        IF (NOPT .LE. 6) THEN
         AVE=AVE+DATA(ICHAN)
        ELSE
         AVE1=AVE1+DATA(ICHAN1)
         AVE2=AVE2+DATA(ICHAN2)
        END IF
   40  CONTINUE
```

```
      IF (NOPT .LE. 6) THEN
       AVE=AVE/1000.
      ELSE
       AVE1=AVE1/1000.
       AVE2=AVE2/1000.
      END IF
      REWIND IFIN1
DO 41 I=1,4
 41    READ (IFIN1,*)
      DO 50 I=1,10000
       DT=1./SAMFREQ
       DATA1=(I-1)*DT
       READ (IFIN1,*) (DATA(J),J=1,NCOL)
       IF (NOPT .LE. 6) THEN
        DATA2=(DATA(ICHAN)-AVE)
       ELSE
        DATA2=(DATA(ICHAN2)-AVE2)-(DATA(ICHAN1)-AVE1)
       END IF
 50    WRITE (IFOUT, 2040) DATA1, DATA2
     END IF
     CLOSE(IFIN1)
     CLOSE(IFOUT)
     GO TO 2500
2000 FORMAT (////////////////////////////)
2001 FORMAT (/' <<< CERL - TEST SERIES FOR MODEL #1 >>>'/)
2002 FORMAT (/'   * ENTER TEST NAME (5 CHARACTERS) *   '/)
2010 FORMAT (//' OPTIONS :'/)
2011 FORMAT ('  1. LOAD-DISPLACEMENT (N CENTER SLAB)')
2012 FORMAT ('  2. LOAD-DISPLACEMENT (E TOP BEAM)')
2013 FORMAT ('  3. TIME HISTORY (BASE ACCELERATION)')
2014 FORMAT ('  4. TIME HISTORY (N CENTER SLAB ACCEL.)')
2015 FORMAT ('  5. TIME HISTORY (E TOP BEAM ACCEL.)')
2016 FORMAT ('  6. TIME HISTORY (BASE DISPLACEMENT)')
2017 FORMAT ('  7. TIME HISTORY (N CENTER SLAB REL. DISP.)')
2018 FORMAT ('  8. TIME HISTORY (E TOP BEAM REL. DISP.)')
2019 FORMAT ('  9. REINFORCEMENT STRAIN (S1..S16)')
2020 FORMAT (' 10. UNASSIGNED')
2021 FORMAT (' 11. NEW TEST')
2022 FORMAT (' 12. EXIT'/)
2025 FORMAT (/' ENTER OPTION(1..12):')
2030 FORMAT (A12,',',A12)
2040 FORMAT (F12.6,',',F12.6)
2052 FORMAT(/'   * TEST NAME : ',A,' *   '/)
C
2500 WRITE (*,2000)
     WRITE (*,2001)
     WRITE (*,2052) TEST
     GO TO 1200
3000 STOP
     END
C
     SUBROUTINE STRAINMAX(NSTR)
     IMPLICIT REAL*8(A-H,O-Y)
     COMMON /FILES/ FILIN1,FILOUT,IFIN1,IFOUT
     COMMON /PARAM/ NAVEDAT,NTOTDAT,ICHAN
     CHARACTER*15 FILIN1, FILOUT
     DIMENSION DATA(5)
     NSTR=NSTR+1
     OPEN (IFOUT,FILE=FILOUT,STATUS='UNKNOWN')
     OPEN (IFIN1,FILE=FILIN1,STATUS='OLD')
     WRITE(*,3200) NSTR,FILIN1,ICHAN
3200 FORMAT('S',I2,'  ',A12,' (Ch=',I2,') ... ')
DO 1 I=1,4
  1   READ (IFIN1,*)
     AVE=0.
     DO 20 I=1,NAVEDAT
      READ (IFIN1,*) (DATA(J),J=1,5)
 20   AVE=AVE+DATA(ICHAN)
     AVE=AVE/NAVEDAT
     REWIND IFIN1
     DO 21 I=1,4
 21   READ (IFIN1,*)
     STMAX=0.
     STMIN=0.
     DO 30 I=1,NTOTDAT
      READ (IFIN1,*) (DATA(J),J=1,5)
      DATA1=DATA(ICHAN)-AVE
      IF (DATA1 .GE. STMAX) STMAX=DATA1
 30   IF (DATA1 .LE. STMIN) STMIN=DATA1
     WRITE (IFOUT,3250) NSTR,STMAX*1E-6,STMIN*1E-6
3250 FORMAT(I2,'  Max',F9.6,'  Min',F9.6)
     CLOSE(IFIN1)
     RETURN
     END
```

APPENDIX B:

RESULTS OF RANDOM TESTS

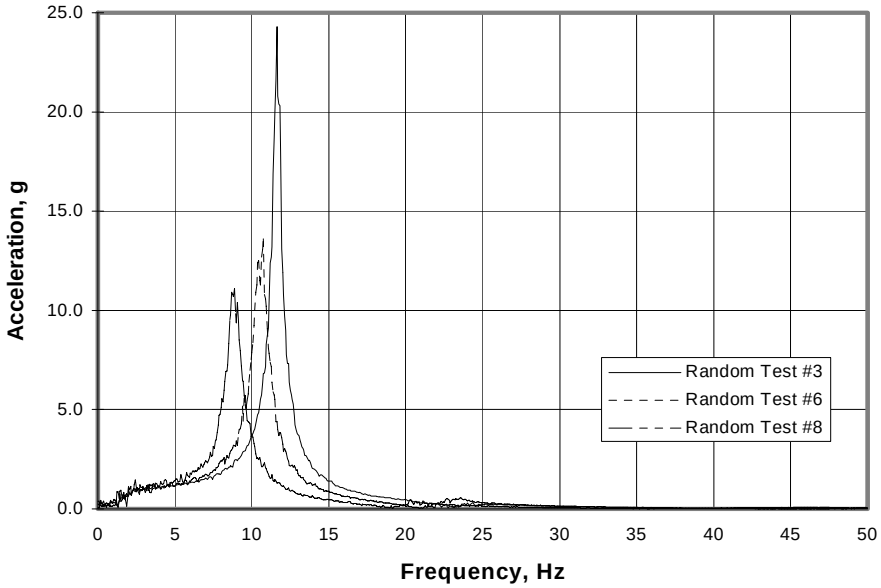

Figure B.1 Random Vibration Response of Model #1

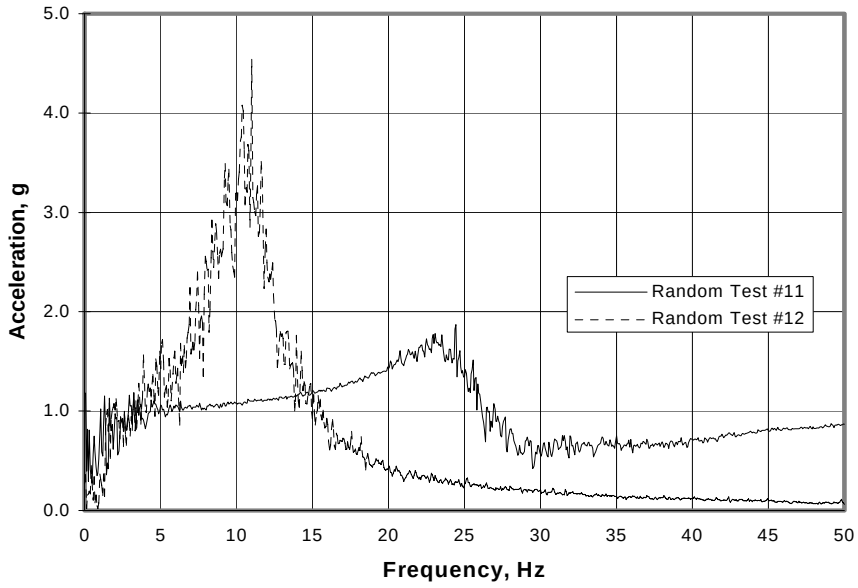

Figure B.2 Random Vibration Response of Model #2

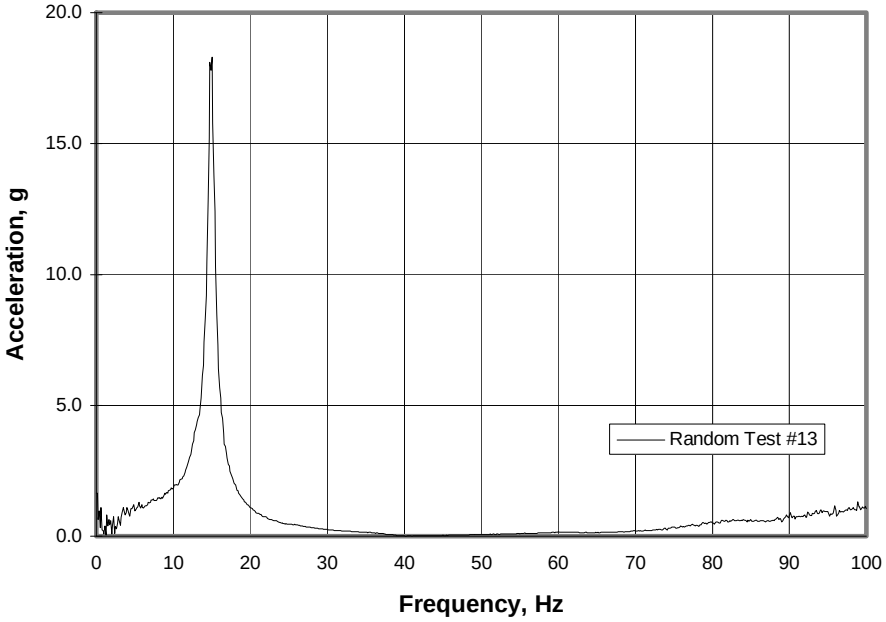

Figure B.3 Random Vibration Response of Model #3

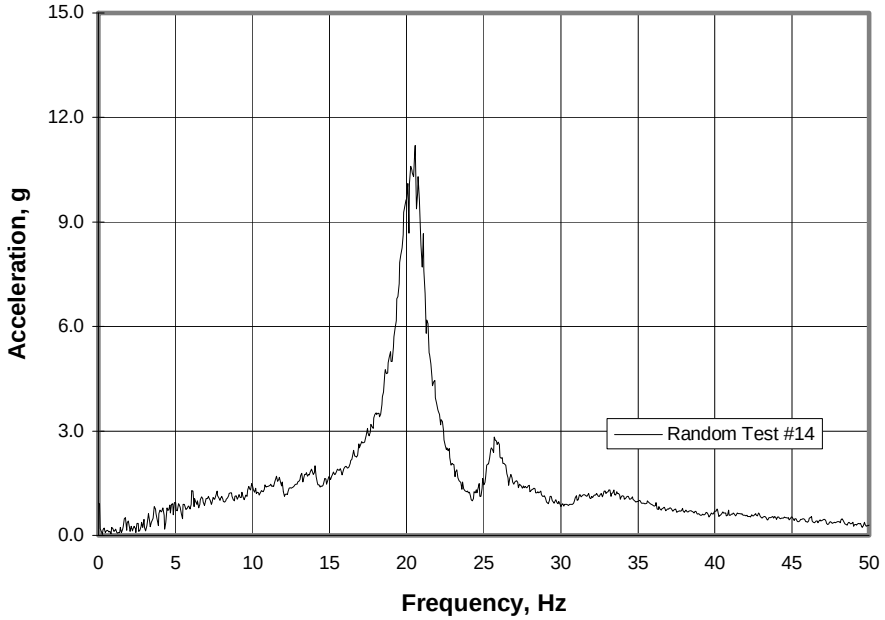

Figure B.4 Random Vibration Response of Model #4

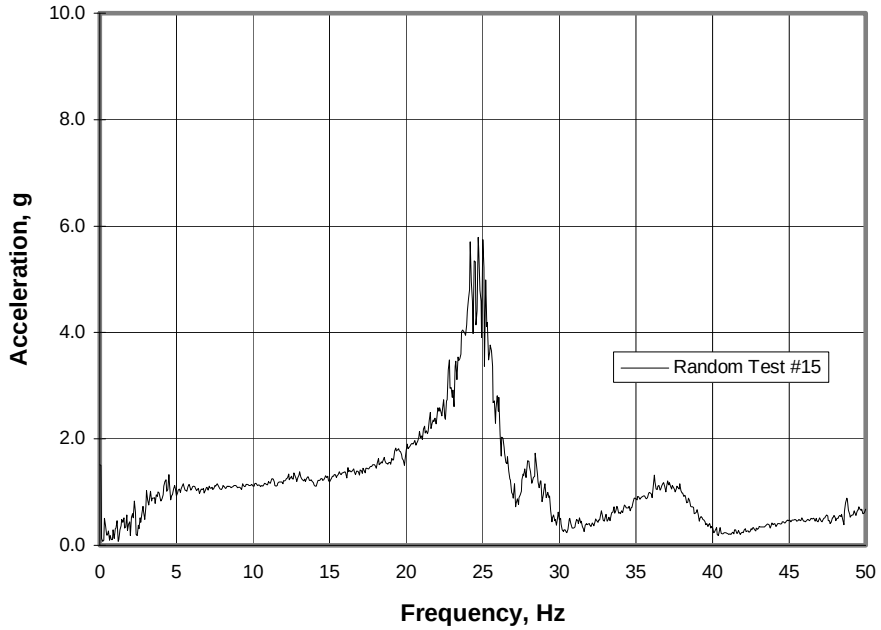

Figure B.5 Random Vibration Response of Model #5

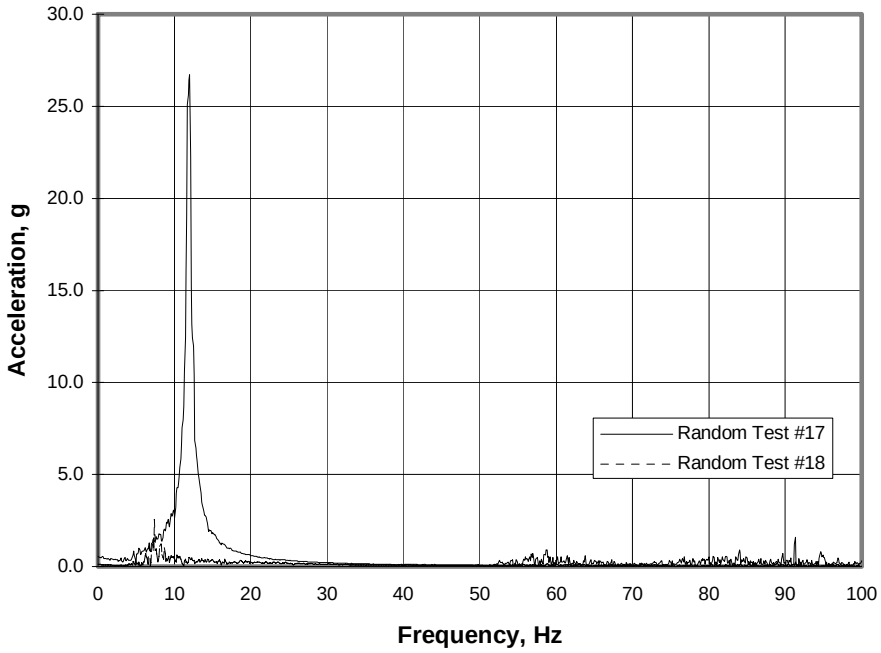

Figure B.6 Random Vibration Response of Model #6

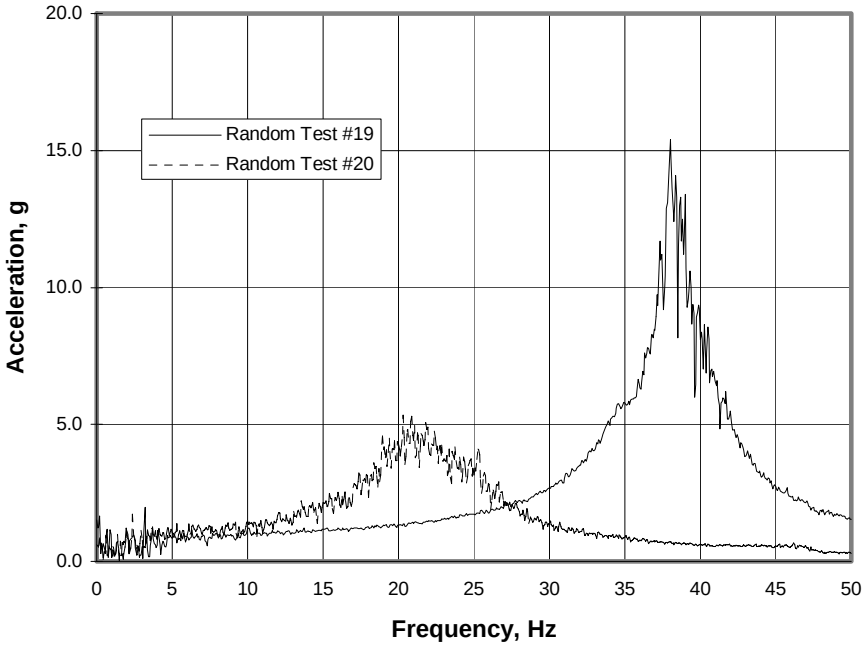

Figure B.7 Random Vibration Response of Model #7

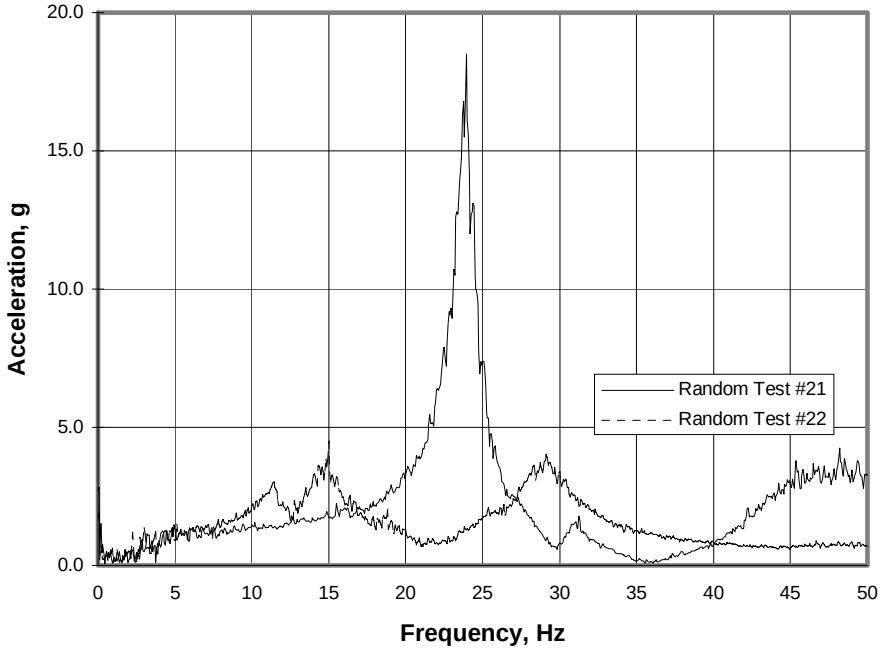

Figure B.8 Random Vibration Response of Model #8